(9) FINAL REPORT,

(6) HYDROSTATIC EXTRUSION,

By

(10) Erastus H. Lee, Russell L. Mallett, Robert M. McMeeking, Oleg D. Sherby, John C. Shyne and Robert T. Whalen

Sponsored by
Defense Advanced Research Projects Agency
ARPA Order No. 2783
Contract Num(15) NØØØ14-75-C-Ø923,
ARPA Order-2783

Scientific Officer: Director, Metallurgy Program
Materials Science Division
Department of the Navy
Office of Naval Research
800 North Quincy Street
Arlington, Virginia 22217

Principal Investigators: Oleg D. Sherby, John C. Shyne & Erastus H. Lee

(11) Mar 1978 (12) 151 P.

(14) SU-DMS-77-T-6

Department of MATERIALS SCIENCE AND ENGINEERING
STANFORD UNIVERSITY

Unclassified
Security Classification

DOCUMENT CONTROL DATA - R & D

(Security classification of title, body of abstract and indexing annotation must be entered when the overall report is classified)

1. ORIGINATING ACTIVITY (Corporate author) Department of Materials Science and Engineering	2a. REPORT SECURITY CLASSIFICATION Unclassified 2b. GROUP

3. REPORT TITLE

Hydrostatic Extrusion

4. DESCRIPTIVE NOTES (Type of report and inclusive dates)
Final Report

5. AUTHOR(S) (First name, middle initial, last name)

Erastus H. Lee, Russell L. Mallett, Robert M. McMeeking, Oleg D. Sherby, John C. Shyne and Robert T. Whalen

6. REPORT DATE	7a. TOTAL NO. OF PAGES	7b. NO. OF REFS
March 1978	147	67

8a. CONTRACT OR GRANT NO.	9a. ORIGINATOR'S REPORT NUMBER(S)
N00014-75-C-0923 b. PROJECT NO. 332 57J c. d.	9b. OTHER REPORT NO(S) (Any other numbers that may be assigned this report)

10. DISTRIBUTION STATEMENT

Unlimited

11. SUPPLEMENTARY NOTES	12. SPONSORING MILITARY ACTIVITY

13. ABSTRACT

Two results have evolved which represent our most significant accomplishments. First, perfection and successful operation of our hydrostatic extrusion press has lead to our ability to extrude ductile materials* up to a reduction ratio of 400 : 1 ($\varepsilon = 6$), and semi-brittle materials** up to reductions of 60 : 1.

* We have extruded aluminum with small percentages of Fe to area reductions of up to 400 to 1. Extruded samples have shown remarkably high yield strengths; for example, an Al-.5%Fe material has a yield strength of approximately 30 ksi. A fine subgrain structure is generated and captured by quenching immediately after extrusion.

** Our studies here have centered on the fabrication of superconducting wire (Nb_3Sn) and on producing high strength steel wire. The Nb_3Sn was processed by a method developed at the Lawrence Berkeley Laboratory. Tin infiltrated into porous niobium compacts were hydrostatically extruded without apparent damage to the infiltrated core. A low alloyed bearing steel (52100) was successfully extruded 60 to 1 in eight passes with no sign of cracking.

Second, initiation of theoretical studies on the extrusion process have led, for the first time, to applying elastic-plastic theory to analyze the process of extrusion. Until now the majority of analytical work has been done using rigid-plastic theory. Although this can be of great value in calculating upper and lower bounds on such things as power requirements, one must consider the materials' elastic properties in order to calculate and predict residual stresses. We have successfully completed the axi-symetric case for extrusion with smooth dies. One very important result of this solution is the generated residual stress distribution in the extrudate.

DD FORM 1 NOV 65 1473

Unclassified
Security Classification

14 KEY WORDS	LINK A		LINK B		LINK C	
	ROLE	WT	ROLE	WT	ROLE	WT
Extrusion						
Hydrostatic Extrusion						
Superconducting Wire						
Aluminum Conductor Wire						
Applied Mechanics						
Residual Stress						
Elastic-plastic Code						
Finite Elements						

TABLE OF CONTENTS

INFLUENCE OF HIGH HYDROSTATIC PRESSURE EXTRUSION ON MECHANICAL BEHAVIOR OF MATERIALS

Introduction and Summary

Hydrostatic extrusion is a promising new metal working technique. In hydrostatic extrusion a large hydrostatic pressure is superimposed on the stress field that normally develops during extrusion. As a result, materials difficult or impossible to extrude by the conventional extrusion process can be extruded hydrostatically. Further, there is evidence that materials formed by hydrostatic extrusion exhibit superior mechanical properties compared to similar materials worked by conventional techniques. At the present time hydrostatic extrusion is not being applied extensively to technological applications in this country (considerably more work is being done in Europe and Japan). A pilot project to hydrostatically extrude copper into wire has been started by Western Electric and this particular operation appears promising. Surprisingly, the basic understanding of the hydrostatic extrusion process, both from the theoretical mechanics point of view and from the standpoint of materials science, remains in quite a primitive state.

The present program is centered on an experimental and analytical study of hydrostatic extrusion. The experimental aspects are described in the first section of this progress report. In the second section we describe the basis for an elastic-plastic code as a means of assessing metal forming operations. This analytical approach is unique and promises to be a very powerful tool in analyzing the extrusion process.

A. OPERATION AND MAINTENANCE OF THE HYDROSTATIC EXTRUSION MACHINE

by Robert T. Whalen and David L. Bourell

For the most part the hydrostatic extrusion machine (Figure 1) has been operating without problems over the last year. However, we decided that several modifications to the extrusion machine would result in a more effective machine operation and better properties of the extruded material. These changes are discussed below.

(1) Installation of Auxillary Pump

One major alteration to the machine was necessary. When testing the high pressure system, a problem arose which required the addition of an auxillary pump to maintain constant extrusion chamber containment pressure. The problem never surfaced during testing with the low pressure system because the containment pressures and extrusion pressures are balanced when line pressure to both the intensifier and extrusion piston are the same, i.e., when both are at system pressure. However, reducing the extrusion chamber diameter by a factor of two (from 3/4" to 3/8") while maintaining equal line pressures to intensifier and piston doubles the clamping pressure on the liner but quadruples the extrusion pressure. Therefore, to maintain the balance between the two, the line pressure to the extrusion piston must be reduced to half the intensifier pressure. The present hydraulic system is not equipped to reliably hold two separate pressures simultaneously. Because the volume of oil being compressed on the high pressure side of the intensifier is so small, normally insignificant leaks at check valves and solenoid valves are causing the intensifier pressure to drop gradually to system pressure, i.e., extrusion piston pressure.

In discussions with Revere Copper and Brass we concluded that success

could only be guaranteed if we went to a system utilizing two hydraulic pumps, both with a 3,000 psi maximum output. The large, high output pump would operate the extrusion piston as well as initially charge the intensifier. The function of the second pump would be to counter-balance the effects of the leaks and maintain a constant 3,000 psi intensifier line pressure during extrusion. The smaller pump was added to the hydraulic system and the intensifier is now holding the proper pressure during extrusion.

(2) Installation of Rapid Quenching System

In order to maximize the mechanical properties and maintain a highly worked structure, we thought it necessary to develop a quenching system. Without some method of cooling, the high material temperatures caused by the adiabatic heating could result in recovery and recrystallization. Therefore we designed and fabricated quenching systems for both direct and indirect extrusion which effectively quench the extruded material immediately on exit from the die.

As shown in Figure 2 the system is best represented as two concentric tubes leading from the die and extrusion chamber to the outside. Liquid enters the machine and flows down the annualar region between the two tubes to the die. At the die, holes are provided to spray the emerging extrusion with liquid. Liquid and extrusion then exit together through the central tube. A quenching system for the indirect mode was somewhat more difficult to achieve. Conceptually the two designs are similar, but for the indirect mode it was necessary to deliver water to the exit of a moving die in the interior of the machine. Again the idea of concentric tubes was used; but in this case a long tube had to pass through a special anvil, then down through the die stem to the die face. As before quenching fluid flows down the outside of the inserted tube to the die face, then exists with material through the tube center.

This method of quenching the extruded billet proved to be very successful. The results of our tests on conductor grade aluminum revealed that a very highly worked state could be preserved by such quenching techniques. The results of this work will be described later in the report.

Also present work is being planned to check if the quenching system prevents dynamic recrystallization during extrusion and also to study the magnitude of strengthening developed by quenching at the die face.

(3) Design Considerations for Warm and Hot Hydrostatic Extrusion

Another goal is to develop capabilities for warm and hot extrusions. Our hydrostatic extrusion machine was not designed specifically for warm extrusion, but we hope someday to develop techniques to allow extrusions approaching 1000°C at pressures of 250,000 psi.

Our first precaution must be to insure against overheating of the hydraulic oil and loss of strength in the die jackets. At higher temperatures, heat retention, thermal shock, thermal expansion and selection of material hydrostatic medium and lubricant are all factors which may be problematic.

We considered both internal and external heating of the billet. The alternative to heat externally and quickly transfer billet and hydrostatic medium offered the best chance for immediate success. Therefore, our efforts have concentrated on perfecting this system. Figure 3 illustrates the modifications of the present system to accomodate warm extrusion (200-750°C). As can be seen in the figure, we have combined the 3/8" die stem and the die stem guide assembly with the 3/4" extrusion chamber. Unfortunately, we had to sacrifice our capability to extrude 3/4" billets in order to gain the requisite amount of insulation

necessary for protection of the die jackets during elevated temperature extrusion. If this system eventually works well, we plan to have different die jackets machined with larger bore diameters.

Our initial attempts have not yet led to successful extrusions. The fact that the glass insulating sleeves (No. 2 in Figure 3b) have so far withheld the pressures for extrusion provides some encouragement. We first encountered problems in material transfer from furnace to extrusion. Once these were solved we still could not extrude material. Dave Bourell, a graduate student, modelled the extrusion chamber and wrote a computer heat flow program. Results from it indicate that even with pre-heating of the extrusion chamber, we will encounter difficulties related to the rapid cooling of the billet and fluid once these are inserted into the chamber.

Figure 4 plots billet centerline temperature vs. time once the heated billet has been inserted into the extrusion chamber. Initial billet temperature was 600°C. As an example, after 10 seconds billet temperature has dropped from 600°C to 350°C. Even pre-heating the chamber to 300°C gains very little - billet temperature still drops to 400°C (see Figure 5).

We plan to return to this problem in the future but for the present room temperature extrusions are providing us with enough material.

(4) Improved Die Design

Die breakage was an occasional problem which has been completely eliminated by the introduction of a new die design. In our hydrostatic extruder the die acts both as a reduction orifice for extruding and as a seal for the pressure transmitting medium. For proper operation the original design required close tolerances on the extrusion liner and die outside diameter. An undersized die might leak and an oversized die would develop high friction forces during indirect extrusion. Although

the extrusion liner does provide some clamping force on the die with the old design, this was often insufficient and die failure resulted.

To solve these problems we developed the die as shown in Figure 6. In our design the die is smaller than the extrusion liner by .004 - .006" on the radius, and a seal is formed through compression of a copper ring at the die orifice. Since the die no longer contacts the liner, close tolerances are unnecessary and changes in liner dimensions do not require re-machining or plating of the dies. The thin annular ring of fluid between die and liner now provides optimum die containment pressure. Additional containment is provided by the copper ring. The fact that the die slips easily off the extruded billet is evidence of the effectiveness of the copper rings ability to hold the die orifice in compression during extrusion. In the last year of operation, we have not broken a die.

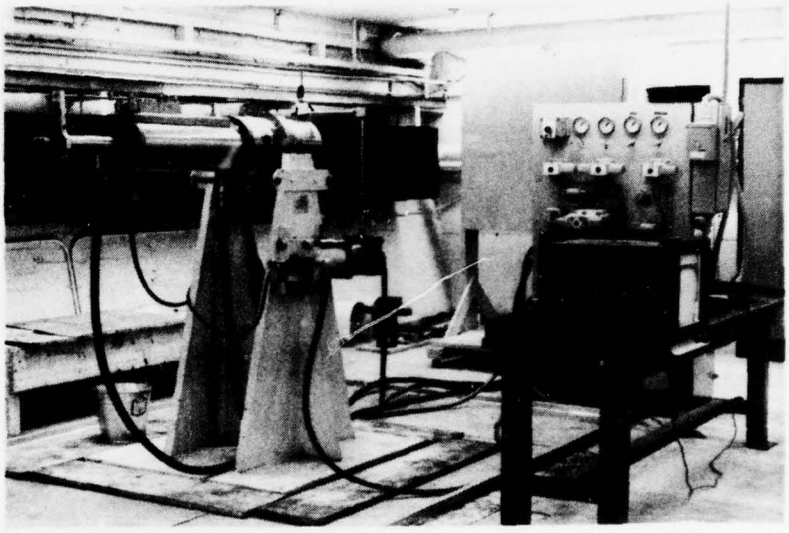

Figure 1. The above photograph shows the hydrostatic extruder in its present location. Both the hydrostatic control panel and protection barrier are visible in the background. The barrier is properly positioned for the direct extrusion mode.

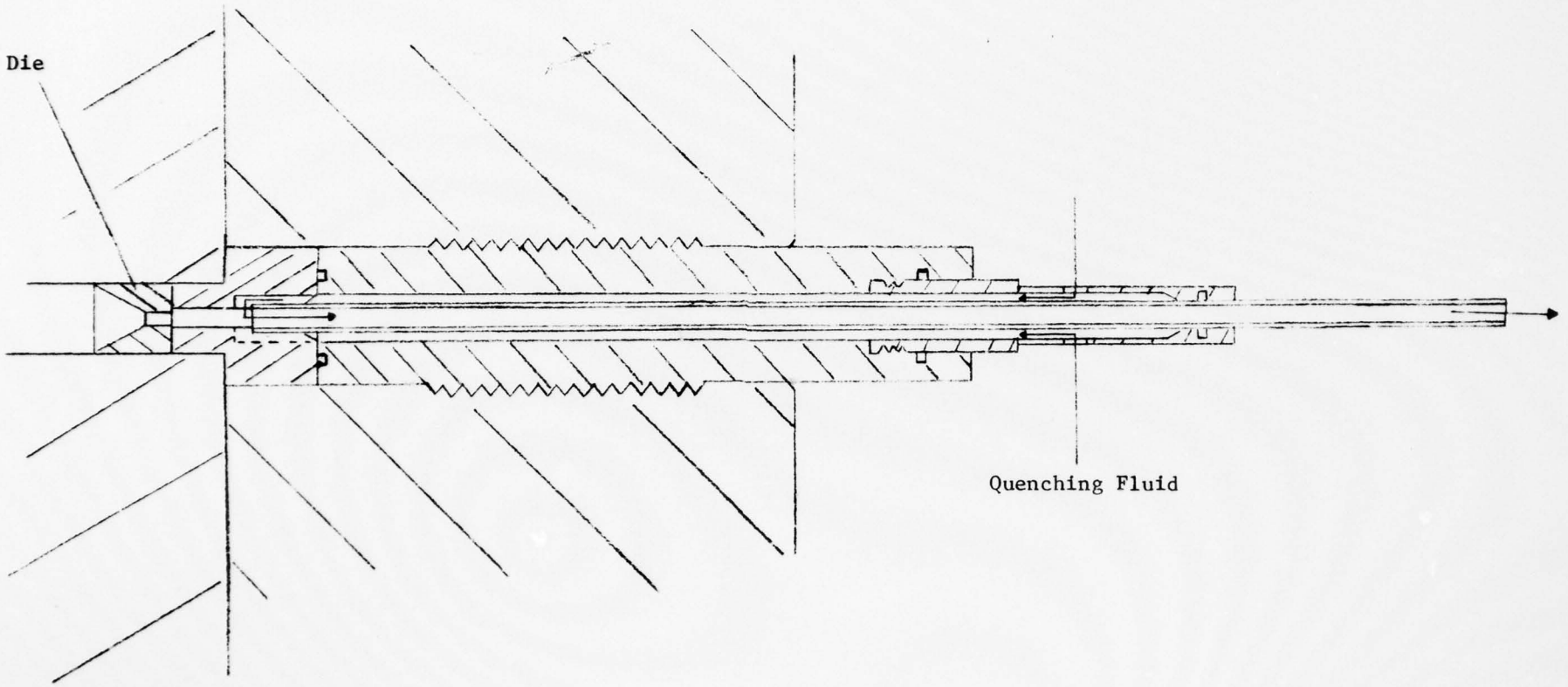

Figure 2. Quenching system for direct extrusion mode. Extruded billet and fluid exit through center tube.

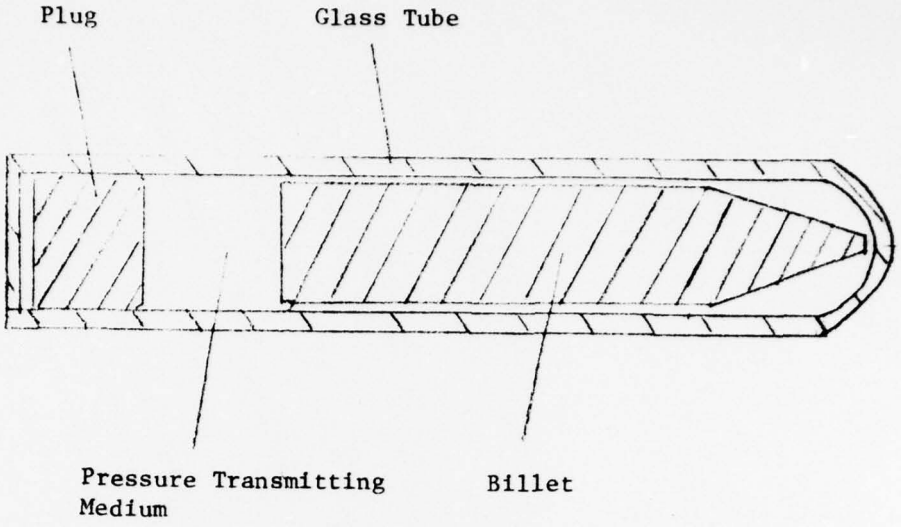

Figure 3a. Preheating container for warm extrusion.

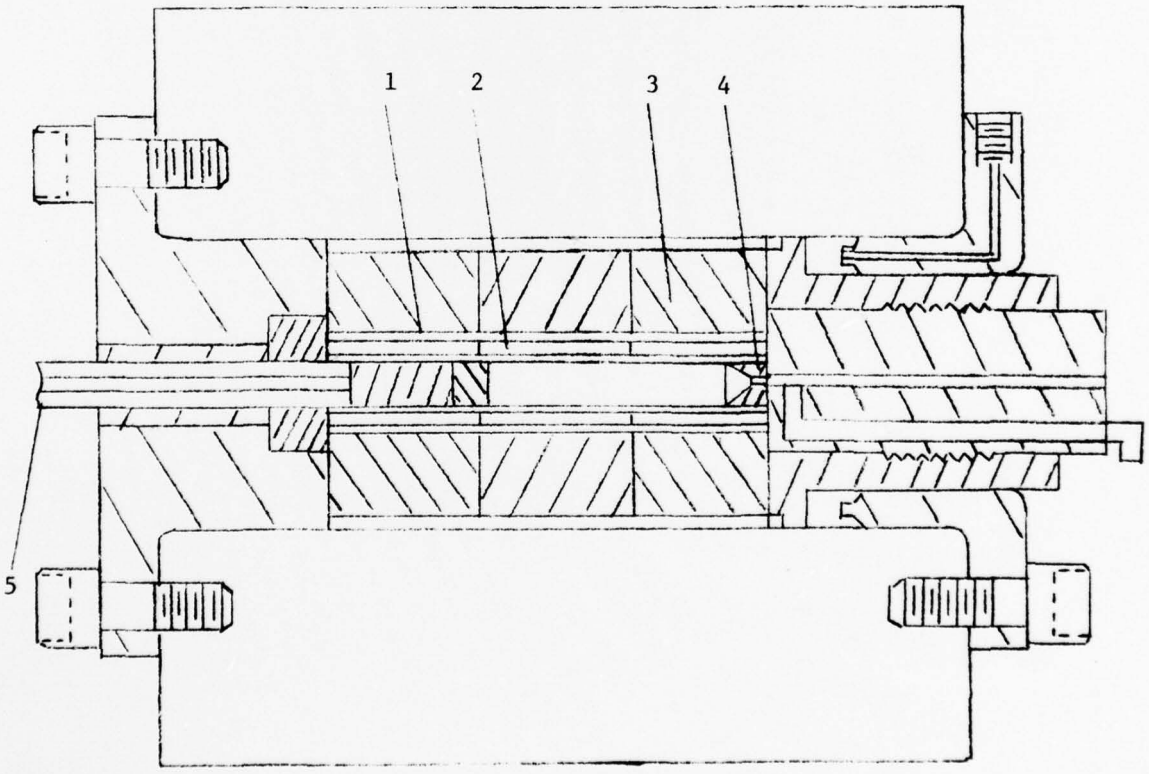

Figure 3b. Extrusion chamber modified for warm extrusion and quenching. (1) Tool steel liner--M2 (2) Insulating sleeves (3) Die jackets (4) Die (5) 3/8 inch die stem

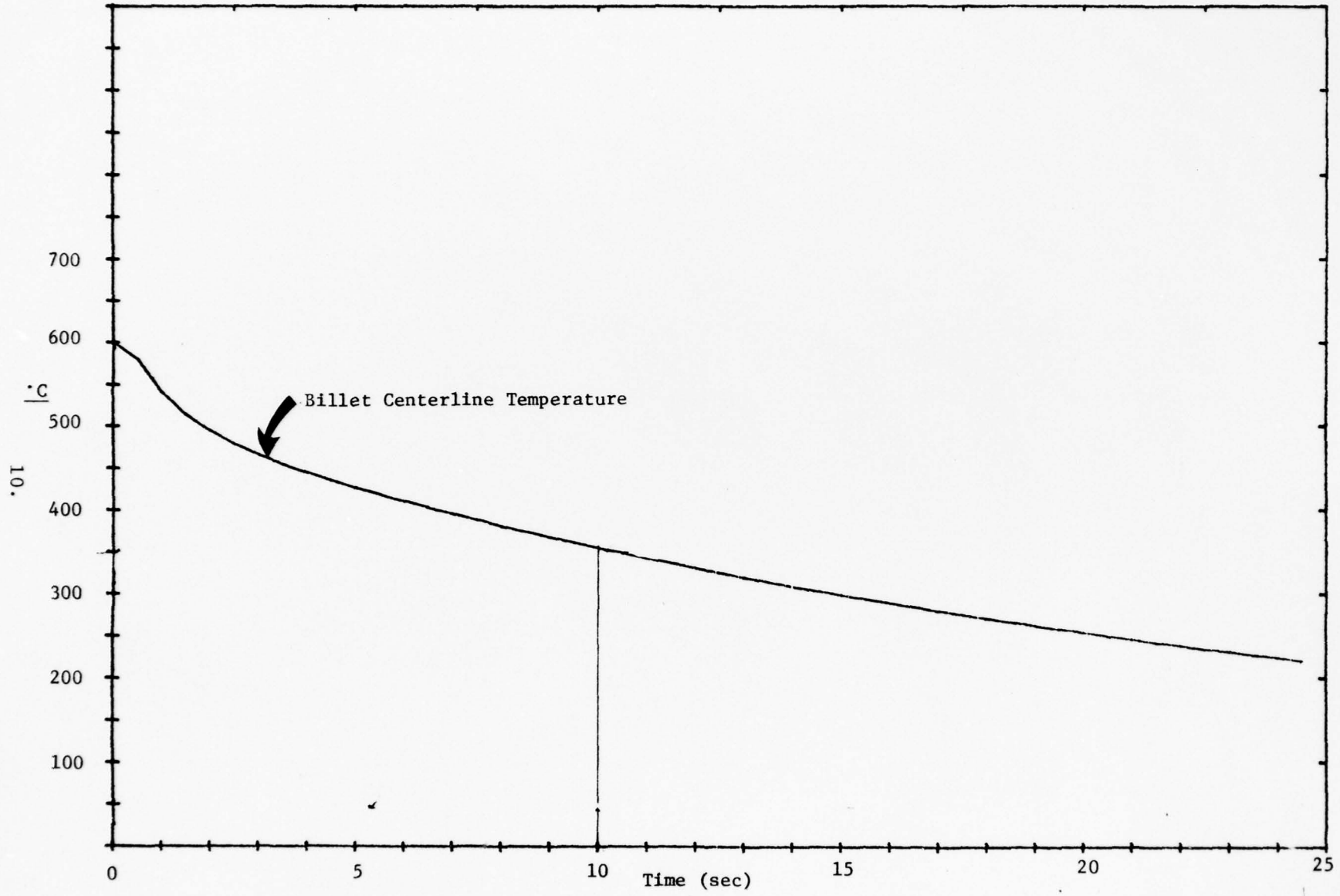

Figure 4. Computer generated results. Cooling rate for a 600 ·C extrusion billet inserted into the extrusion chamber. The graph represents the billet centerline temperature. Chamber was not preheated.

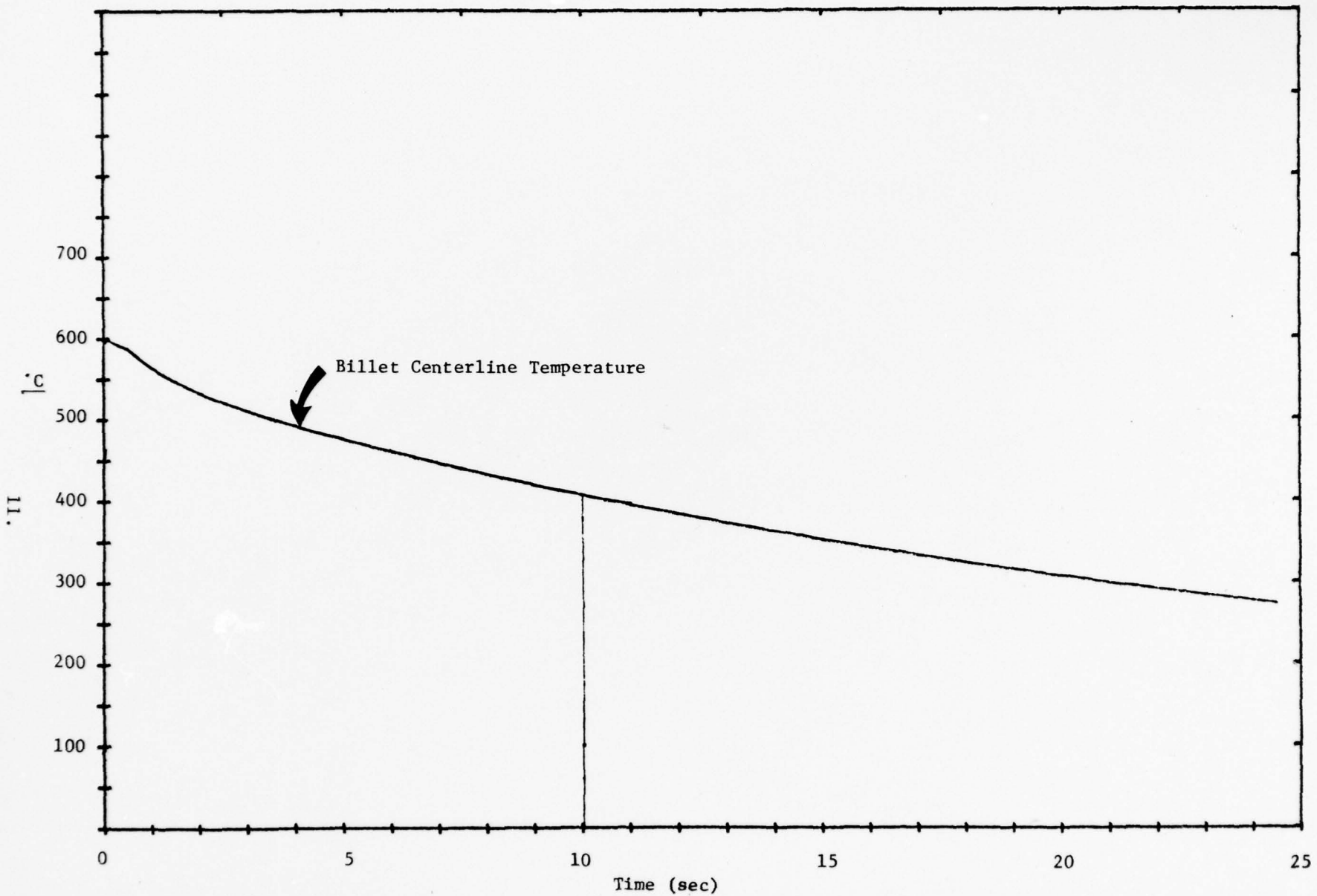

Figure 5. Computer generated results. Cooling rate for a 600 °C extrusion billet inserted into the extrusion chamber. The graph represents the billet centerline temperature. Extrusion chamber was preheated to 300 °C.

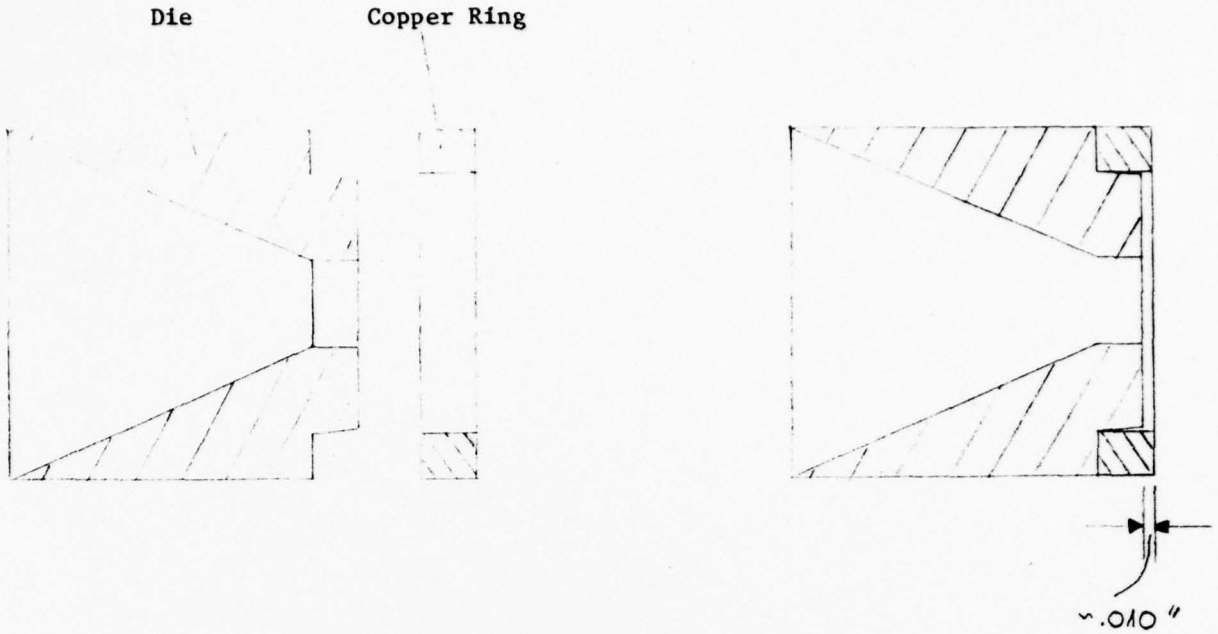

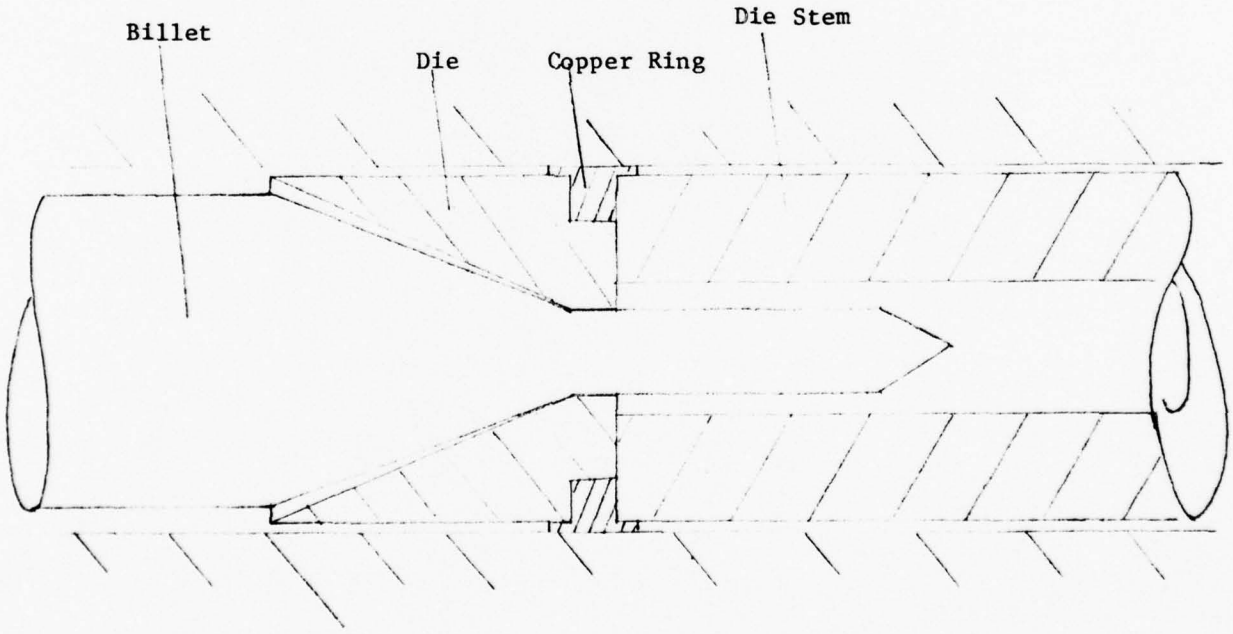

Figure 6. Modified die design.

B. HYDROSTATIC EXTRUSION OF SELECTED MATERIALS

We are presently using the hydrostatic extrusion machine to pursue several independent research directions at Stanford. Experimental work at Stanford has concentrated on the extrusion and testing of electrical conductor (EC) grade aluminum with small additions of iron (.05 W/% - 0.5 W% Fe). This work has demonstrated the capability of fabricating very strong EC grade aluminum wire. In addition to the aluminum work,we have assisted the Berkeley group, led by Professor M. R. Pickus, in their studies on the processing of A15 superconductor wire.

The remaining projects are briefly summarized to indicate the various directions of the Stanford program. Also, for the most part, these studies have only recently begun, and very little analyzed data is available to report.

(1) Electrical Conductor Grade Aluminum

Aluminum wire became a substitute for copper wire in electrical applications in about 1954. The major reason for this change was due to the high cost of copper. The low strength of electrical conductor grade aluminum, however, has been a problem ever since.

There have been extensive efforts to develop strong electrical conductor grade (EC Grade) aluminum. The electrical conductivity of aluminum is more than twice that of copper on an equal weight basis and it is also less expensive. In many applications a major disadvantage of EC grade aluminum is its low strength.

EC aluminum can be strengthened by alloying it with small amounts of highly insoluble elements which form intermetallics which do not increase the electrical conductivity as much as elements that go into solution. Strengthening can also be obtained by thermo-mechanical processing with

little effect on the conductivity of EC aluminum.

Because of the requirement of high conductivity, the alloy additions were usually limited to within one percent. As mentioned earlier solid solution alloys show lower conductivities than alloys whose alloying elements exist as precipitates. Table I shows the effect of elements on the resistivity of aluminum.

TABLE I

Element	Maximum solubility in Al, %	Average increase in resistivity per wt. %, microhm-cm In solution	Out of solution (a)
Chromium	.0.77	4.00	0.18
Copper	.5.65	0.344	0.030
Iron	.0.052	2.56	0.058
Lithium	4.0	3.31	0.68
Magnesium	.14.9	0.54 (b)	0.22(b)
Manganese	1.82	2.94	0.34
Nickel	0.05	0.81	0.061
Silicon	.1.65	1.02	0.088
Titanium	1.0	2.88	0.12
Vanadium	0.5	3.58	0.28
Zinc	82.8	0.094 (c)	0.023 (c)
Zirconium	0.28	1.74	0.044

Add above increase to the base resistivity for high-purity aluminum, 2.65 microhm-cm at 20 C (68 F) or 2.71 microhm-cm at 25 C (77 F).

(a) Limited to about twice the concentration given for the maximum solid solubility, except as noted. (b) Limited to approximately 10%. (c) Limited to approximately 20%.

Source: L. A. Willey, Alcoa Research Laboratories

TABLE I. Effect of Elements In and Out of Solid Solution on the Resistivity of Aluminum.

To take an appropriate example, iron increases the resistivity of aluminum 2.56 microhm-cm/wt % in solution but only 0.058 microhm-cm/wt % when out of solution. Therefore, alloy additions must be chosen which have a very limited solid solubility and form very stable precipitates which will not dissolve or coarsen during processing.

Once the composition has been fixed, the strength of the alloy is solely dependent upon the wire processing. Because of the high stacking fault energy, alumimum can easily develop well-defined subgrains during deformation even if the working temperature is relatively low (such as 0.3-0.4 T_m). Ball[1] and Lake[2] showed that an increase in the yield strength of polycrystalline and single cryatalline alumimum is achieved by decreasing the subgrain size. Therefore, the production of a fine and stable subgrain structure is the main concern in the processing of alumiumum electrical conductor wire. Two different processes, multi-step wire drawing and hydrostatic extrusion, have been developed to increase the strength of wire by decreasing the subgrain size[3,4]. Hydrostatic extrusion can prevent microvoids from forming, and can potentially eliminate pre-existing defects, such as pores and cracks. In addition, the ductility of the material can be increased by the high superimposed hydrostatic pressure[5]. Large amounts of cold deformation can be accomplished in a single step with hydrostatic extrusion. Reduction ratios of as high as 1000 to 1 have been successfully achieved with commerically pure alumimum.[6] But with wire drawing, large amounts of deformation can only be achieved by multi-step drawing with intermediate annealing. It has been reported that hydrostatically extruded wire has superior mechanical properties to cold-drawn wire.[7]

---

(1) C. J. Ball, The Flow Stress of Polycrystalline Aluminum, Phil. Mag., 2, 1957, p. 1011.

(2) J. S. H. Lake, Substructure Strengthening in Aluminum. Trans. of ASM, 61, 1968, p. 829.

(3) D. Kalish, Subgrain Strengthening of Aluminum Conductor Wires, Met. Trans. 6A, 1975, p. 1319.

(4) P. F. Hettwer, Alumimum Wire by Cold Hydrostatic Extrusion. Trans. of ASME, 1969, p. 822.

(5) H.L.D. Pugh, The Mechanical Behavior of Materials under Pressure, Elsevier, 1970.

(6) H. Hero and J. A. Mikkelsen, Mechanical and Structural Properties of Hydrostatically Extruded Aluminum and Aluminum Alloys, J. of Inst. of Metals, 97, 1969, p. 18.

(7) P. F. Hettwer, Alumimum Wire by Cold Hydrostatic Extrustion, Trnas. of ASME, 1969, p. 822.

The reason has been attributed to fewer microcracks and finer subgrains in the hydrostatically extruded wire. Efforts to develop continuous hydrostatic extrusion have been pursued during recent years. If and when this process is available and refined, its potential for wire production will be significant.

The initial rod condition has been demonstrated to have a significant effect on the subsequent strength-subgrain relationship in drawn wires[8]. Equivalent experiments have not been done on hydrostatically extruded aluminum. We believe that the initial rod condition; that is, the prior thermal treatment, might influence the properties of hydrostatically extruded wire. This investigation was undertaken in order to understand some of the factors which affect subgrain formation and mechanical behavior of aluminum hydrostatically extruded to large strains (i.e., greater than 100%).

8. H. Hero and J. A. Mikkelsen, Mechanical and Structural Properties of Hydrostatically Extruded Aluminum and Aluminum Alloys, J. of Inst. of Metals, 97, 1969, p. 18.

(1a) HIGH STRENGTH EC GRADE ALUMINUM WIRE
BY HYDROSTATIC EXTRUSION AT ROOM TEMPERATURE

By

Lawrence E. Eiselstein

And

Robert T. Whalen

STANFORD UNIVERSITY
STANFORD, CALIFORNIA 94305

JUNE 1977

INTRODUCTION

The strength of pure aluminum can be increased by alloying it with a small amount of iron. The maximum solubility of iron in aluminum is approximately .05% by weight (Figure 1). By solution heat treating at 640°C (1184°F) and water quenching an aluminum alloy supersaturated with iron is formed. This supersaturated alloy can then be cold worked to large strains to produce a high dislocation density. Heat treatment of this material should then cause fine subgrains to form and at the same time the excess iron in solution is forming Al_3Fe precipitates. The Al_3Fe precipitates should pin the subgrains as they form, thereby strengthening the aluminum to a greater extent than if the iron remained in solution.

Kalish and LeVevre[1,2] have produced an EC grade aluminum wire with fine subgrains by large strain deformation using a multistep wire drawing process. In the following papers we will discuss the production of fine subgrains by large strain deformation using a single step hydrostatic extrusion process. It will be shown that such a process will lead to strong EC grade aluminum wire.

EXPERIMENTAL PROCEDURE AND MATERIALS

(a) Hydrostatic extrusion is a metal working operation that consists of forcing metal through a die as in conventional extrusion but with the addition of a superimposed hydrostatic pressure. A schematic representation of metal forming with hydrostatic pressure is shown in Figure 2. A cross-sectional drawing of Stanford's hydrostatic extrusion machine is given in Figures 3 and 4 for comparison. The term hydrostatic extrusion is actually a misnomer since material under hydrostatic pressure only undergoes a volume change, i.e., no shear deformation. For material to flow through a die during extrusion, shear deformation must take place. Thus, in the region of the die, the billet is in a complex stress-strain state[3]. The basic idea behind hydrostatic extrusion is the minimization of the tensile stress component in the die region by the superposition of a high hydrostatic compressive stress. In addition a thin film of fluid is maintained between the die and billet during extrusion. This hydrodynamic lubrication results in a drastic reduction in die friction and great

uniformity of material deformation.

A quenching system was added to the hydrostatic extrusion system to quench in the as-extruded structure. In this way the strength can be maximized by "capturing" the cold worked structure that under normal conditions would have annealed from adiabatic heating. The direct mode quenching system (Figure 5) is best described as two concentric tubes leading from the die and extrusion chamber to the outside. Liquid enters the device and flows down the annular region between the two tubes to the die. At the die, holes are provided to spray the emerging extrusion with liquid. The liquid and the extrusion then exit together through the central tube. Examples of typical extrusions are shown in Figure 6.

(b) Materials and Heat Treatment

The materials examined were castings of high purity aluminum with .05%, .50%, and 1.0% iron by weight. Table I gives the chemical condition of the aluminum castings studied. Extrusion billets were machined from these cast ingots. Billet dimensions were standardized to a diameter of .725 inches with a cone angle on the front of 36° to initiate extrusion.

All the extrusion billets were solution heat treated in air at 640°C (1184°F) for 1.25 hours and immediately water quenched. These billets were then given various pre-hydrostatic extrusion anneals (Table II). The billets were then extruded to give true strains of 3.58 (about 36:1 reduction) and 4.39 (about 81 to 1 reduction). These extrusions were water quenched at the die exit.

(c) Microscopy

The microstructure of the aluminum extrusions were investigated by both optical and transmission electron microscopy. Thin foils were taken perpendicular to the wire axis and prepared by a technique developed by Rack and Cohen[4]. Final polishing was done with an electrolyte of 3 parts mechanol and one part nitric acid in an ice bath. The thin foils were then examined in a Phillips 201 microscope operated at 100 KV.

TABLE I : Chemical Composition of the Aluminum-Iron Billets

FE	Mg	Cu	BAL
.054	.004	.003	Al
.527	.001	.003	Al
1.028	.001	.004	Al

weight percent

Analysis made by

Metallurgical Laboratories
1142 Howard St.
San Francisco, Calif.

TABLE II: Wire Processing Parameters

EXTRUSION NUMBER	% FE	PRE-EXTRUSION HEAT-TREATMENT	EXTRUSION TRUE STRAIN	EXTRUSION RATIO
17	.05	None	4.41	(81:1)
18	.50	"	"	"
19	1.00	"	"	"
20	.05	"	3.52	(36:1)
21	.50	"	"	"
22	1.00	"	"	"
23	.05	200°C(392°F)/2.25 hrs.	4.41	(81:1)
24	.50	"	"	"
25	1.00	"	"	"
26	.05	310°C (590°F)/2 hrs.	3.52	(36:1)
27	.50	"	"	"
28	1.00	"	"	"

(d) Mechanical Testing

Because of the difficulties associated with the tension testing of small diameter wires, compression samples were machined with a length to diameter ratio of 3:2. This ratio is typically used to minimize the effects of barrelling and buckling.

All compression tests were performed at room temperature on an Instron machine. The initial strain rate for all tests was $\dot{\epsilon} = 1.2 \times 10^{-3} sec^{-1}$.

RESULTS AND DISCUSSION

The first billets hydrostatically extruded showed irregular variations in the wire diameter. This variation in the wire surface is caused by the phenomenon known as "stick-slip". "Stick-slip" occurs because of the difference in the static and hydrodynamic friction coefficient and can be controlled by adjusting the extrusion rate. Once this adjustment was made no other precautions were necessary to insure a good surface finish on the wire. The .725 inch (1.9 cm) billets were hydrostatically extruded as machined at various reductions and the resulting wire showed consistently good, defect-free surface finishes (Fig. 7).

The influence of subgrain size on the room temperature yield strength of EC grade alumimum is illustrated in Figure 8. The data are from Kalish and LeFevre (2). The subgrain sizes were obtained from a multi-step wire drawing process. On the same graph we show the yield strength of hydrostatically extruded high purity aluminum containing .05, 0.5 and 1.0% iron. The compression strengths are high and considerably above those obtained for EC grade aluminum by the wire drawing process.

Annealing studies on hydrostatically extruded high purity aluminum containing 0.5% Fe reveal that this material exhibits strength stability over a wide range of temperatures. Figure 9 illustrates that annealing for 2.25 hours at 200°C led to no significant softening. The wire drawn aluminum alloy studies by Kalish and

LeFevre (drawn to $\varepsilon = 3.19$) exhibited recovery effects after 1 hour at 150°C even though this wire is more highly alloyed and annealed for shorter times than the hydrostatically extruded wire. Extrapolation of the above results suggests that material extruded at ratios greater than 81:1 may be expected to be stronger and more thermally stable than those shown in Figure 9.

The room temperature true stress versus true strain diagram for a hydrostatically extruded and heat treated wire of aluminum with .5% iron is shown in Figure 10. This material was solution annealed at 640°C (1184°F) for 1.25 hours then given a pre-extrusion anneal of 200°C (392°F) for 2.25 hours and was then hydrostatically extruded at an extrusion ration of 81:1. Compression samples were then machined from this wire with an initial diameter of .080 inches (2 mm) and initial high of .120 inches (3 mm). The compression sample was given a heat treatment of 200°C (392°F) for 2.25 hours just before testing. This material showed some strain softening and a .2% flow stress of over 30 ksi (207 MPa). This material is considerably stronger than the EC grade aluminum wire made by the multi-step wire drawing process. The highest .2% flow stress achieved by the multi-step process was not over 25 ksi (172 MPa) (2). This shows that through hydrostatic extrusion and heat treatment the strength of EC grade aluminum can be raised to over 30 ksi (207 MPa).

The effect of pre-extrusion anneals (Figs 11a,b,c) and the effect of the extrusion ratios (Figs 12a,b,c) on the annealing behavior of all three aluminum-iron alloys were investigated. From this data a number of conclusions can be drawn. The most obvious conclusion is that the yield strength increases as the iron content and extrusion ratio increases. To illustrate this effect one can look at high purity annealed aluminum and hydrostatically extruded aluminum with

.05% iron. The yield strength of high purity annealed aluminum is below 4 ksi (27.6 MPa). However, by the addition of .05% iron, hydrostatically extruding to large strains, and proper heat treatment, yield strengths of 27 ksi (186 MPa) can be obtained. Small iron additions, hydrostatic extrusion, and thermal treatments are a very effective strengthening process for high purity aluminum.

A comparison with the wire drawn aluminum alloy (Al - .7 Fe - .15 Mg) again shows that all extrusions to 81:1 reductions of the .5% and 1% iron compositions exhibited equal or superior yield strength. All the tests again showed more resistance to recovery (softening) with increasing annealing temperatures than the wire drawn material.

Most of the annealing diagrams also showed a slight increase in the yield strength at an annealing temperature of 200°C (392°F). It is believed that this increase in yield strength could come from the formation of subgrains.

An investigation of the structure of these wires by transmission electron microscopy showed small, well defined subgrains. Very few fine Al_3Fe precipitates were found pinning subgrains. Figure 13 shows a typical substructure. The lack of small precipitates was surprising and further transmission electron microscopy is planned to detail the nature, distribution and morphology of the subgrains and the precipitate particles in the hydrostatically extruded aluminum-iron alloys.

SUMMARY AND CONCLUSIONS

The major purpose of this investigation was to show that high strength EC grade aluminum wire could be developed. To achieve this goal hydrostatic extrusion was used. Hydrostatic extrusion provided a method of cold working aluminum to large strains in a single operation and the wire that results is relatively defect-free.

This research has shown that the development of EC grade aluminum wire with yield strengths in excess of 30 ksi (207 MPa) is easily attainable and this material is more resistant to thermal softening than the conventional wire drawn EC wire.

REFERENCES

1. D. Kalish and B. G. LeFevre, Met. Trans. 6A, 1975, 1319.
2. D. Kalish, B. G. LeFevre, and S. K. Varma, Met. Trans. 8A, 1977, 204.
3. O. D. Sherby , J. C. Shyne, and E. H. Lee, Report No. SU-DMS 75-T-32, Department of Materials Science and Engineering, Stanford University, Stanford, California 1975.
4. H. J. Rack and M. Cohen, Met. Trans. Vol. 1, 1970, 1050.

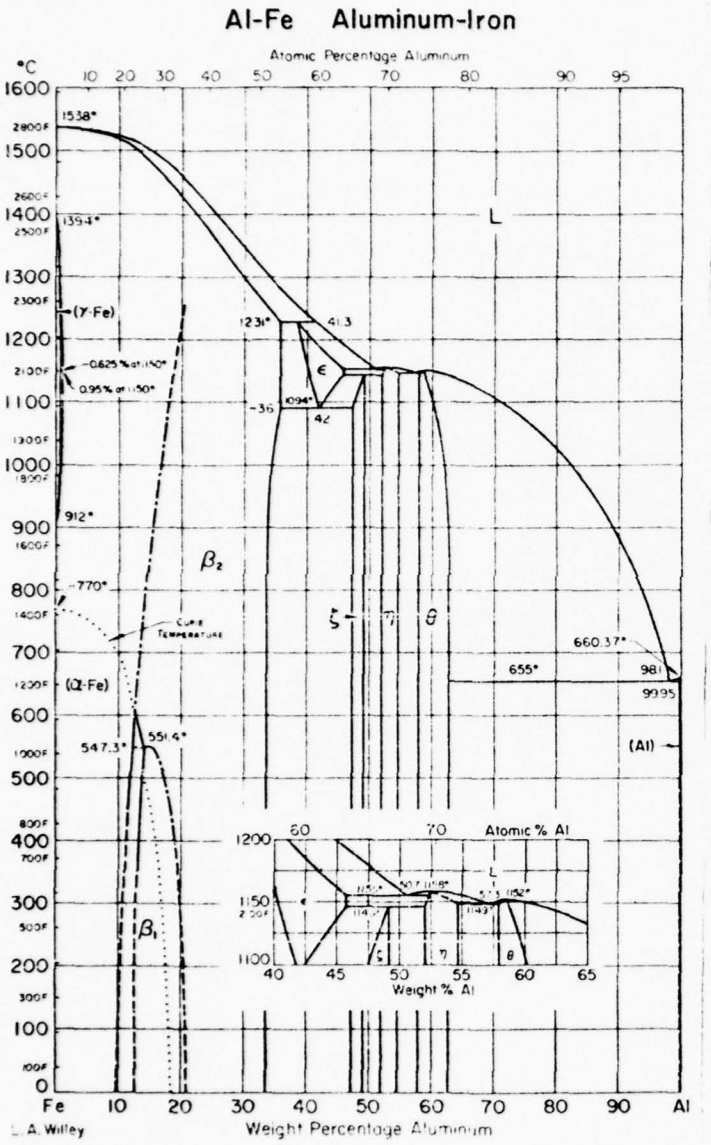

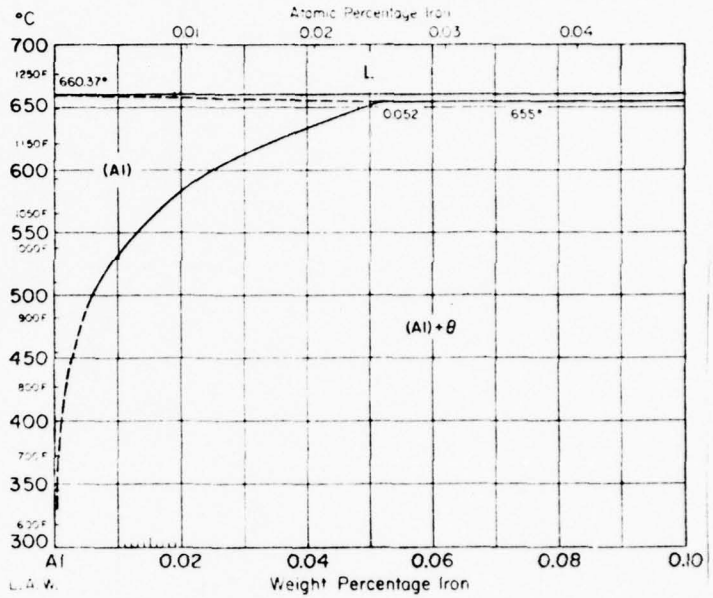

Figure 1 Aluminum-Iron Phase Diagram

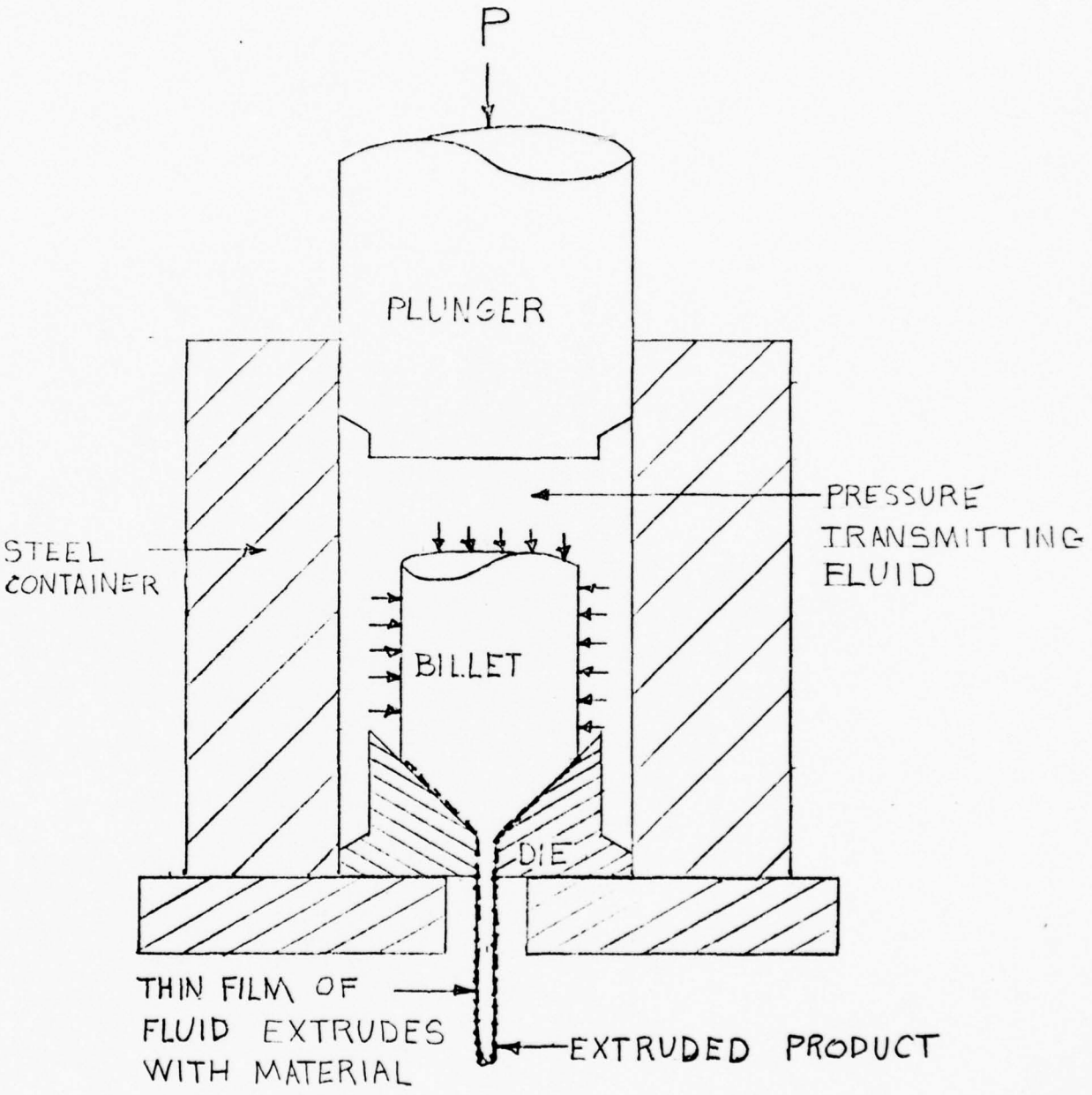

Figure 2: Schematic Representation of Hydrostatic Extrusion

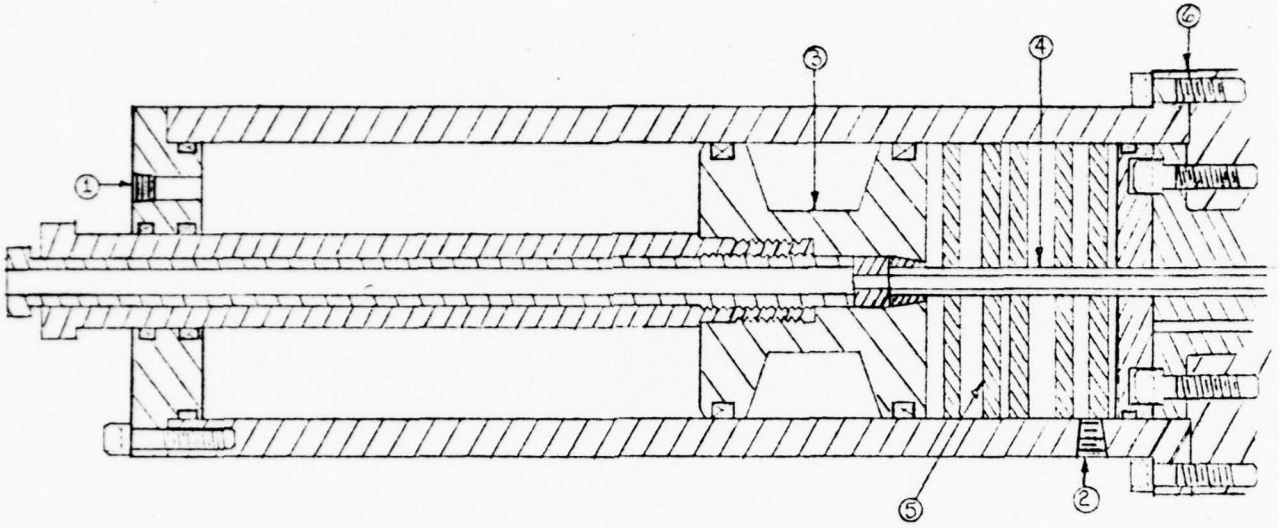

Figure 3. Cross sectional drawing of extrusion piston, die stem and die stem guides. (1) Hydraulic port--extruding (2) Hydraulic port--retracting (3) Piston (4) Die stem (5) Die stem guide, and (6) Beginning of extrusion load chamber.

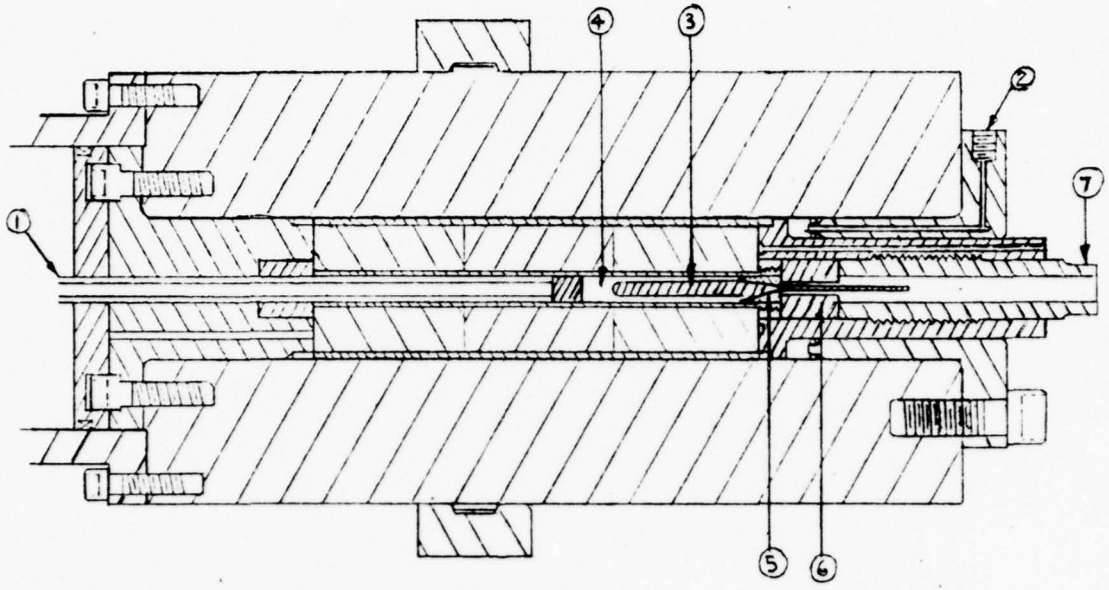

Figure 4. Cross sectional drawing of high pressure extrusion cylinder. (1) Die stem (2) Pressure intensifier inlet (60 KSI) (3) Billet (4) Castor oil (5) Die (6) Tungsten carbide anvil, and (7) Breech plug.

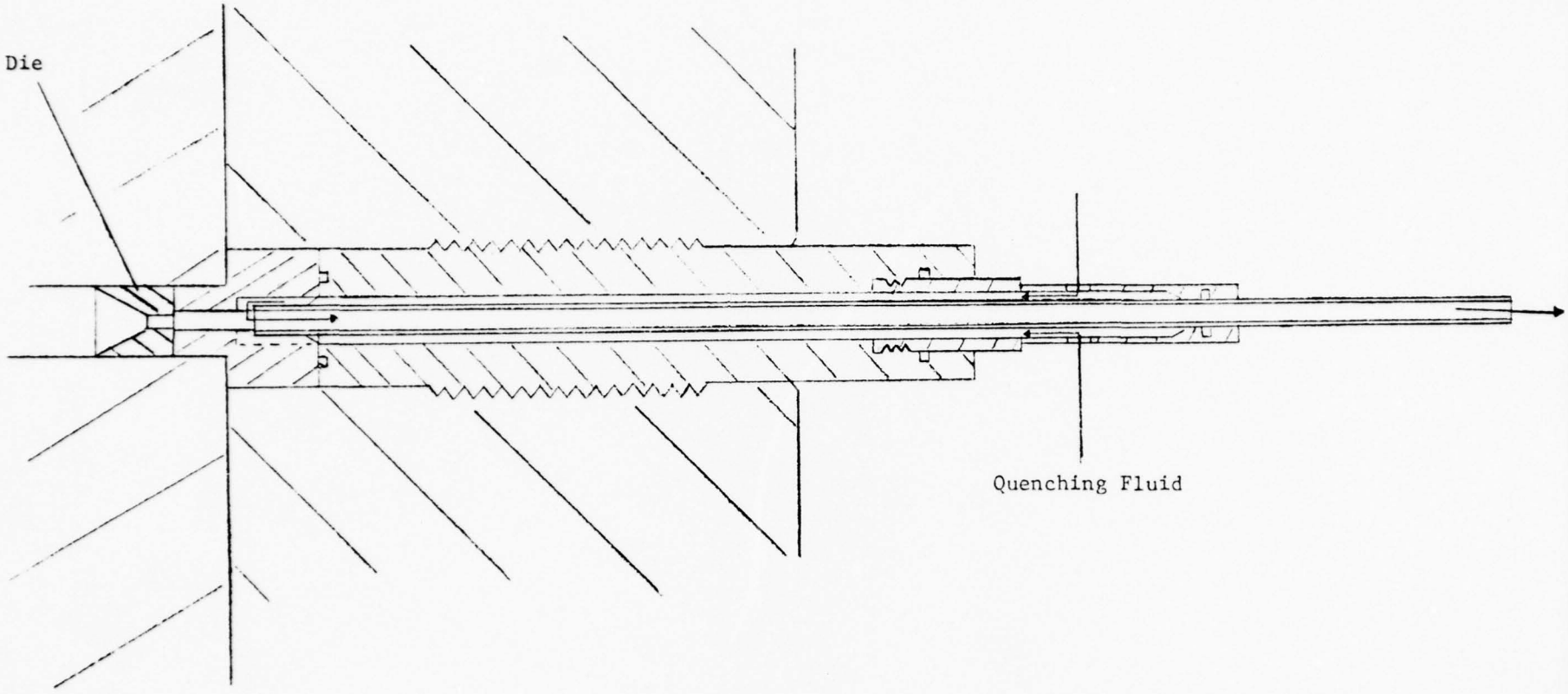

Figure 5. Quenching system for direct extrusion mode. Extruded billet and fluid exit through center tube.

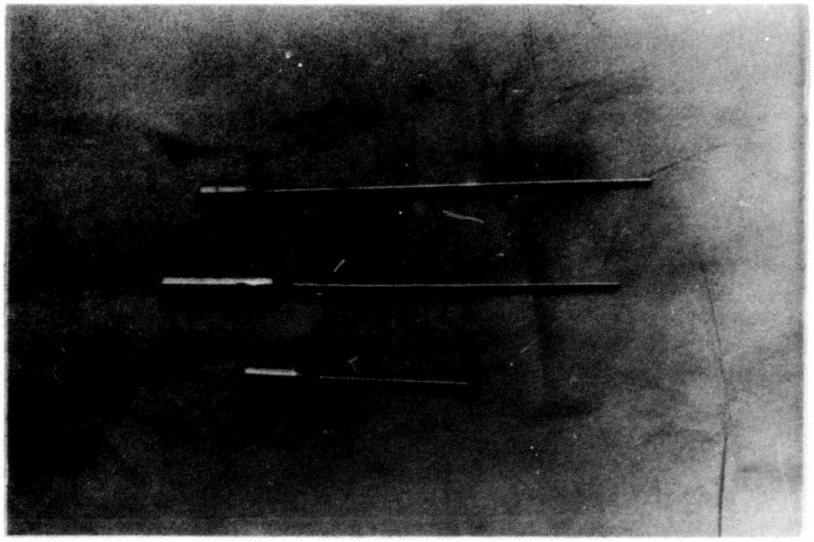

Figure 6. Sample aluminum extrusions. Initial billet diameter was .750". Listing from top to bottom, the exytusion ratios are 16:1, 25:1, 36:1.

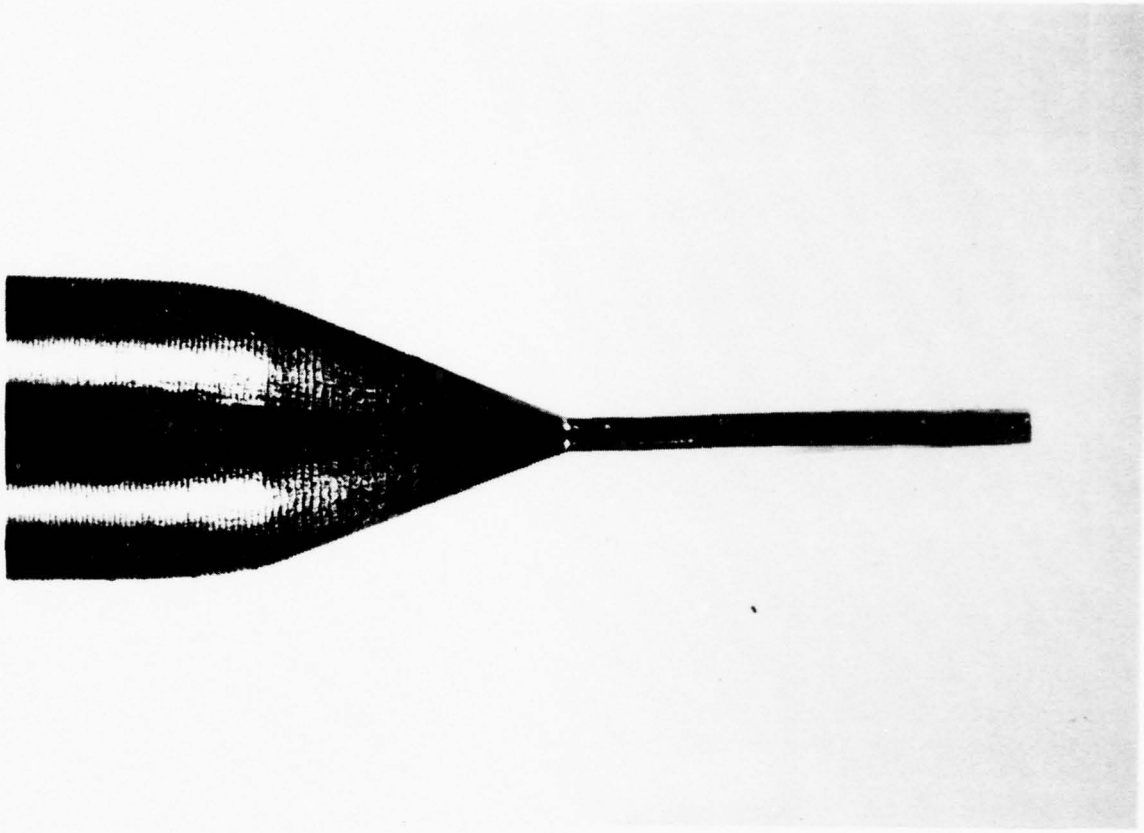

Figure 7. Surface finish on hydrostatically extruded billet. Extrusion ratio of 81:1.

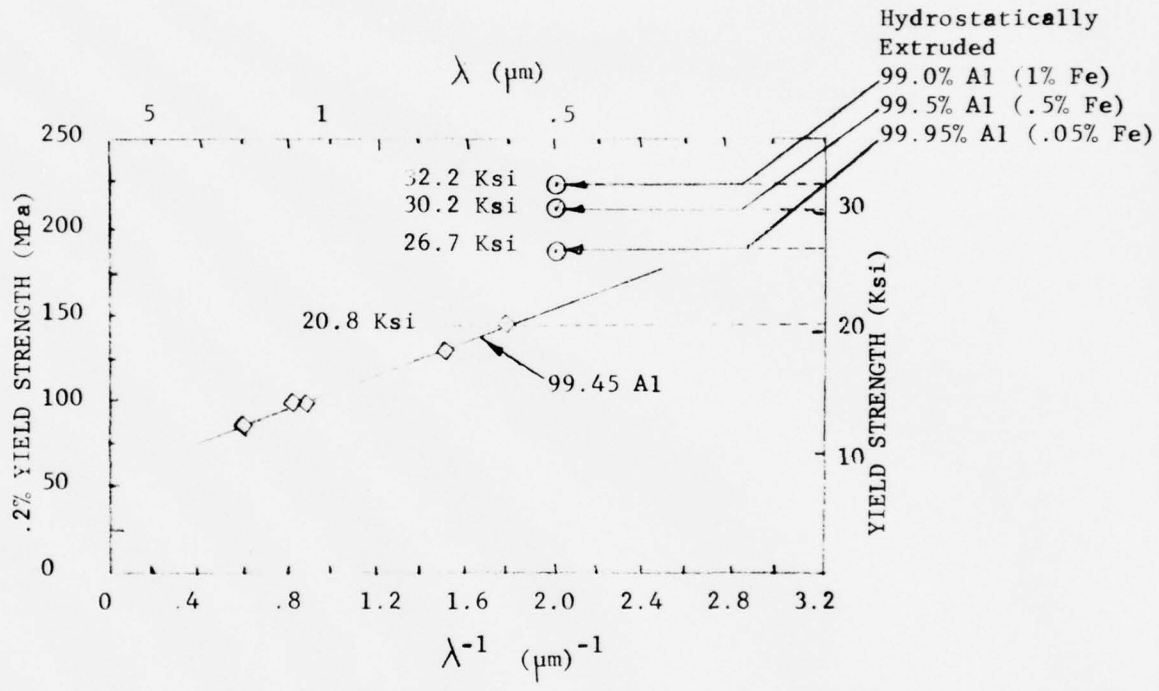

Figure 8. The effect of subgrain size on the room temperature yield strength of EC grade aluminum.

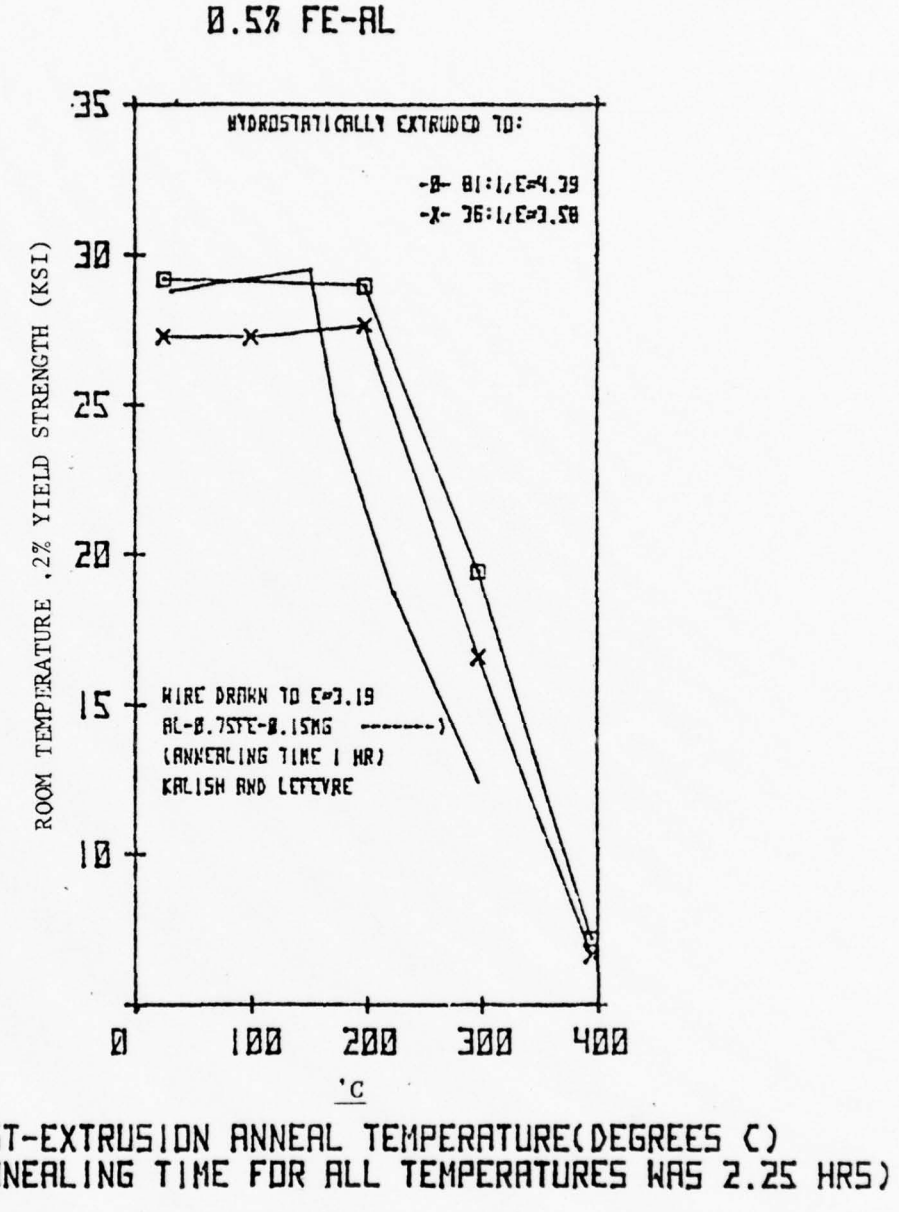

Figure 9. Annealing study on hydrostatically extruded high purity aluminum containing .5% iron.

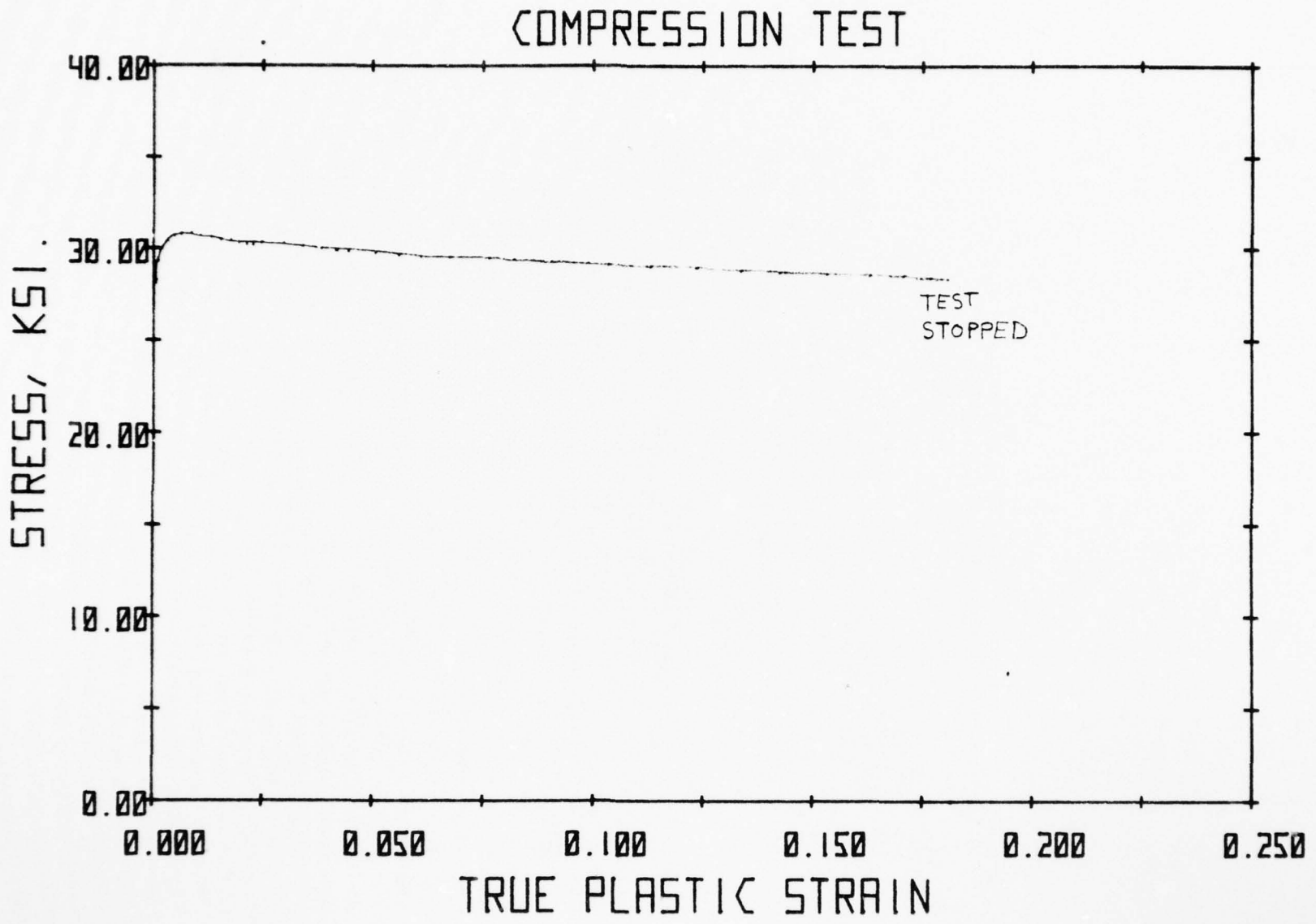

Figure 10. Room temperature true stress-true strain diagram for a hydrostatically extruded and heat treated wire of aluminum with .5% iron. Solution annealed at 640°C/1.25 hr. Pre-extrusion annealed at 200°C/hr. Extrusion ratio of 81:1. Pre-testing anneal of 200°C/2.25 hr. Tested at an initial strain rate of $\dot{\varepsilon} = 1.2 \times 10^{-3}$ sec^{-1}.

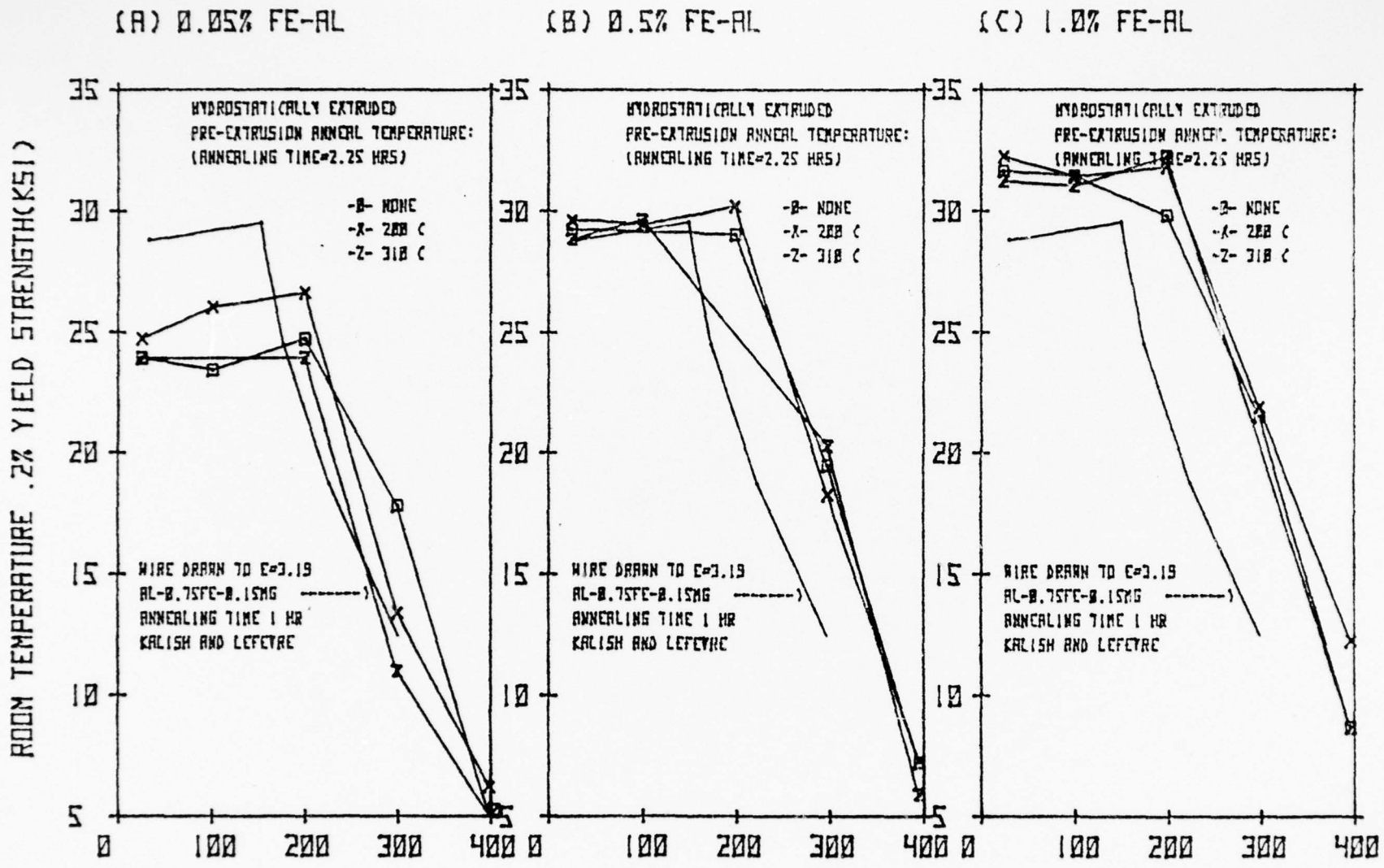

FIGURE 11 A/B/C: THE EFFECT OF PRE-EXTRUSION AND POST-EXTRUSION ANNEALING ON THE YIELD STRENGTH OF THREE COMPOSITIONS OF FE-AL. THE EXTRUSION RATIO WAS 81:1, OR E=4.39.

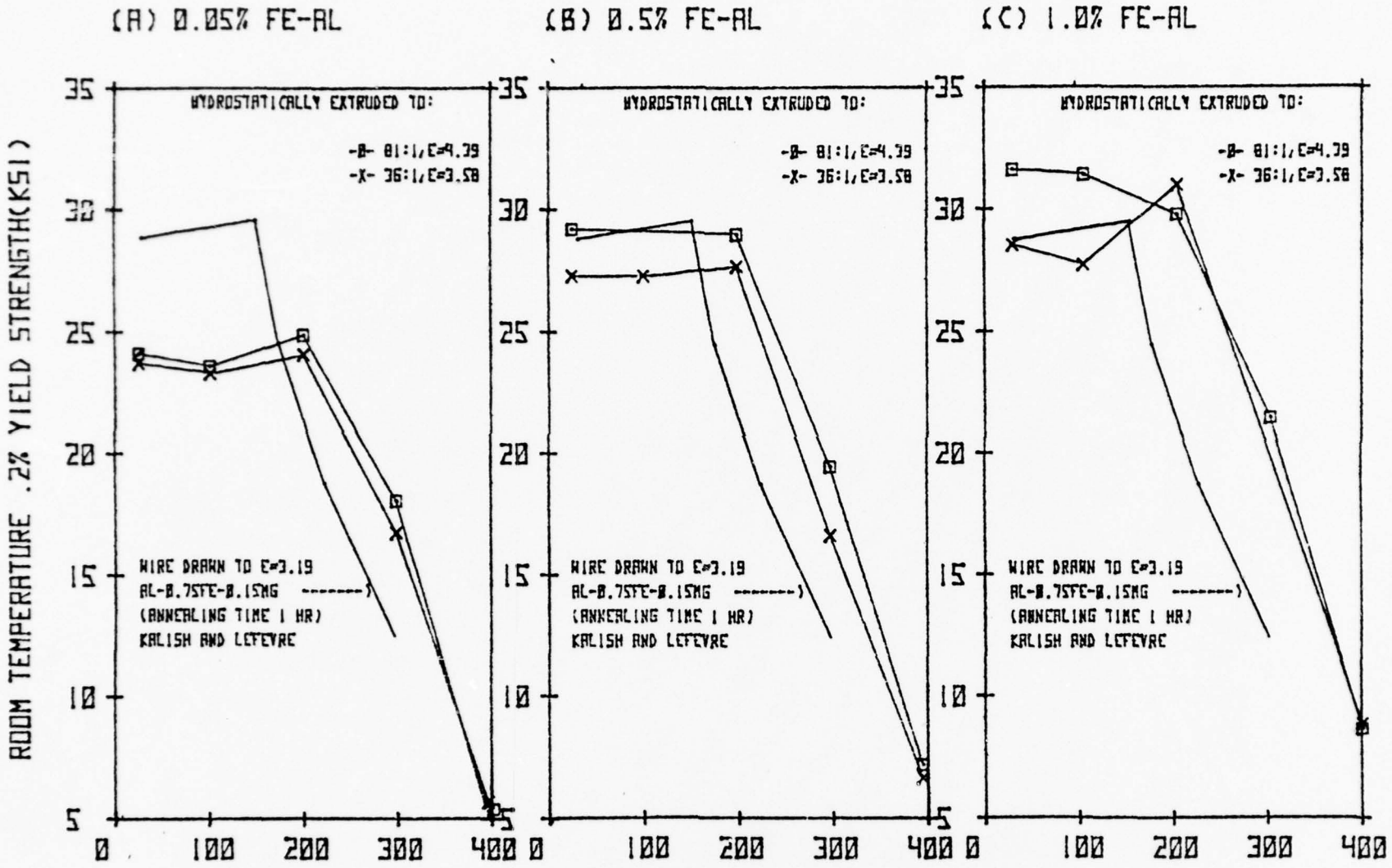

FIGURE 12 A/B/C: THE EFFECT OF EXTRUSION RATIO AND POST-EXTRUSION ANNEALING ON THE ROOM TEMPERATURE YIELD STRENGTH OF THREE COMPOSITIONS OF FE-AL. NO PRE-EXTRUSION ANNEAL WAS DONE.

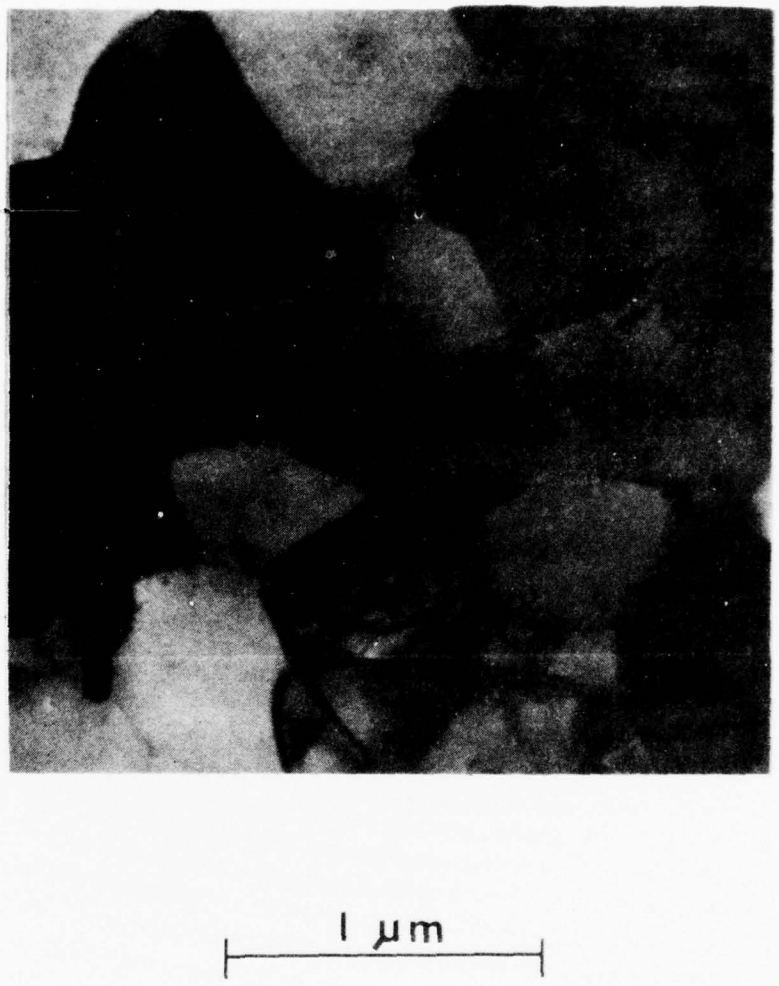

Figure 13. Typical subgrain structure of aluminum - .5% iron hydrostatically extruded to an extrusion ratio of 36:1.

(1b)

INFLUENCE OF THERMAL HISTORY ON THE PROPERTIES OF HYDROSTATICALLY EXTRUDED Al-Fe ALLOYS

By

Li-Lien Lee

Graduate Research Assistant
Department of Materials Science and Engineering

STANFORD UNIVERSITY
STANFORD, CALIFORNIA 94305

December, 1977

The following research work was done by Li-Lien Lee as partial fulfillment for the degree of Engineer at Stanford University. Our earlier work had suggested that super-saturating an aluminum matrix with iron would lead to high strengths. Further, it was assumed that the higher strengths were the result of finer stabilized subgrains. However, the precise interaction mechanism between the iron and aluminum was unclear. This paper is an attempt to clarify these points.

ABSTRACT

Aluminum alloys with 0.5 wt % and 0.05 wt % Fe have been hydrostatically extruded with a reduction in area of 81 to 1. Two difference types of heat treatment were employed. One group of samples were solution treated at 640°C then water quenched and a second group was furnace cooled after solution treating at 640°C. Both heat treatments were performed before extrusion. It was found that the excessive amount of iron in the solution treated and quenched samples helped develop fine subgrain structures during hydrostatic extrusion. The superior wire obtained from solution treatment and quenching was also found to be more thermally stable in subsequent annealing studies.

ACKNOWLEDGEMENTS

The author is particularly grateful for the invaluable guidance provided by his advisor, Professor O. D. Sherby, during every phase of this investigation.

The author would like to express his special appreciation to Robert Whalen, Larry Eiselstein for their contributions to this investigation. In addition the author would also like to express his gratitude to S. G. Roberts at Kaiser Aluminum in Pleasanton, California for his help in conductivity measurements.

INTRODUCTION

Aluminum wire became a substitute for copper wire in electrical applications in about 1954. The major reason for this change was due to the high cost of copper. The low strength of electrical conductor grade aluminum, however, has been a problem ever since.

High strength aluminum conductors have been developed through alloying or through mechanical working. Because of the requirement of high conductivity, the alloy additions were usually limited to within one percent. In addition, whether or not the alloying elements are in solution must be taken into consideration. Solid solution alloys usually show lower conductivities than alloys whose alloying elements exist as precipitates. For example, iron increases the resistivity of aluminum 2.56 microhm -cm/wt % in solution but only 0.058 microhm-cm/ wt % when out of solution (1). Alloying additions, therefore, must be chosen which have a very limited solit solubility and form very stable precipitates which will not dissolve during processing.

Once the composition has been fixed, the strength of the alloy is solely dependent upon the wire processing. Because of the high stacking fault energy, aluminum can easily develop well-defined subgrains during deformation even if the working temperature is relatively low (such as 0.3 - 0.4 T_m). That an increase in the yield strength of polycrystalline and single crystalline aluminum may be achieved by decreasing the subgrain size has been shown experimentally by Ball (2), Lake (3) and others (4-8). Therefore, the production of a fine and stable subgrain structure as a means of strengthening is a main product of wire processing of aluminum conductors. Two different processes, multi-step wire drawing and hydrostatic extrusion have been used to increase the strength successfully by

decreasing the subgrain size (7,9). Hydrostatic extrusion can prevent microvoids from forming and eliminate defects such as pores and cracks that are already in existence. In addition, the ductility of the material can be increased by the high pressurized environment (10). Large amounts of cold deformation can be accomplished by hydrostatic extrusion within one single step. Reduction ratios of as high as 1000 to 1 have been successfully achieved with commercially pure aluminum (11). But, in wire drawing, large amounts of deformation can only be achieved by multi-step drawing and intermediate annealing is sometimes required. It has been reported that hydrostatically extruded wire has superior mechanical properties to cold-drawn wire (9,11). The reason has been attributed to fewer microcracks and finer subgrains in hydrostatically extruded wire. Although hydrostatic extrusion has been known for years, there are still very few commercial installations. This is probably due to: (1) The uncertainty in safety and reliability of such equipment, (2) the relatively large investment of funds required for installation, and (3) the capacity of material is limited by the size of the pressure chamber. Efforts to develop continuous hydrostatic extrusion have been pursued during recent years. If this process is available, its potential for wire processing may be significant.

The initial rod condition has been demonstrated to have a fignificant effect on the subsequent strength-subgrain relationship in drawn wires (11). Equivalent experiments have not been done on hydrostatically extruded aluminum. We believed that the initial rod condition, that is, the prior thermal treatment, might influence the properties of hydrostatically extruded wire. This investigation was undertaken in order to understand some of the thermal-mechanical processing factors which affect subgrain formation and

mechanical behavior of hydrostatically extruded aluminum with a high reduction in cross sectional area.

MATERIALS AND EXPERIMENTAL PROCEDURES

The materials used for this study were supplied by Aluminum Company of America as cast ingots. The chemical compositions in wt% are tabulated as follows:

Table 1

The compositions of the Al-Fe alloys employed in this study

Alloy designation	Fe	Mg	Cu	Al
0.5%Fe-Al	0.527	0.001	0.003	Balance
0.05%Fe-Al	0.054	0.004	0.003	Balance

Three quarter inch (19mm) diameter extrusion billets were machined and heat treated in the following ways:

A: Heat to 640°C for 1.5 hrs., then quench in water

B: Heat to 640°C for 1.5 hrs., furnace cool to 500°C. Anneal for 12 hrs at 500°C, then furnace cool to room temperature.

We felt that thermal treatment A would put as much iron in solution as possible and thermal treatment B would do the opposite, that is, the iron would be mostly in precipitate form. It was noted that a smooth finish in machining the billets was unnecessary. Billets with smooth surfaces require higher extrusion pressures than similar billets with rough surfaces. This effect is due to the mechanism involved in setting up a full-fluid film lubricant condition. According to the mechanism (13), the lubricant does not flow freely between the die and billet, but is carried into the die by the billets. The billets machining marks may be carried through the product. Nevertheless the surface finishes of

extruded wires still compared favorably with drawn wires.

After heat treatment, an 1/8 inch (0.317mm) thick disk sample was cut from each billet. The resistivity of these disks were measured by eddy current measurement. Knowing the resistivity, ρ, the amount of iron in solution can be calculated as follows (1):

$$\rho = 2.71 + 2.56 \cdot X + 0.058 \cdot (X_o - X)$$

where X is the amount of iron in solution, X_o is the total iron content, 2.56 (microhm - cm) is the average increase in resistivity per wt% of iron in solution, 0.058 (microhm - cm) is the average increase in resistivity per wt% of iron out of solution, and 2.71 (microhm - cm) is the resistivity of high purity aluminum at 25°C.

All the billets were extruded with the same area of reduction, 81:1, with the Stanford Hydrostatic Extrusion press. A device was used to water quench the wire at the die opening in an effort to maintain the hydrostatically worked structure. The extrusions were conducted in such a way that the wire was still connected to the undeformed portion of the billet after hydrostatic extursion. By doing this, the metallographic work was made much easier.

Compression specimens with a height to diameter ratio of 1.5 were machined from the extruded wires. Room temperature compression tests were carried out using an Instron machine with an initial strain rate of 0.016 min^{-1}. A few tension specimens were prepared from extruded wires in order to get some idea of the tensile properties, such as percent of elongation and reduction of area, and to compare the yield strengths with those determined from the compression tests. We had a hard time making a successful tension test at the beginning, because we were trying to prepare it mechanically. Eventually this difficulty was eliminated by using a cylindrical cathode to

electropolish the gage portion of the tension specimens. Room Temperature tensile tests were carried out with an Instron machine using a initial strain rate 0.01 min^{-1}. Annealing studies on the hydrostatically extruded wires were performed at a series of different temperatures, from 125°C to 325°C, for two and one half hours. The annealed samples were compression tested to determine the thermal stability of the extruded materials.

Lateral sections of the end of wires, as shown in Figure 1, were prepared for optical microscopy. The specimens were electropolished at 80°C, 17 volts in a solution of 100 ml distilled water, 160 gm chromium trioxide, 820 ml phosphoric acid and 135 ml sulfuric acid. They were then anodized at room temperature in a solution of 5% fluoboric acid and 95% distilled water. An optical microscope with polarizer attachment was used for metallography study.

Transmission electron microscopy (TEM) studies were conducted on a Phillips EM 200 electron microscope. Thin films were prepared as follows. The hydrostatically extruded wires were sawed into 0.4 mm discs. They were then ground on emery paper to about 0.15 mm thick discs and were then electrothinned in a double jet polishing unit at -30°C, 17 volts in a solution of 3 parts methanol and 1 part nitric acid. TEM was used with a high tension of 100 KV in examining all of the specimens.

RESULTS AND DISCUSSION

The results of the conductivity measurements are shown in Table 2. The resistivity ρ (microhm - cm) = 172.41/% IACS. By knowing the total iron content, the percent of iron in solution can be calculated by the method previously described. These results are also tabulated in Table 2.

Table 2

Conductivity and wt% of iron in solution before extrusion

Material designation	heat treatment	conductivity % IACS	resistivity microhm-cm	calculated wt% iron in solution	microprobe analysis
0.5%Fe-Al	640°C→W.Q.	59.5	2.89	0.0628	~.05
0.5%Fe-Al	640, FC→500°C 500°C, FC→RT	61.4	2.81	0.0269	~.02
0.05%Fe-Al	640°C→W.Q.	61.4	2.81	0.0379	
0.05%Fe-Al	640, FC→500°C 500°C, FC→RT	61.5	2.80	0.0361	

It is known that the maximum solubility for Fe in Al is 0.052 wt% (14). From our calculated values one percentage was as high as 0.0628 wt%. The reason for this was probably due to neglecting the contribution to electrical resistivity of the other solute atoms present. Therefore, the calculated values in Table 2 can be taken only as a first order approximation. Still, it is likely that a high superaturation of iron was obtained in the water quenched samples as we expected.

The true stress-true plastic strain curves obtained from compression tests for the extruded wires are shown in Figures 2 and 3. They are plotted by assuming that the samples were uniformly deformed during compression test. This was true for all our compression tests. It was found that the heat

treatment before extursion strongly influenced the strength of the extruded wire for the 0.5% Fe-Al material (Figure 2), but was not a minor factor for the case of the 0.05% Fe-Al material (Figure 3). The difference in strength noted from heat treatment appears to be due to the amount of supersaturated iron. For the 0.5% Fe-Al material, when we double the amount of iron in solution before extrusion the strength of the extruded wire was increased by 60% (Figure 2). For the 0.05% Fe-Al material, we were able to change the amount of iron in solution only slightly and the strengths of the extruded wires in this case were almost exactly the same (Figure 3). In order to check our conjecture about the supersaturated iron, one more 0.5% Fe-Al wire was extruded. The heat treatment before extrusion was 640°C for 1.5 hrs, then furnace cooled to room temperature. Such a treatment should retain more iron in solution than the sample which was isothermal annealed at 500°C then furnace cooled but should contain less iron in solution than the solution treated and quenched sample. The third heat treatment lead to a compression stress-strain curve which falls in between the previous two curves, as expected (Figure 2).

Figure 4 summarizes the results of the annealing studies. In this figure the room temperature yield strength (0.2% offset) is plotted as a function of annealing temperature. The compression test curves for constructing Figure 4 are given in the Appendix. The data in Figure 4 show that all the different strength wires were fully recrystallized when annealed at 325°C for 2.5 hrs. The results show that the pre-extrusion solution treatment not only raised the strength of the extruded wire but also increased the resistance to thermal softening. We believe that the dissolved iron can aid in substructure stabilization since the iron solute atoms can hinder subgrain growth and boundary migration by pinning the dislocation

boundaries as Cottrell atmospheres. It is also possible that iron in solution may lower the stacking fault energy of aluminum, which in turn, may inhibit cross slip as well as decrease the climb rate (8). Even when the annealing temperature is as high as 225°C, our strongest wire didn't show any softening at all. It was noted that the weakest wire has the least amount of iron in solution before extrusion. All the curves in Figure 4 show a slight increase in strength from low temperature annealing. Possible reasons for this effect may be attributed to the effect of strain aging or to an increase in subgrain boundary perfection.

Since most of the stress-strain curves of the compression tests show a negative slope (that is, strain softening) in the plastic region, tensile instability should occur at small strains in a tension test. The results of room temperature tensile tests on hydrostatically extruded 0.5%-Al are shown in Figure 5. Both curves in Figure 5 showed that the specimens started to neck just as soon as yielding took place. This is consistent with the negative strain hardening exponent of the previous compression tests. Therefore, although the hydrostatically extruded wire exhibited ductile fracture with reduction in area greater than 80%, the tensile elongation was less than 5% in the 1 inch gage length samples tested. The yield strengths obtained from the tensile tests were fairly close to those obtained in the compression tests, suggesting that the extruded material may have a relatively isotropic structure.

Figures 6 to 21 are the results of optical microscopy. Because of the different thickness of the anodized film, adjacent grains showed a difference in color under polarized light. The grain size before extrusion was large, varying from 0.4 mm to 3 mm, for all our billets. No difference between samples of different pre-extrusion heat treatment could be observed optically

for a given total iron content. The polarized light photomicrographs taken after hydrostatic extrusion give a hint that the elongated grains may have broken up into small grains (Figure 9). The Al_3Fe precipitates are segregated at the interdendritic regions before extrusion and distributed homogeneously after extrusion. This difference can be readily seen from the micrographas taken without polarized light (for example, see Figures 10 and 11).

Figures 22 and 25 show electon micrographs of the as-extruded wires from the TEM studies. The type of substructure noted are summarized in Table 3.

Table 3

Summary of TEM studies on hydrostatically extruded Al-Fe alloys

material designation	pre-extrusion heat treatment	TEM observations
Al-0.5%Fe	640°C→W.Q.	Uniform subgrain size λ = 0.5 micron (dislocation present in 10% of the subgrains)
Al-0.5%Fe	640°C, FC→500°C 500°C, FC→RT	mixed subgrain structure 35% coarse, λ = 2 micron (dislocation free in all subgrains) 65% fine, λ = 0.75 micron (dislocation present in 10% of the subgrains)
Al-0.05%FE	640°C→W.Q.	uniform subgrain size λ = 0.65 micron (dislocation present in 10% of the subgrains)
Al-0.05%Fe	640°C, FC→500°C 500°C, FC→RT	uniform subgrain size λ = 0.65 micron (dislocation present in 10% of the subgrains)

It was found that the strongest wire has the smallest subgrain size and

the weakest wire has the largest subgrain size. The existence of coarse subgrains in the weakest wire was probably due to the ease of dynamic recovery during the extrusion process. Sherby, Klundt and Miller (15) have proposed that the subgrain size at a given σ/E decreases with decreasing stacking fault energy. If the stacking fault energy is decreased by the presence of excessive iron in solution, then the subgrain size may decrease by this effect. This may be one explanation. Another contribution to subgrain size refinement may arise from the precipitation of Al_3Fe during the extrusion process. The most likely factor controlling the subgrain size during hydrostatic extrusion, however, is likely associated with the amount of iron present in supersaturated solution in aluminum. For 0.05% Fe-Al material, both heat treatments showed almost the same amount of dissolved iron, and the same size of subgrains developed in both cases. The 0.5% Fe-Al material, solution treated at 640°C then isothermal annealed at 500°C and furnace cooled, precipitated more iron out of solution than the 0.05% Fe-Al material thermally treated in the same way (Table 2). This is possibly due to the greater amount of eutectic Al_3Fe present in the 0.5% Fe-Al material which may have acted as nucleation sites for the iron solute atoms. The small amount of iron in solution for the slowly cooled 0.5% Fe-Al material, we believe, lead to the coarse subgrain size observed.

Adiabatic heating during hydrostatic extrusion process could cause the iron atoms to move to preferential sites for precipitation, which in turn, would pin the dislocations at subgrain boundaries. The distance of diffusion, X, for Fe in Al can be calculated if the temperature from adiabatic heating is known and the time at temperature is known. The increase in temperature due to adiabatic heating is calculated as follows:

$$\Delta W \cong \sigma \cdot \varepsilon = C_p \cdot \Delta T$$

where ΔW is the work done during hydrostatic extrusion, σ is the flow stress, ε is the total strain during extrusion ($\varepsilon = 4.4$ for a 81:1 reduction), C_p is the specific heat (0.215cal/gm-°C for pure Al (16)), and ΔT is the temperature change. The flow stress during extrusion, σ, is not known but a reasonable assumption might be 25 ksi (the yield strength of the hydrostatically extruded material). Substituting the proper conversion factors ΔT can be readily calculated, and was determined to be $\Delta T \cong 313°C$. Therefore the temperature, T, at the die exit is about 610°K.

The distance of iron solute atom diffusion in aluminum is now readily calculated from the following relation(17).

$$X = 2\sqrt{Dt}$$

where t is the diffusion time and D is the diffusion coefficient of Fe in Al (18) given as $D_{\text{Fe in Al}} = 4.1 \times 10^{-9} \exp\left(\frac{-13900 \text{ cal/mole}}{RT}\right) \text{cm}^2/\text{sec}$. Assuming t at 610°K is equal to 1 second (likely a maximum since the extruded billet was directly water quenched upon exiting the die), we calculate that $X \cong 4.14 \times 10^{-7}$ cm. Since the closest approach of atoms in Al is 2.86×10^{-8} cm (16), X is equal to 15 atom spacings. This diffusion distance may be overestimated since t can be much smaller than 1 second in reality. Still, the calculations suggest that theiron solute atoms may move several atom spacings if adiabatic heating occurs during hydrostatic extrusion. This, in turn, can permit some pinning of subgrain boundaries by Cottrell atmospheres of iron. Such an agrument suggests that the influence of iron in solution can play an important role in the various strengths observed (Figures 2 and 3).

Let us now consider the annealing experiments and the observation of anneal hardening (Figure 4). In the same way as above we can determine the diffusion distance for Fe in Al at 150°C where the maximum increase in

room temperature strength was observed. The same formula $X \cong 2\sqrt{Dt}$ was used with t = 2.5 hrs. and D = $2.7 \times 10^{-16} cm^2/sec$ at 150°C, X was calculated to be about 109 atom spacings which is about 0.06 of the fine subgrain size observed. This significant amount of diffusion can explain the increase in yield strength of the hydrostatically extruded wire observed with annealing. Furthermore, this annealing could improve the conductivity of the wires as a result of the segregation of iron atoms to subgrain boundary sites, either as Cottrell atmospheres or as minute precipitates. Further studies by TEM and by microprobe analysis can prove ver useful. Electrical conductivity measurements on the extruded wires, before and after annealing, could yield useful information with respect to deducing the various atomic mechanisms discussed above regarding subgrain boundaries, solute and precipitate segregation and subgrain size.

CONCLUSIONS

1. The Al-Fe alloys studied could easily develop well defined subgrains by hydrostatic extrusion with an extrusion ratio of 81 to 1.

2. The amount of supersaturated iron appears to be very important for subgrain size control. It is proposed that the more iron in solution, the smaller the subgrains that can be developed, leading to high strength. Thermal stability of the mechanical properties could also be improved by the presence of supersaturated iron.

3. Strain softening characterized the plastic flow behavior of the hydrostatically extruded wire. As a result, tensile instability in tension tests was noted which is an undesirable characteristic.

4. It is suggested that the solution treatment before extrusion should be done as well as possible. After extrusion, the wire could be annealed at about 200°C for a period of time in order to improve the conductivity without hurting the strength.

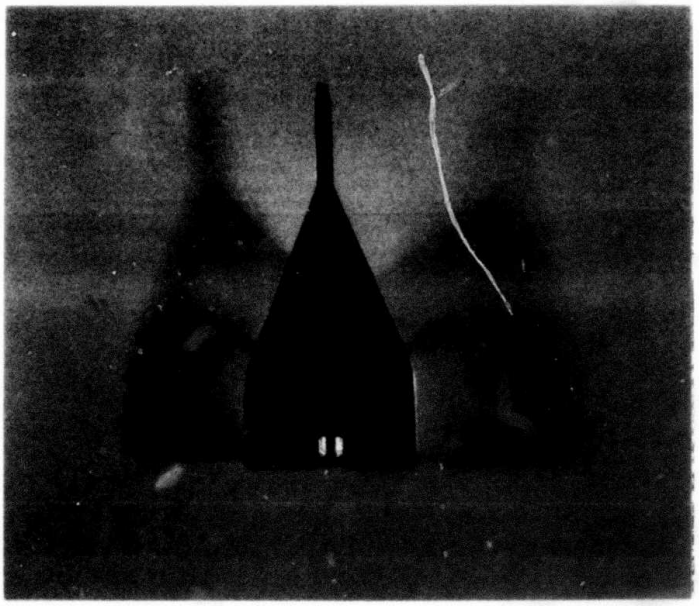

Figure 1. The above photograph illustrates a half section of the extruded sample. Such extruded billets were utilized to study their structure by optical microscopy.

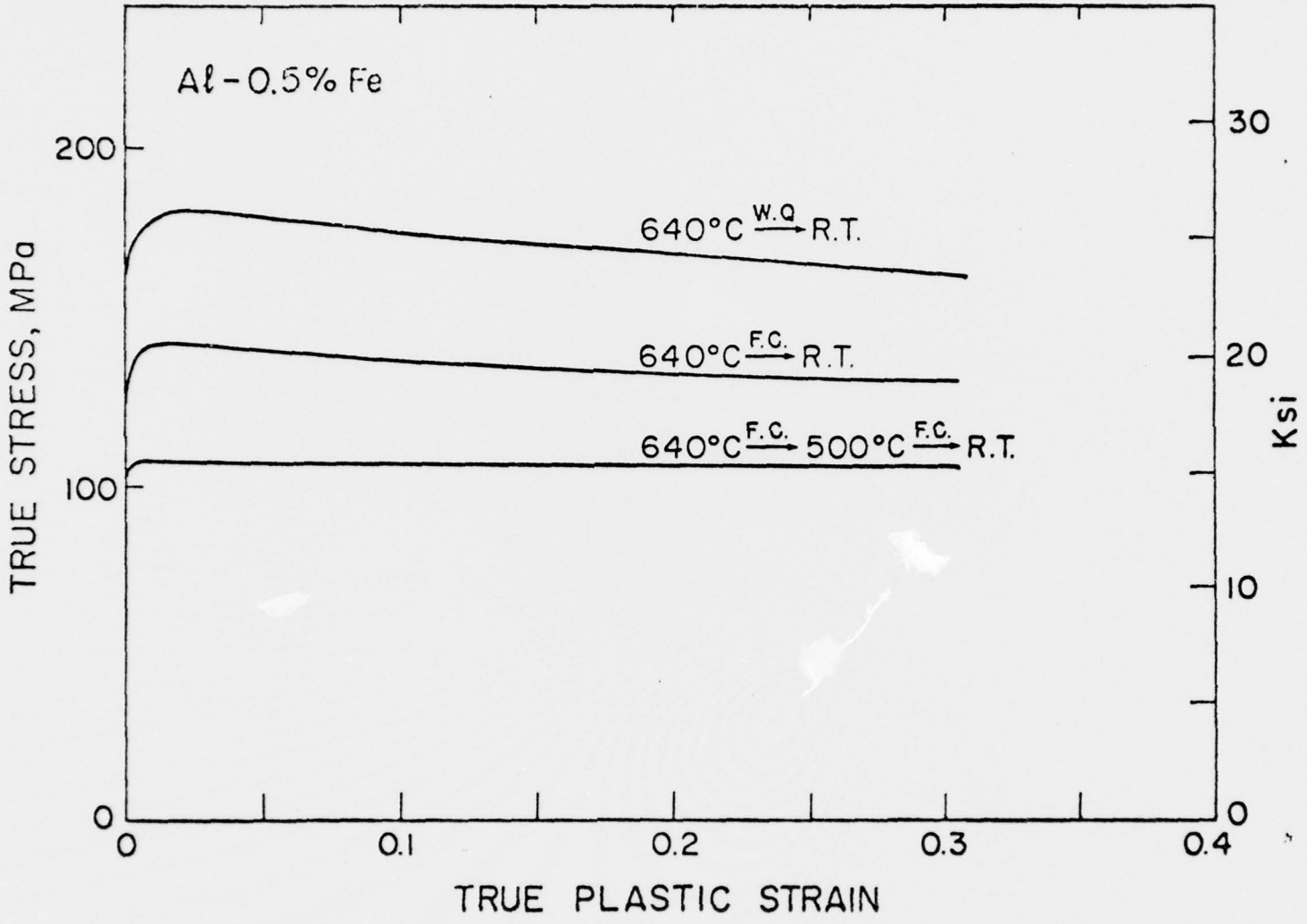

Figure 2. Compression stress-strain curves at room temperature for hydrostatically extruded 0.5% Fe-Al as influenced by various thermal treatments prior to extrusion.

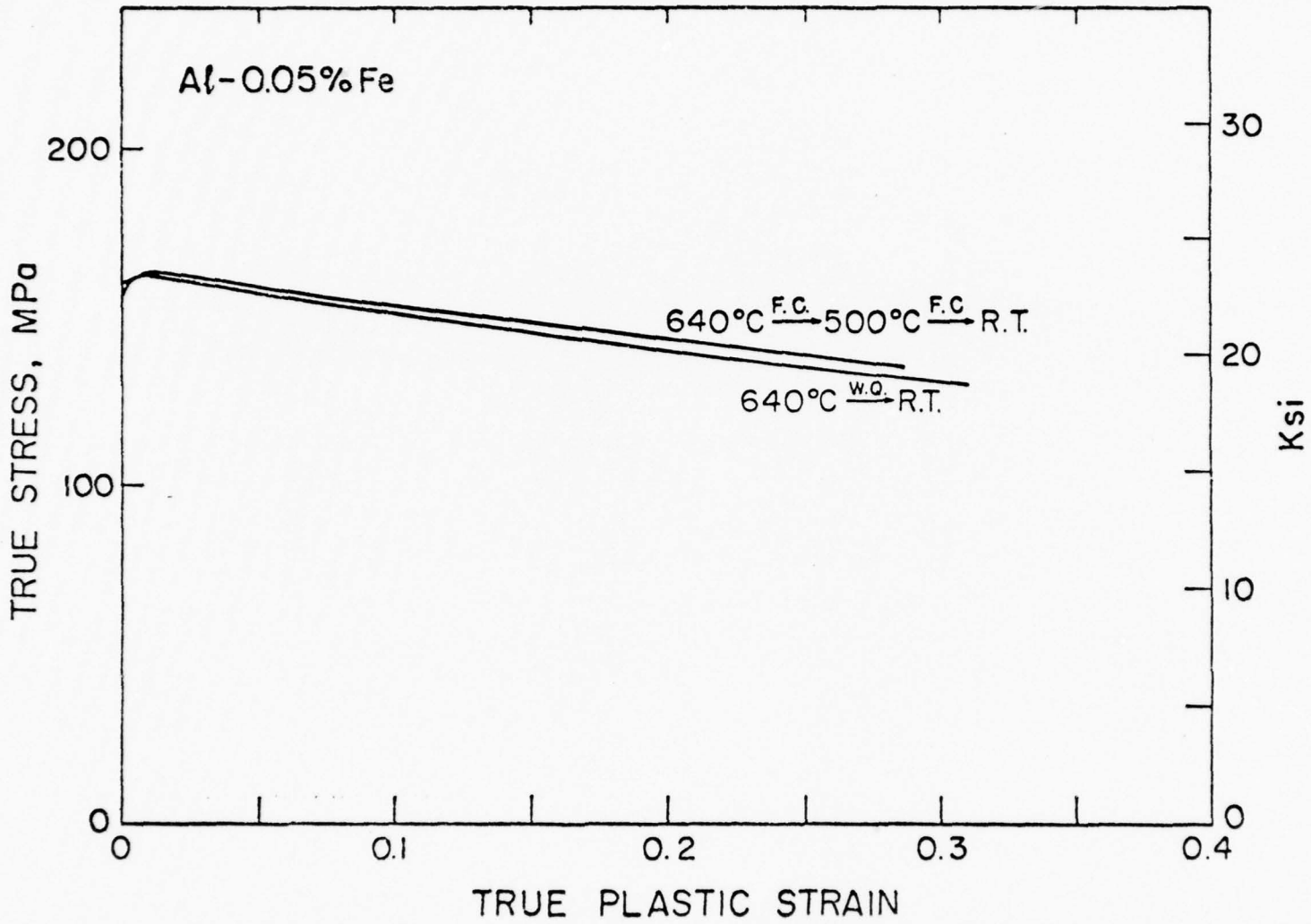

Figure 3. Compression stress-strain curves at room temperature for hydrostatically extruded 0.05% Fe-Al as influenced by various thermal treatments prior to extrusion.

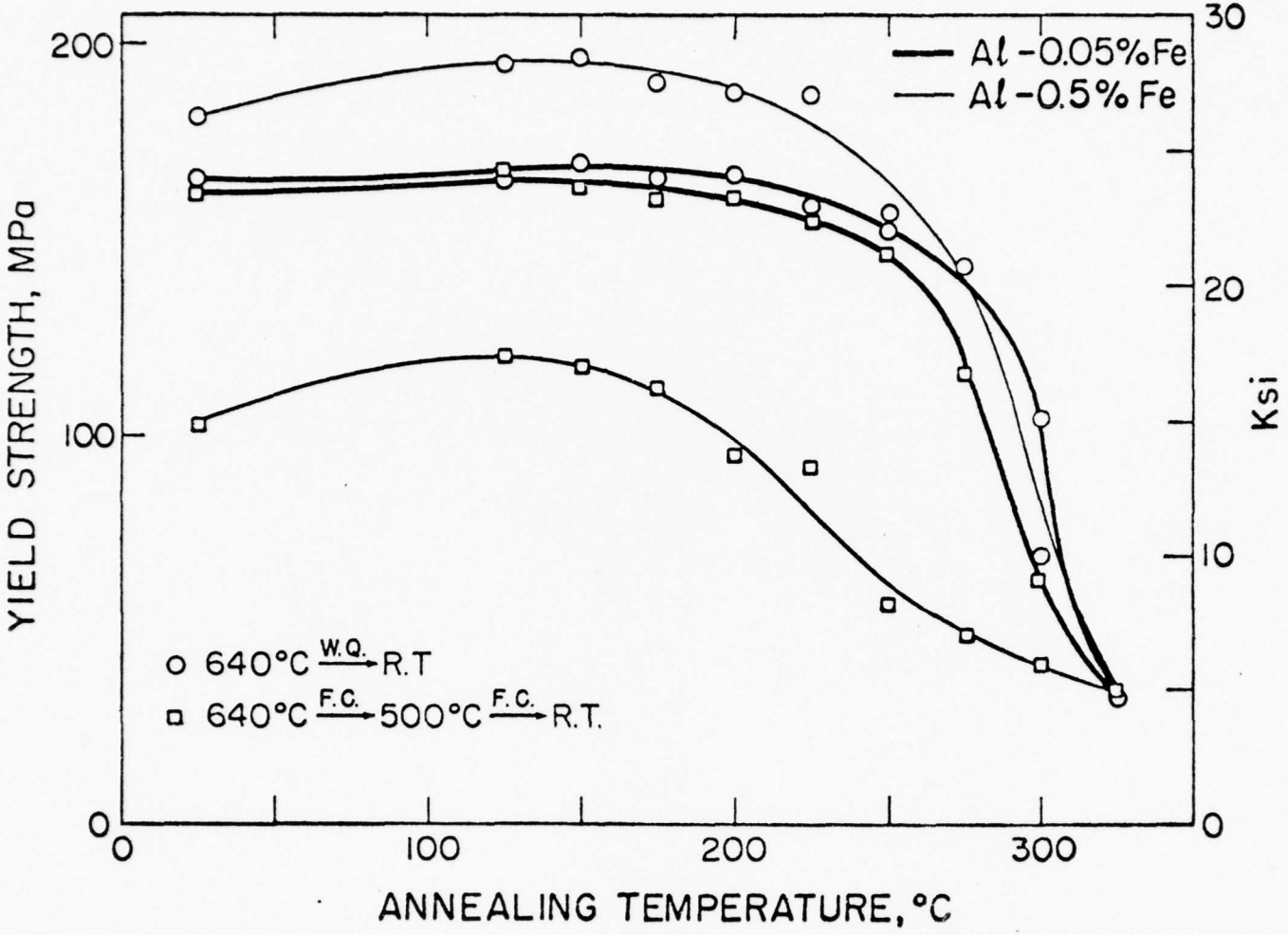

Figure 4. The room temperature yield strengths of the hydrostatically extruded wires after annealed for 2.5 hrs. at different temperatures.

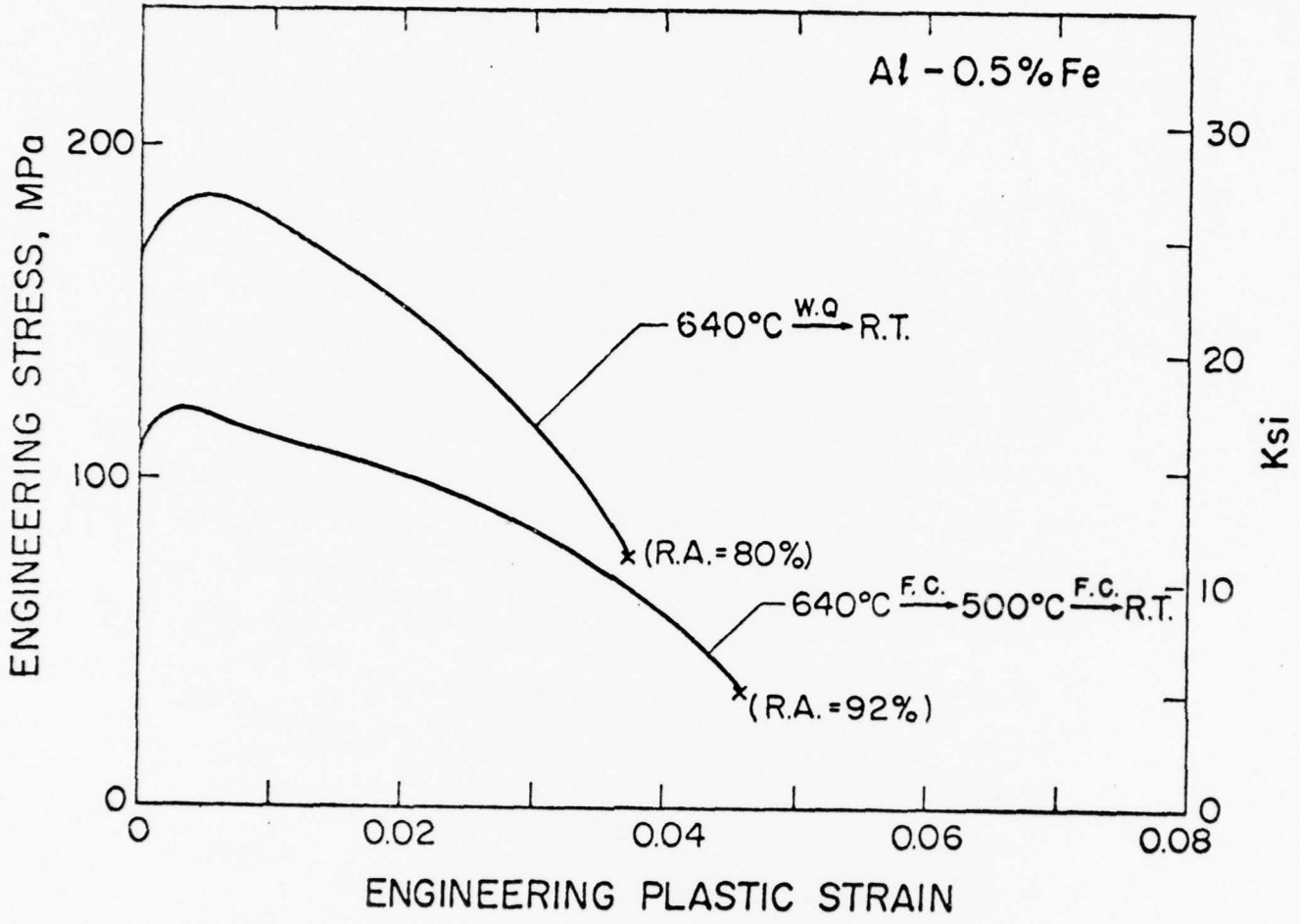

Figure 5. The room temperature tensile test curves of the hydrostatically extruded Al-0.5% Fe wires.

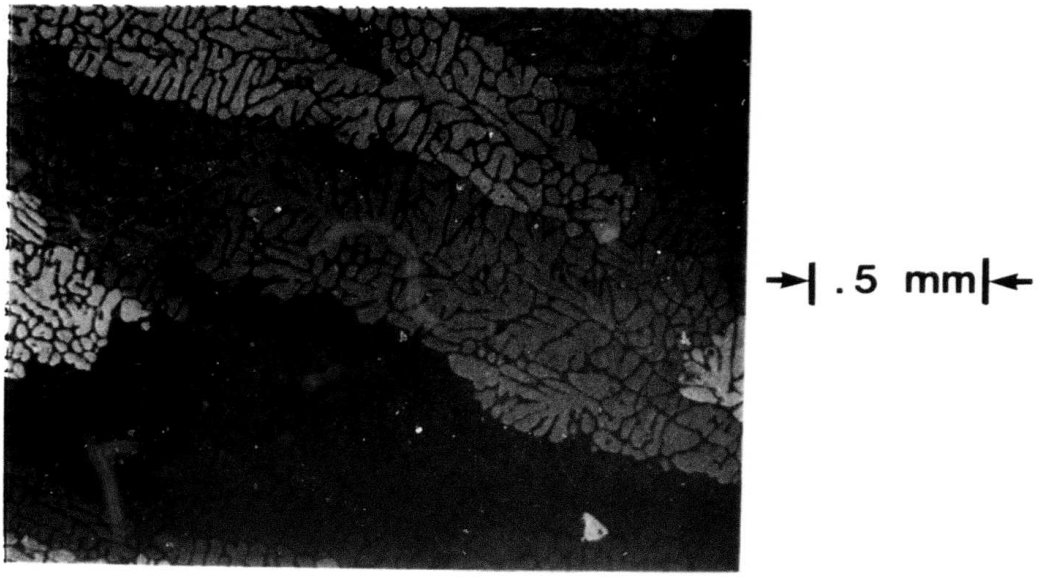

Figure 6. Solution treated and quenched Al-0.5% Fe before extrusion. Polarized light was used.

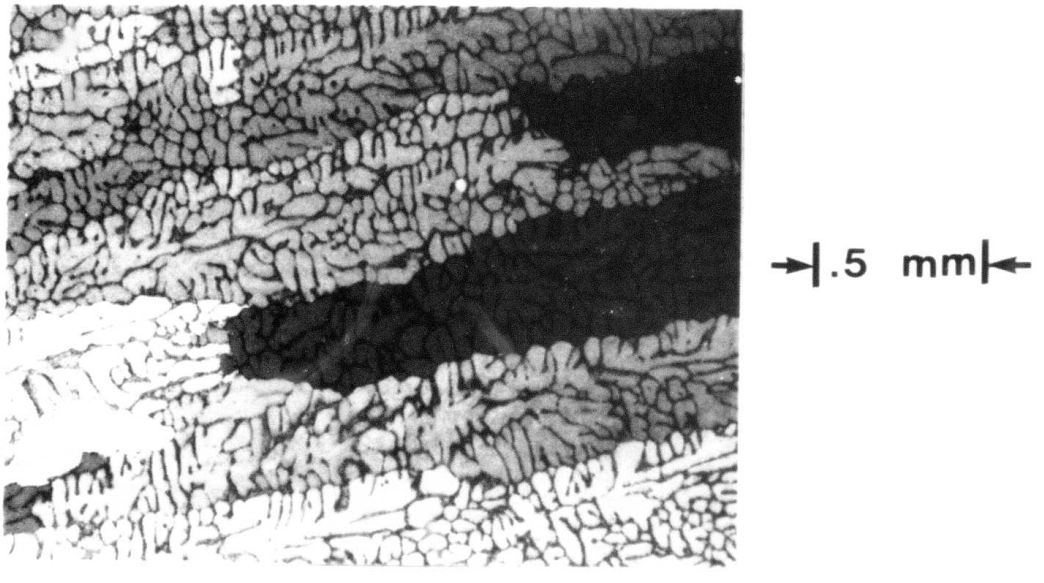

Figure 7. Solution treated and furnace cooled Al-0.5% Fe before extrusion. Polarized light was used.

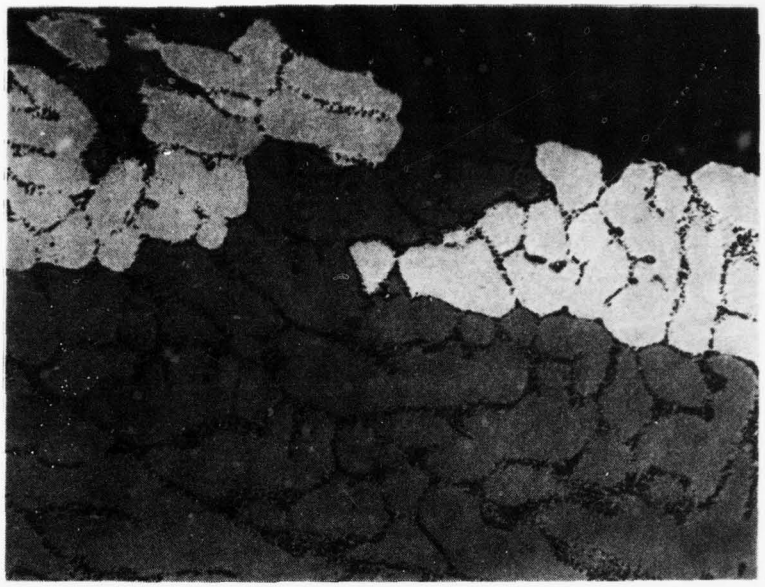

Figure 8. Solution treated and quenched Al-0.5% Fe before extrusion. Polarized light was used.

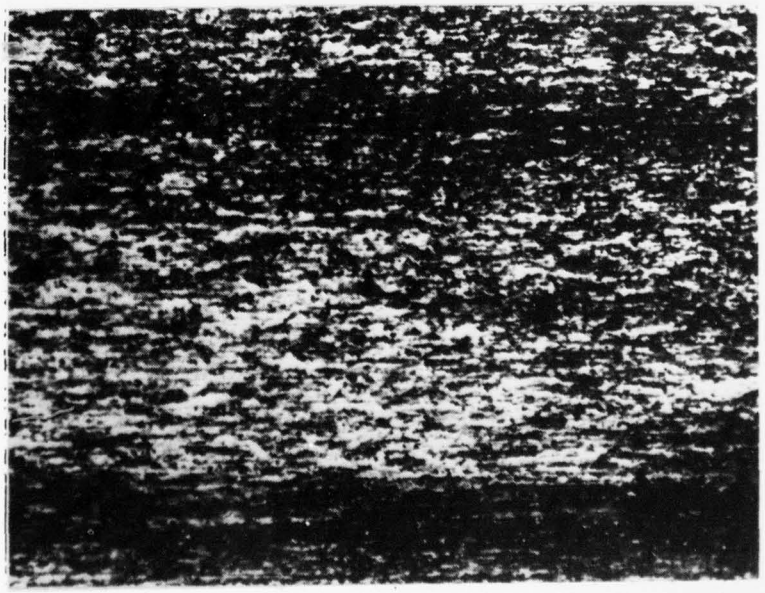

Figure 9. Longitudinal section of hydrostatically extruded wire of the same material as in Figure 8. Polarized light was used.

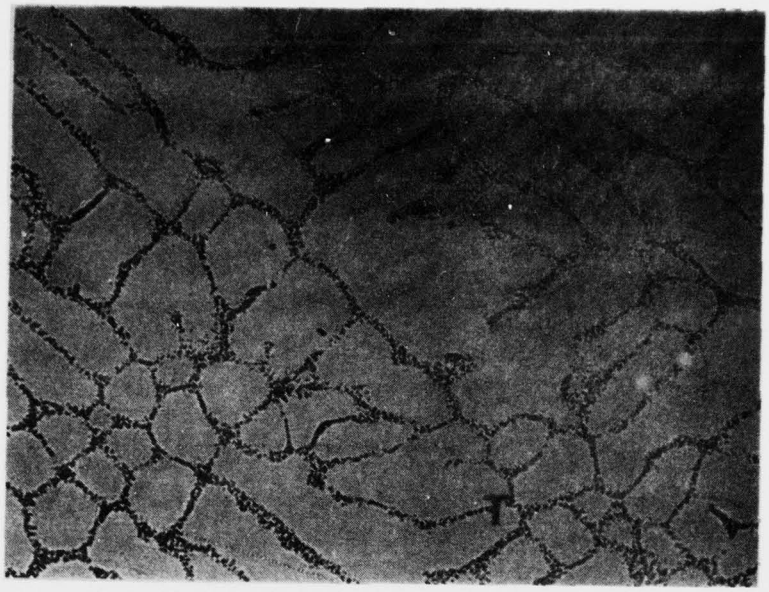

Figure 10. Same as Figure 8 without polarized light.

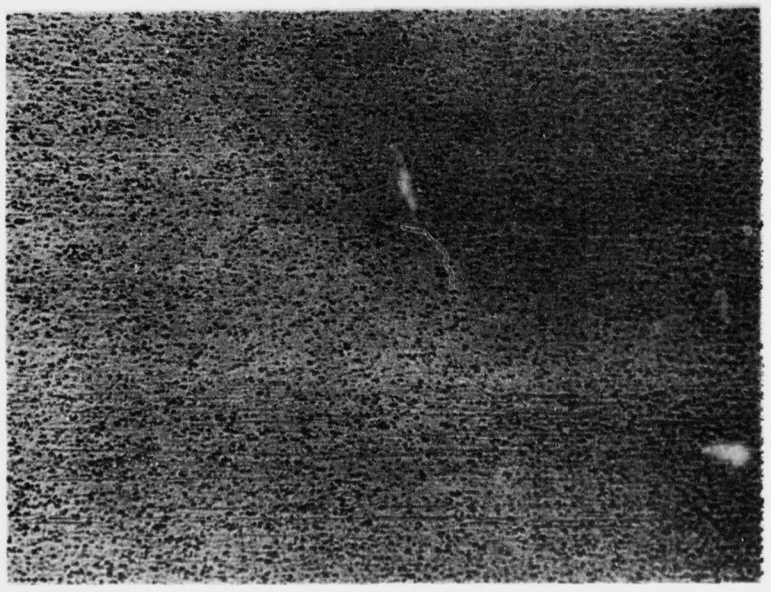

Figure 11. Same as Figure 9 without polarized light.

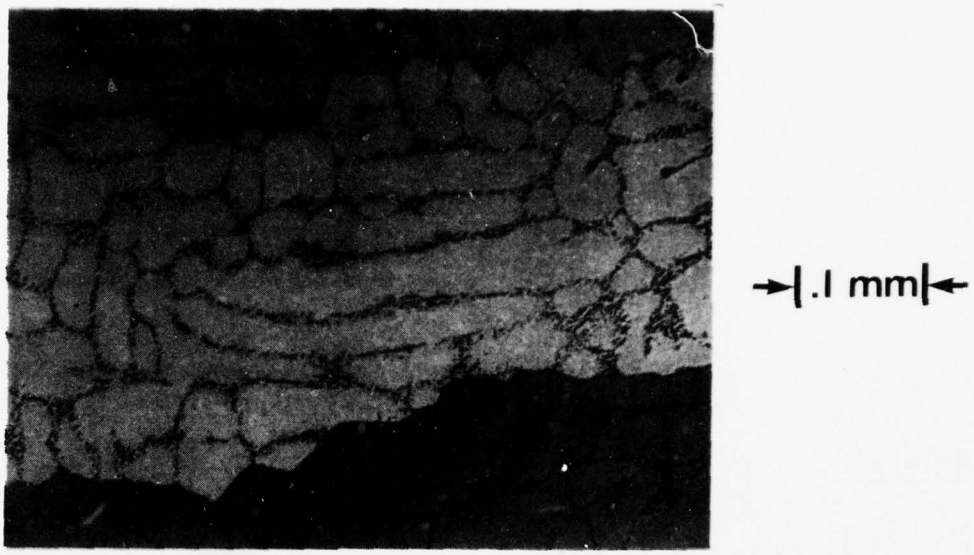

Figure 12. Solution treated and furnace cooled Al-0.5% Fe before extrusion. Polarized light was used.

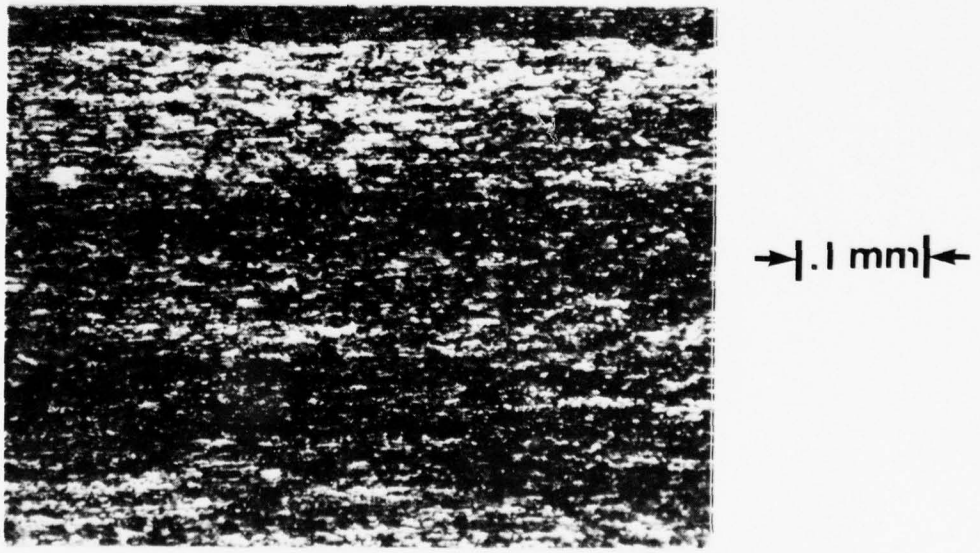

Figure 13. Longitudinal section of hydrostatically extruded wire of the same material as in Figure 12. Polarized light was used.

Figure 14. Same as Figure 12 without polarized light.

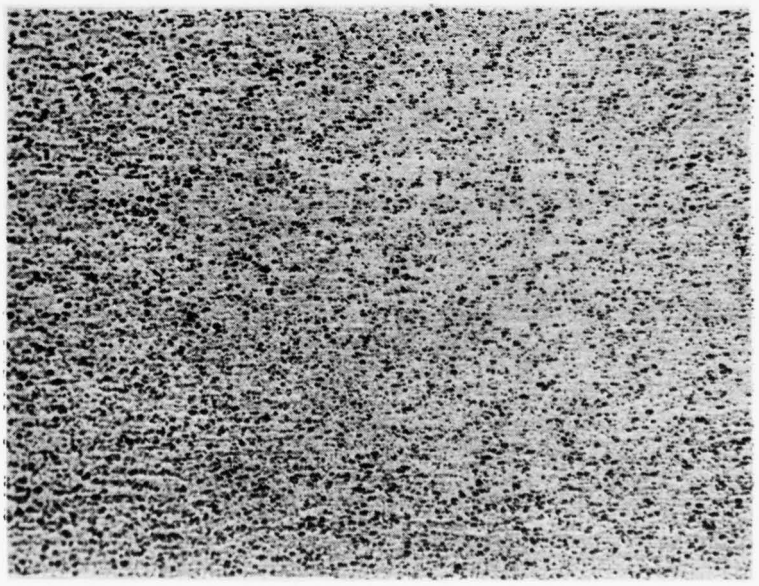

Figure 15. Same as Figure 13 without polarized light.

Figure 16. Solution treated and furnace cooled Al-0.5% Fe before extrusion. Polarized light was used.

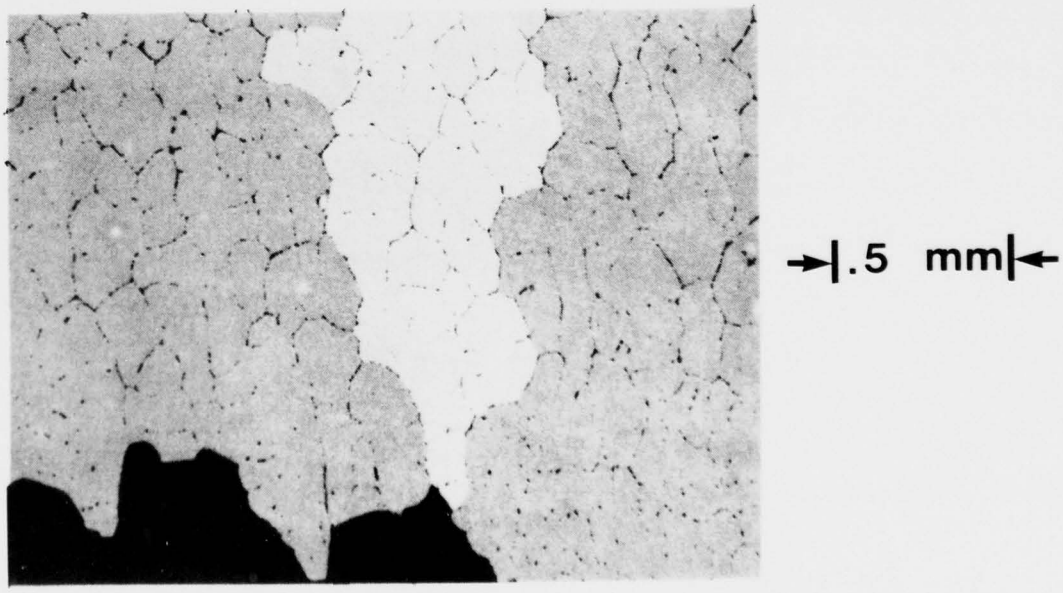

Figure 17. Same as Figure 16 but different area. Interdendritic Al_3Fe are present. Polarized light was used.

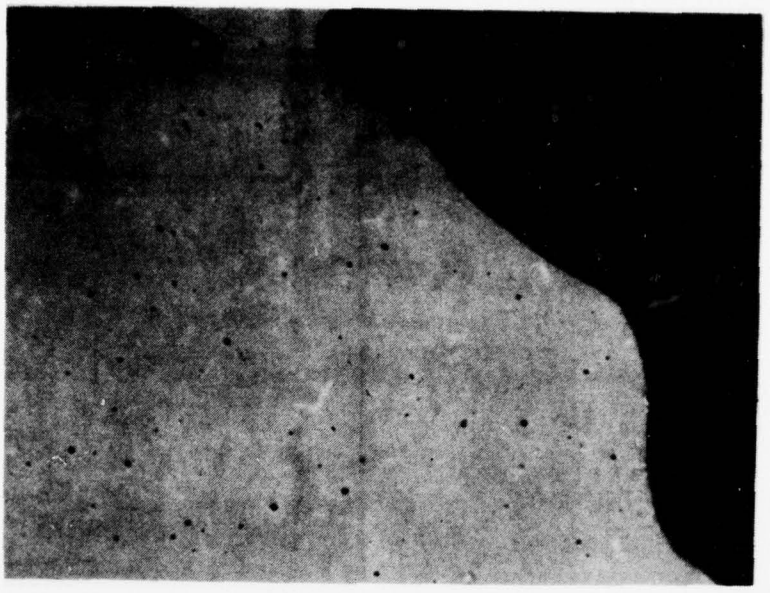

Figure 18. Solution treated and furnace cooled Al-0.5% Fe before extrusion. Polarized light was used.

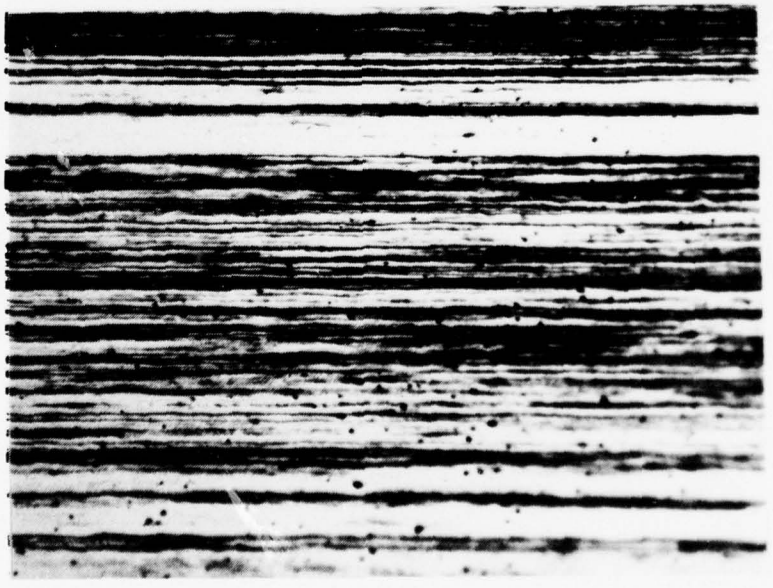

Figure 19. Longitudinal section of hydrostatically extruded wire of the same material as in Figure 18. Polarized light was used.

Figure 20. Same as Figure 18 without polarized light.

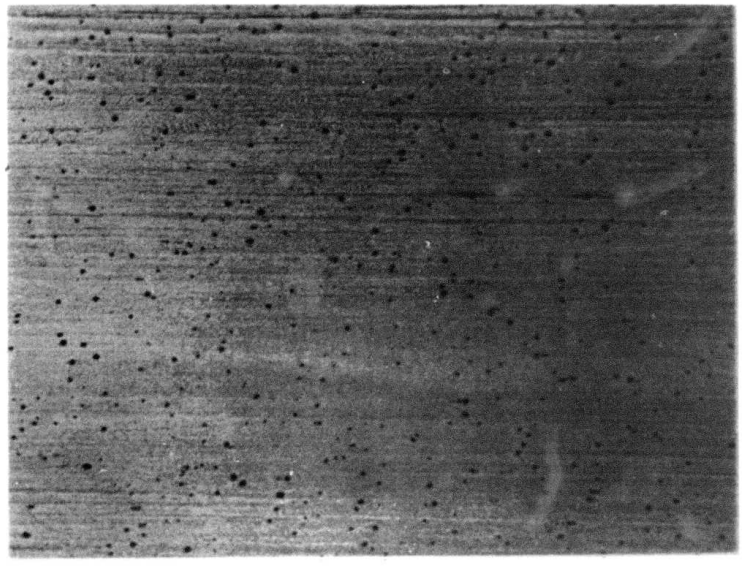

Figure 21. Same as Figure 19 without polarized light.

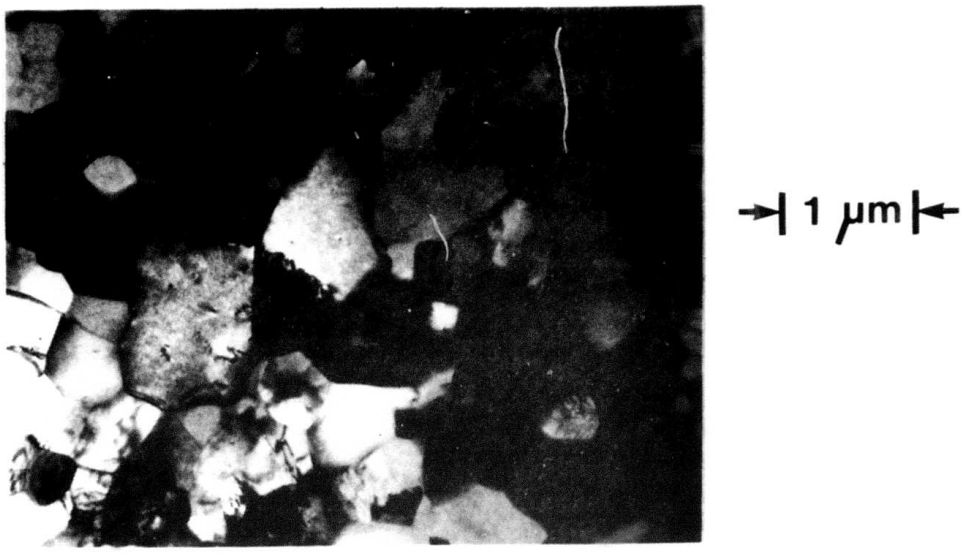

Figure 22. Electron micrograph of hydrostatically extruded Al-0.05% Fe wire. Solution treated and quenched before extrusion.

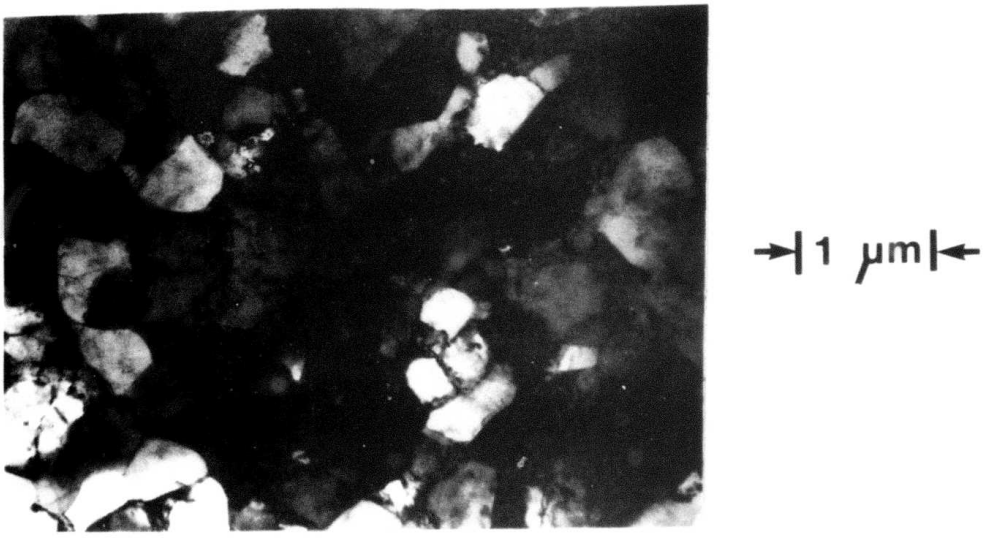

Figure 23. Electron micrograph of hydrostatically extruded Al-0.05% Fe wire. Solution treated and furnace cooled before extrusion.

Figure 24. Electron micrograph of hydrostatically extruded Al-0.5% Fe wire. Solution treated and quenched before extrusion.

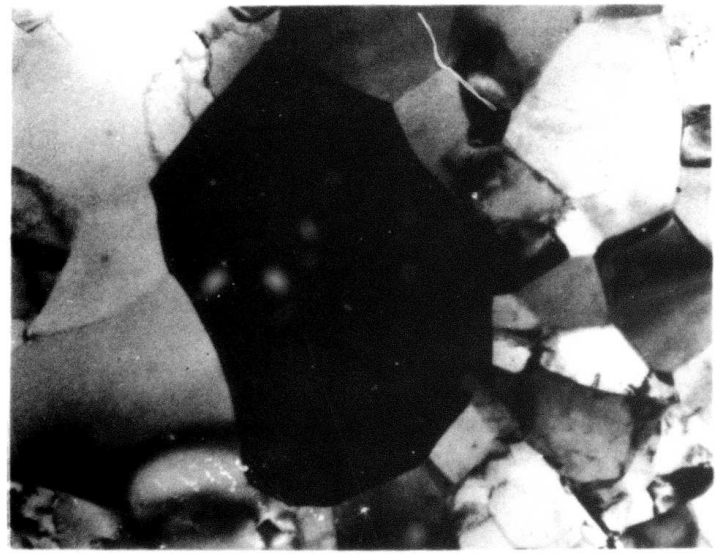

Figure 25. Electron micrograph of hydrostatically extruded Al-0.5% Fe wire. Solution treated and furnace cooled before extrusion.

APPENDIX

Room Temperature Stress-Strain Curves of Compression Tests for Annealing Studies in Al-Fe Alloys.

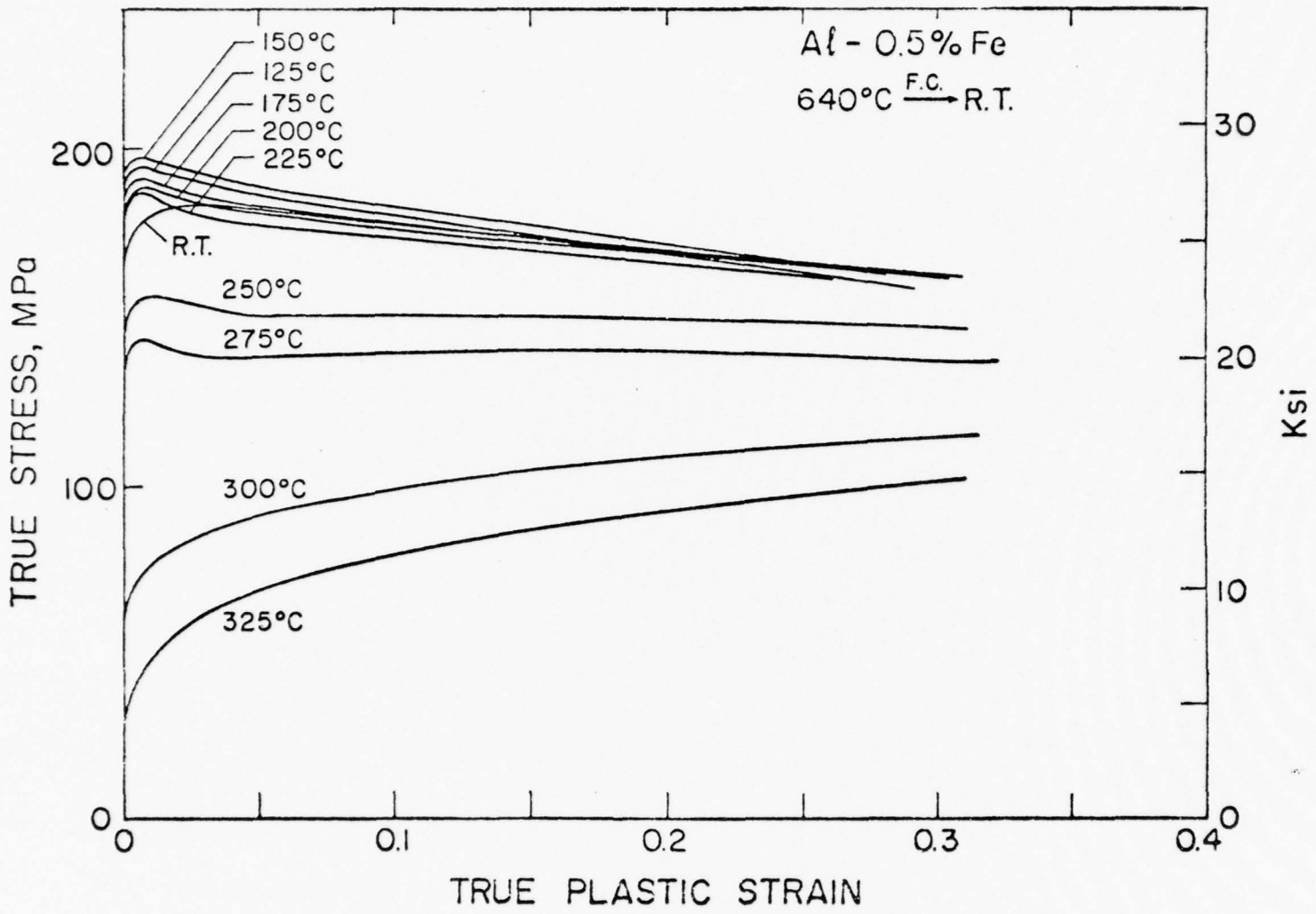

Figure A1. Compression true stress-true strain curves at warm temperature for hydrostatically extrudedAl-0.5%Fe as a function of annealing temperature (2.5 hours at temperature). The material was solution treated at 640°C and water quenched prior to hydrostatic extrusion.

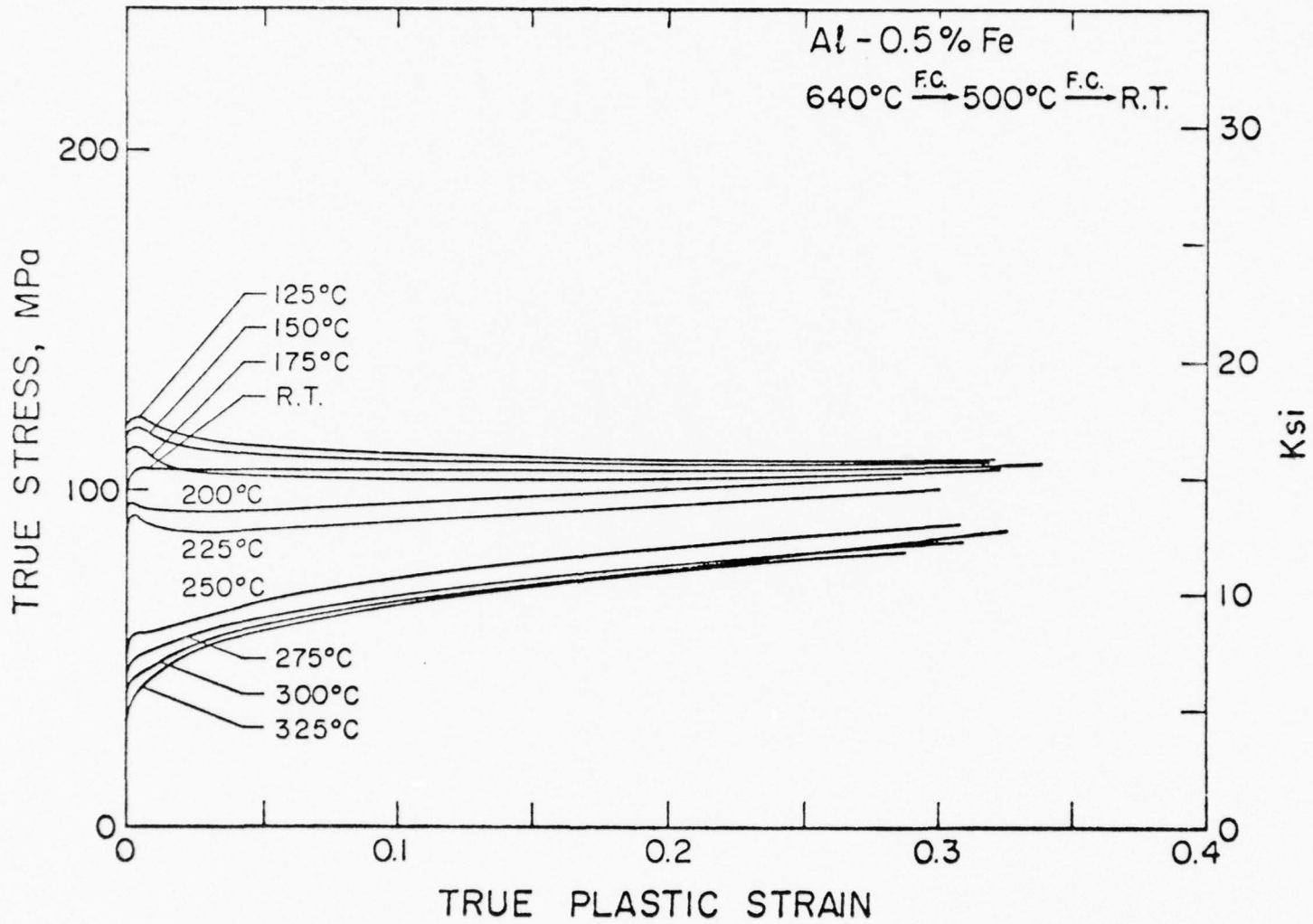

Figure A2. Compression true stress-true strain curves at room temperature for hydrostatically extruded Al-0.5%Fe as a function of annealing temperature (2.5 hours at temperature). The material was solution treated at 640°C and furnace cooled prior to hydrostatic extrusion.

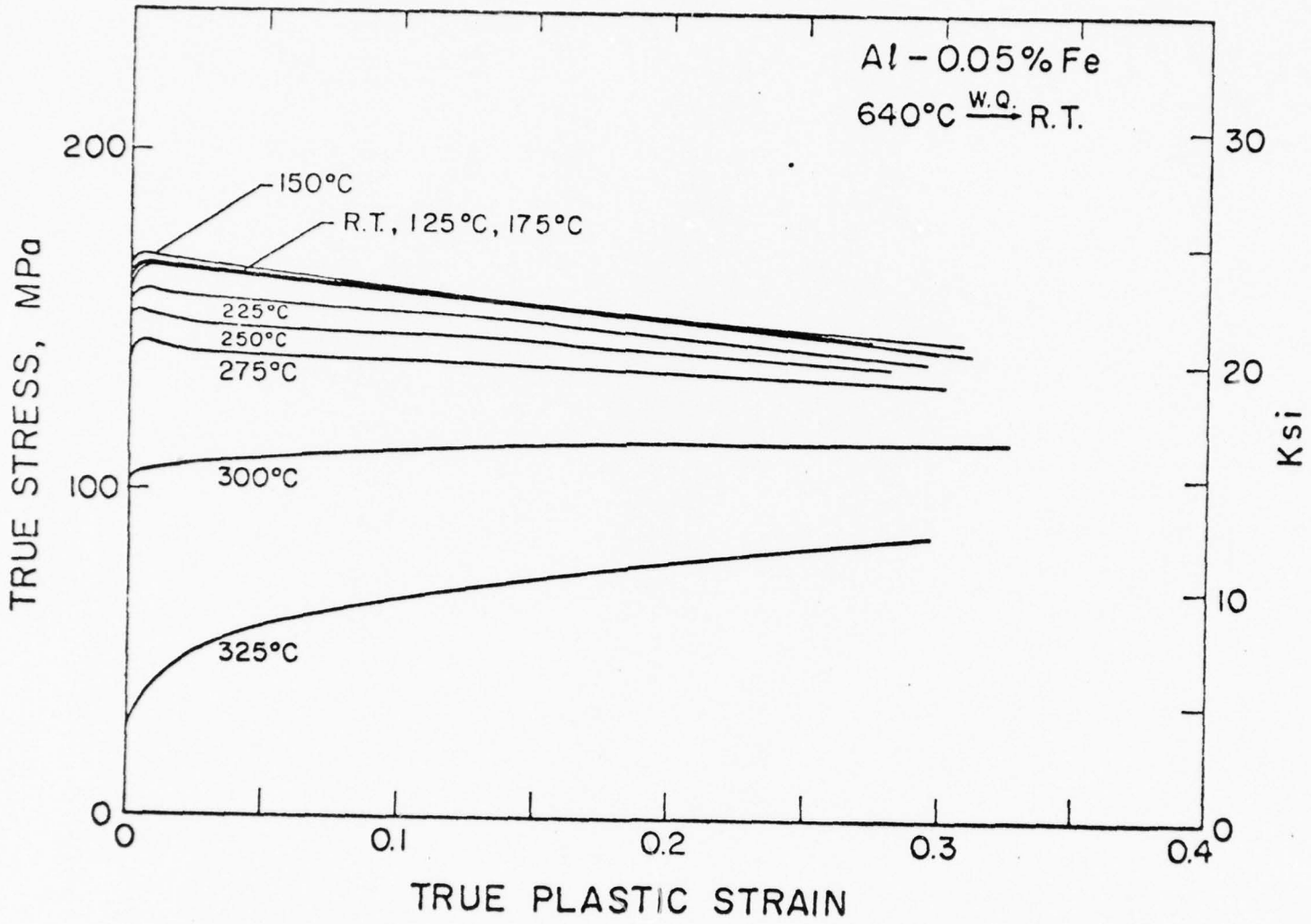

Figure A3. Compression true stress-true strain curves at room temperature for hydrostatically extruded Al-0.05%Fe as a function of annealing temperature (2.5 hours at temperature). The material was solution treated at 640°C and water quenched prior to hydrostatic extrusion.

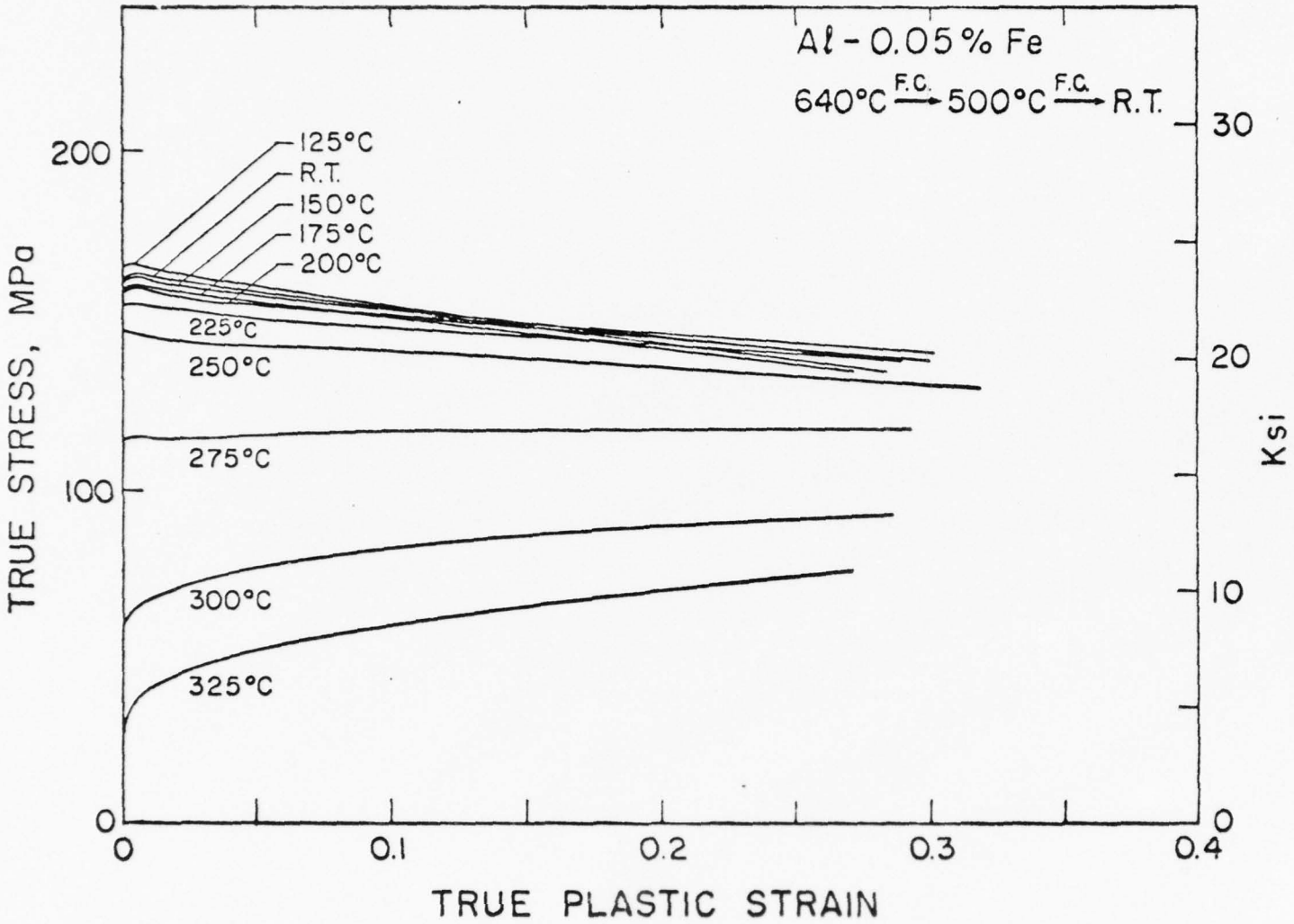

Figure A4. Compression true stress-true strain curves at room temperature for hydrostatically extruded Al-0.05%Fe as a function of annealing temperature (2.5 hours at temperature). The material was solution treated at 640°C and furnace cooled prior to hydrostatic extrusion.

REFERENCES

1. K. R. van Horn, Aluminum, vol. 1, Metals Park, Ohio, 1967, p. 174.

2. C. J. Ball, The Flow Stress of Polycrystalline Aluminum, Phil. Mag., 2, 1957, p. 1011.

3. J. S. H. Lake, Substructure Strengthening in Aluminum, Trans. of ASM, 61, 1968, p. 829.

4. J. E. Hockett and H. J. McQueen, Second International Conference on the Strength of Metals and Alloys, 30 Aug - 4 Sept. 1970, Asilomar, California, ASM p. 991-995.

5. D. J. Abson and J. J. Jonas, The Hall-Petch Relation and High Temperature Subgrains, Met. Sci. J., 4, 1970, p. 24.

6. D. Kalish, Effect of Alloying and Processing on the Subgrain-Strength Relationship in Aluminum Conductor Alloys, Met. Trans., 8A, 1977, p. 204.

7. D. Kalish, Subgrain Strengthening of Aluminum Conductor Wires, Met. Traans. 6A, 1975, p. 1319.

8. E. H. Chia and E. A. Starke, Jr., Application of Subgrain Control to Aluminum Wire Products, Met. Trans., 8A, 1977, p. 825-832.

9. P. F. Hettwer, Aluminum Wire by Cold Hydrostatic Extrusion, Trans. of ASME, 1969, p. 822.

10. H. L. D. Pugh, The Mechanical Behavior of Materials under Pressure, Elseview, 1970.

11. H. Hero and J. A. Mikkelsen, Mechanical and Structural Properties of Hydrostatically Extruded Aluminum and Aluminum Alloys, J. of Inst. of Metals, 97, 1969, p. 18.

12. O. D. Sherby, Second Semi-annual Technical Report on Hydrostatic Extrusion, Stanford University, 1975.

13. B. Avitzur, Study of Flow Through Conical Converging Dies, Lehigh U. Bethlehem, Penn., 1974, p. 34.

14. M Hansen, Constitution of Binary Alloys, McGraw-Hill, 1958, p. 90.

15. O. D. Sherby, R. H. Klundt, and A. K. Miller, Flow Stress, Subgrain Size, and Subgrain Stability at Elevated Temperature, Met. Trans. 8A, 1977, p. 849.

16. Metals Handbook, 8th Edition, vol. 1, Metals Park, Ohio, 1961, p. 46.

17. A. H. Cottrell, Theoretical Structural Metallurgy, 2nd Edition, Eward Arnold Publ. 1965, p. 181.

18. K. I. Hirano, R. P. Agarwala, M. Cohen, Diffusion of Iron, Nickel and Cobalt in Aluminum, Acta Met., 1962, 10, p. 857.

(2) An Investigation of Hydrostatic Extrusion and Other Deformation Modes for the Fabrication of Multifilamentary Niobium-Tin Superconductors by a Powder Metallurgy Approach

Glen Earl MacCleod

Presently, the most promising materials in terms of superconducting properties are the brittle A-15 compounds, for example Nb_3Sn. Therefore, extensive research is being done in the field of materials fabrication in an effort to move A15 superconductors from the study of an exciting phenomenon to the realm of practical applications.

Berkeley investigators are using hydrostatic extrusion in their attempts to develop viable processing techniques for superconducting wire.

The following paper was written by Glen MacCleod as partion fulfillment for the Master of Science Degree in Mechanical Engineering at Berkeley. It details Berkeley's initial efforts in the fabrication of Nb_3Sn wire by tin infiltration of sintered niobium billets.

This paper has been edited to include only those topics which appear relevant to hydrostatic extrusion. We reproduce the paper here with full permission from Professor Milton R. Pickus.

AN INVESTIGATION OF HYDROSTATIC EXTRUSION AND OTHER DEFORMATION MODES FOR THE FABRICATION OF MULTIFILAMENTARY NIOBIUM-TIN SUPERCONDUTORS BY A POWDER METALLURGY APPROACH

BY

Glen Earl MacCleod
(M.S. Thesis, U.C. Berkeley)

June, 1977

Glen Earl MacLeod

Materials and Molecular Research Division

Lawrence Berkeley Laboratory

and

Department of Mechanical Engineering

University of California

Berkeley, California 94720

ABSTRACT

Various aspects of a powder metallurgy approach to fabricate filamentary niobium-tin superconducting wire were investigated . Difficulties occured due to lack of complete tin infiltration of the sintered niobium rod, formation of intermetallics during infiltration, and both cladding and core fracture during mechanical reduction. The influence of sintering time, infiltration temperature, and deformation mode was investigated. Progress is reported on the clarification of the role of several of the important process parameters.

INTRODUCTION

In 1911, H. Kamerlingh Onnes[1] observed that mercury lost all electrical resistance at 4.2°K. This phenomenon became known as superconductivity. During the next fifty years, little research was done in the area of superconductivity because no known superconductors had practical application. Then in 1961, Kunzler, et al.,[2] discovered that Nb_3Sn remained superconductive in high magnetic fields - the first superconductor found to do so.

Extensive work has since been done in the area of superconductor fabrication. Many of the high field superconductors, particuarly those having the A15 structure, like Nb_3Sn, are inherently brittle and must be subjected to special fabricating processes to make them useable. Neither the Bell Telephone process[2] or the General Electric tape process[3], two of the first successful fabrication processes developed, produced multifilamentary conductors.

Multifilamentary wire was developed by Tachikawa[4] in Japan in 1967, and has since been studied extensively in this country by Suenage, et al.,[5,6] working at Brookhave National Laboratory. Tachikawa's original process and its modifications have become known as the "bronze process". The bronze process has found commercial acceptance due to the relative flexibility and intrinsic stability of the wire. This stability is due to the multifilamentary morphology of the wire and is described by Wilson, et al.[7]

At the Lawrence Berkeley Laboratory, multifilamentary Nb_3Sn superconducting tape and wire have been made using a unique powder metallurgy approach to fabrication.[8] Babu,[9] Garrett,[10] and Hemachalam[11] have optimized the process parameters and characterized the resulting tape. Since multifilamentary tape

is less stable than multifilamentary wire, the tape process was modified to produce wire. Hemachalam[12] was able to fabricate Nb_3Sn superconducting wire that had a higher current density at high fields than commercially available wire. Hemachalam began with 0.19 in. rods and was only able to make 20 foot lengths.

One objective of this work was to scale up the existing powder metallurgy process in order to make long lengths of Nb_3Sn superconducting wire (a few hundred feet). The ability to make long lengths of wire would demonstrate the practical feasibility of the process and with long lengths of wire a superconducting solenoid could be made and tested.

It was originally envisioned that the powder metallurgy process could be directly scaled up by simply increasing the billet diameter (the billet length is fixed due to the furnace geometry) and leaving other process parameters the same. However, core and cladding fracture during wire drawing have now indicated that the process parameters must be re-evaluated.

The effects of sintering time and infiltration temperature were investigated. Hydrostatic extrusion was used as an alternative to form rolling and wire drawing. The nominal diameters of the infiltrated cores employed in this work were 1/2 in. and 3/4 in. as contrasted with the 3/16 in. cores used by Hemachalam.

EXPERIMENTAL PROCEDURE

Processing of the Wire

The powder metallurgy process requires six steps to go from a powder to the final superconducting wire. These steps are: 1) isostatic compaction of the niobium powder to impart the required porosity and green strength; 2) sintering of the niobium rod to give it strength and ductility; 3) infiltration of the rod with tin, thereby filling the pores with an inter-connected network of tin;

4) cladding of the rod to facilitate mechanical deformation; 5) mechanical reduction of the rod to produce a multifilamentary structure of tin in the niobium, and 6) diffusion treatment to form Nb_3Sn filaments. A schematic of the process is shown in Fig. 1.

Niobium powder was isostatically compacted in rubber tubes to pressures of from 25 ksi to 50 ksi. A minimum pressure was required to give the compact adequate green strength. Porosity of the green compact was controlled by the compaction pressure (Fig. 2).

Green compacts were vacuum sintered at 2200°C to 2300°C for 5 min. to 40 min. at a pressure of 10^{-5} mm Hg, and then they were infiltrated with tin at 500°C to 750°C for 30 seconds. Both sintering and tin infiltration were carried out in an Abar furnace.

On all but a few specimens, cladding was used to facilitate mechanical deformation and maintain integrity of the infiltrated rod. Monel, bronze (92% Cu, 8% Sn), or OFHC Cu was used as the cladding material. An intermediate sheath of tantalum prevented reaction between the cladding and the infiltrated tin. Tantalum or niobium could not be used as cladding material since they tend to gall on the dies.

The primary modes of deformation were wire drawing and hydrostatic extrusion. Form rolling was required on billets larger than 0.34 in. diameter since this was the largest size that could be wire drawn on the available equipment. Swaging was used to initially impart good mechanical bonding between the core and claddings and to point the wire for drawing. Hydrostatic extrustion was performed on a 250,000 psi 0.750 in. bore machine located at Stanford University, Department of Materials Science and Engineering. Figure 3 shows the hydrostatic extrusion machine from the rear along the projectile barrier,

the pumping station, and the protective screen around the control panel. Figure 4 is a side view of the machine with the water cooling system attached.

Compression tests were made on various cladding materials, niobium (both wrought and from powder) and Nb-Sn as-infiltrated compacts for estimating material flow stresses at hydrostatic extrusion strain rates.

RESULTS AND DISCUSSION

Compact Processing

Initial attempts to directly scale up the powder metallurgy process for making Nb_3Sn superconducting wire using Hemachalam's parameters were unsuccessful. Consequently, the influence of powder size, compaction pressure, sintering time, and infiltration temperature was evaluated. Niobium powder of -270 mesh from Wah Chang was used. The green porosity as a function powder size fraction and compaction pressure is shown in Fig. 2. An isostatic compaction pressure of 30 ksi gave adequate porosity along with the required green strength. Sintering temperatures of 2250 and 2300°C appeared to be satisfactory. Infiltration temperatures of 700°C and 750°C were found to cause the formation of Nb_6Sn_5. Rods that have been infiltrated at these temperatures tended to fracture at the early stages of wire drawing. Rods infiltrated at lower temperatures did not always wet completely which resulted in areas that were void of tin. To resolve this problem, the sintered rod was preheated to 600°C and infiltrated with tin at 600°C. The result was a completely infiltrated rod with no Nb_6Sn_5 present, provided that the tin bath was reasonably clean.

Besides core fracturing encountered during wire drawing, cladding fracture also occurred. Annealed monel was used as cladding for wire drawn rods since Hemachalam had the most success with it in his work. During form rolling, which was required for the initial size reduction, the cladding was subjected to large alternating strains. This plastic cycling of the monel usually resulted in

the eventual fracture of the cladding, either in the last stages of form rolling or during the pointing of the wire on the swaging machine. To circumvent the problem of sleeve fracture two rods, one 0.19 in. diameter and the other 0.45 in. diameter, were deformed without cladding. The exposed tin on the surface of the rods both prevented galling and acted as an excellent lubricant. The drawing force appeared to be much less for these unclad rods than for clad rods. The 0.19 in. diameter rod was reduced in area by a factor of 50 and still had tin remaining in it. The 0.45 in. diameter rod was reduced in area by a factor of 800 and had no tin remaining. The tin apparently squeezed out of the rod on the up stream side of the die. It was therefore deemed necessary to have cladding to prevent tin squeeze out during wire drawing at higher reductions.

Hydrostatic Extrusion

Because of the difficulties encountered with wire drawing, hydrostatic extrusion was tried as an alternate method of mechanical reduction. Hydrostatic extrusion of Nb_3Sn wire and NbTi wire have been reported in references 13 and 14. Hydrostatic pressure has been shown to increase the ductility of various materials that are subjected to tension[15]. An application of this finding was to extrude materials under hydrostatic pressure; in addition to increasing the ductility of the material being extruded, hydrostatic extrusion eliminates the container wall friction associated with conventional extusion and also provides for a certain amount of lubrication between the billet and the die[16,17].

Hydrostatic extrusion was initially attempted on two 0.5 in diameter as-infiltrated rods (No. 1 and 2, Table 1), and a 0.625 in. diameter sintered Nb rod (No. 3, Table 1). In these first extrusions billet design was somewhat arbitrary and both core instability and cladding fracture were encountered.

Rather than proceeding blindly to determine under what conditions a successful extrusion could be made, B. Avitzur[18,19] was consulted because he had done much work in the area of how process parameters affect both wire drawing and hydrostatic extrusion. He has also determined under what conditions successful coextrusions can be made[14,20,21]. Recently, Avitzur has developed a computer code based on theoretical analysis to determine acceptable core to sleeve diameter ratios and acceptable reductions to prevent core or sleeve fracture fiven the die angle, flow stress ratios, and billet-die friction coefficient[22]. To determine the flow stresses for the various materials that were extruded compression tests were made at different strain rates. Flow stress versus strain rate was plotted on a log-log graph (Fig. 5), since most metals follow the relationship $\sigma_f = \sigma_o \dot{\varepsilon}^m$ where σ_o and m are constants[23]. In this way, the flow stress at strain rates encountered during extrusion can be extrapolated. Based on information given by the code a fourth billet was designed and extruded (No. 4, Table I). A comparison between Nos. 3 and 4 is made in Fig. 6. The results seem to correspond well to Avitzur's predictions since the process parameters of No. 3 were within the core instability or fracture region given by his computer code and No. 4 was not.

Since billet No. 4 extruded successfully, five more billets (Nos. 5 through 9) were either made or modified to conform to Avitzur's criteria. Figures 7 and 8 are photographs of billets Nos. 5 and 8 before their first extrusion pass. Figure 9 is a photograph of billet No. 8 after its first pass, and Fig. 10 shows it made into a billet for a second reduction. The billets had mild steel plugs at the ends so that the extrusion would stall out prior to reaching the end of the billet. Billet No. 6 virtually exploded out of the machine in many pieces (Fig. 11), and billett No. 9 did not extrude at a 94% reduction in area, and the machine broke down when a reduction of 88% was tried.

Billets Nos. 5,7 and 8 extruded with uniform cores on the first reduction and no sleeve fractures except for billet No. 5 pass 3 (Figs 12,13 and 15). During this extrusion, the Nb-Sn core appeared to have pulled the monel in tension and fractured it. This was attributed to the relatively high cladding to core flow stress ratio and therefore monel is not recommended for use as cladding material. The second extrusion of billet No. 8 resulted in a fractured product (Fig. 14). Photomicrographs of the Nb-Sn cores of billets Nos. 5 and 8 after a 69% and 77% reduction, respectively, reveals a fairly uniform dispersion of Sn filaments (Figs. 15 and 16). At a total reduction in area of 95% for billet No. 8 fissures appeared towards the centerline of the core and oriented themselves approximately 45° to the core axis (Fig. 17). Also, it was observed that tin tends to flow into these fissures. A similar observation was made for billet No. 7 (Fig. 18). It seems plausible that this tin segregation may have resulted from pressure differentials between interconnected pores due to the low flow stress of tin particularly in the liquid state (all the extrusions of Nb-Sn showed evidence of tin melting despite water cooling of the extrusion product during deformation). Lending support to this explanation for the tin segregating: Rogers, et al.[24] has determined stress solutions for sheet drawing by slip-line analysis which reveals a hydrostatic compression component near the dies but a hydrostatic tensile component at the centerline of the sheet. Although Roger's data cannot be directly related to axisymmetric extrusion, Lambert and Kobayashi[25] have demonstrated similar trends for axisymmetric extrusion. An as-infiltrated rod wire drawn to a total reduction in area of 91% exhibits the same segregation of tin to the center of the rod (Figs. 19 and 20).

CONCLUSIONS

1. Increasing the diameter of infiltrated compacts to produce long lengths of multifilamentary Nb_3Sn wire as suggested by Hemachalam proved to be more

difficult than expected. Re-evaluation and refinement of the process parameters has been made but more work in this area is required.

2. The optimum temperature for tin infiltration now appears to be 600°C provided that the sintered rod is preheated to 600°C prior to infiltration. This procedure will ensure proper wetting of the niobium rod resulting in complete infiltration and will prevent the formation of the brittle Nb_6Sn_5 phase.

3. Form rolling prior to wire drawing usually results in cladding failure. A larger and more sophisticated draw bench would eliminate the need for form rolling.

4. Reduction in areas of up to 80% could be achieved by hydrostatic extrusion without apparent damage to the infiltrated core.

5. It appears desirable to maintain the ratio of the cladding flow stress to core flow stress close to or less than 1.

ACKNOWLEDGEMENT

The author wishes to thank Professor M. R. Pickus for his guidance. Additional thanks to Dr. J. L-F Wang for his comments and suggestions, and to Dr. K. Hemachalam for his help in the early stages of this work. The technical advice of J. T. Holthuis was of great value. The assistance of J. A. Jacobsen with metallographic techniques was greatly appreciated.

Special thanks are due to Professor O. D. Sherby of Stanford University for his interest in this project, and for not only making available the use of the hydrostatic extrusion machine, but also for setting up a cooperative effort with their research technician, Rob Whalen, whose contributions were invaluable. Thanks also to Professor B. Avitzur of Lehigh University for his recommendations regarding optimization of the extrusion parameters. I greatly appreciate the fruitful discussions with Professors F. E. Hauser and S. Kobayashi of the University of California at Berkeley.

This work has been accomplished under the auspices of the U. S. Energy Research and Development Administration through the Materials and Molecular Research Division of the Lawrence Berkeley Laboratory.

TABLE I

Billet No.	Core and Diameter (in.)	Cladding and Diameter (in.)	Pass No.	Die Angle	Diameter Ratio Core/ Cladding	Flow Stress Ratio Cladding/ Core	Reduction in Area	Extrusion Pressure (psi)	Final Diameter (in.)	Remarks	Figure Nos.
1	Nb-Sn 0.450	Brass 0.735	1	45°	0.6	0.90	75%	* N/A	0.375	Sleeve fracture.	
2	Nb-Sn 0.450	None	1	45°	---	---	N/A	---	---	Billet buckled.	
3	Nb 0.625	Cu 0.735	1	45°	0.85	0.70	75%	N/A	0.367	Good extrusion.	
	0.312	0.735	2	45°	0.42	0.70	75%	N/A	0.375	Core fractured.	18
4	Nb 0.250	Bronze 0.360	1	22°	0.69	1.38	73%	152,000	0.187	Good extrusion, uniform core.	18
5**	Nb-Sn 0.450	Monel 0.640	1	22°	0.70	1.35	80%	250,000	---	Did not extrude.	
	0.450	0.640	2	22°	0.70	1.35	69%	160,000	0.355	Uniform core, rough surface.	19, 24, and 27.
	0.450	0.600	3	22°	0.75	1.35	65%	160,000	0.357	Nb-Sn forced out cladding fracturing it in tension.	
6	Nb-Sn 0.723	None	1	22°	---	---	75%	152,000	0.360	Fractured into many pieces.	23
7	Nb-Sn 0.40	Nb 0.535	1	22°	0.75	0.74	88%	N/A	0.187	Uniform core, rough surface.	25, 30, and 32.
	0.140	0.187	2	22°	0.75	0.74	55%	N/A	0.125	Uniform core, smooth surface.	
8**	Nb-Sn 0.400	OFHC Cu 0.555	1	22°	0.72	0.52	77%	160,000	0.266	Uniform core, smooth surface.	
	0.190	0.266	2	22°	0.72	0.52	78%	N/A	0.125	Both core and cladding fractured.	20, 21, 22, 26, 28, and 29.
	0.190	0.266	3	22°	0.72	0.52	78%	N/A	0.125	Both core and cladding fractured.	
9	Nb-Sn 0.400	OFHC Cu 0.556	1	22°	0.72	0.52	94%	250,000	0.125	Did not extrude.	
	0.400	0.556	2	22°	0.72	0.52	88%	---	---	Seals ruptured on machine.	

* N/A - Not available.
** Intermediate sheath of Tantalum tube 0.02 in. thick was put between core and cladding.

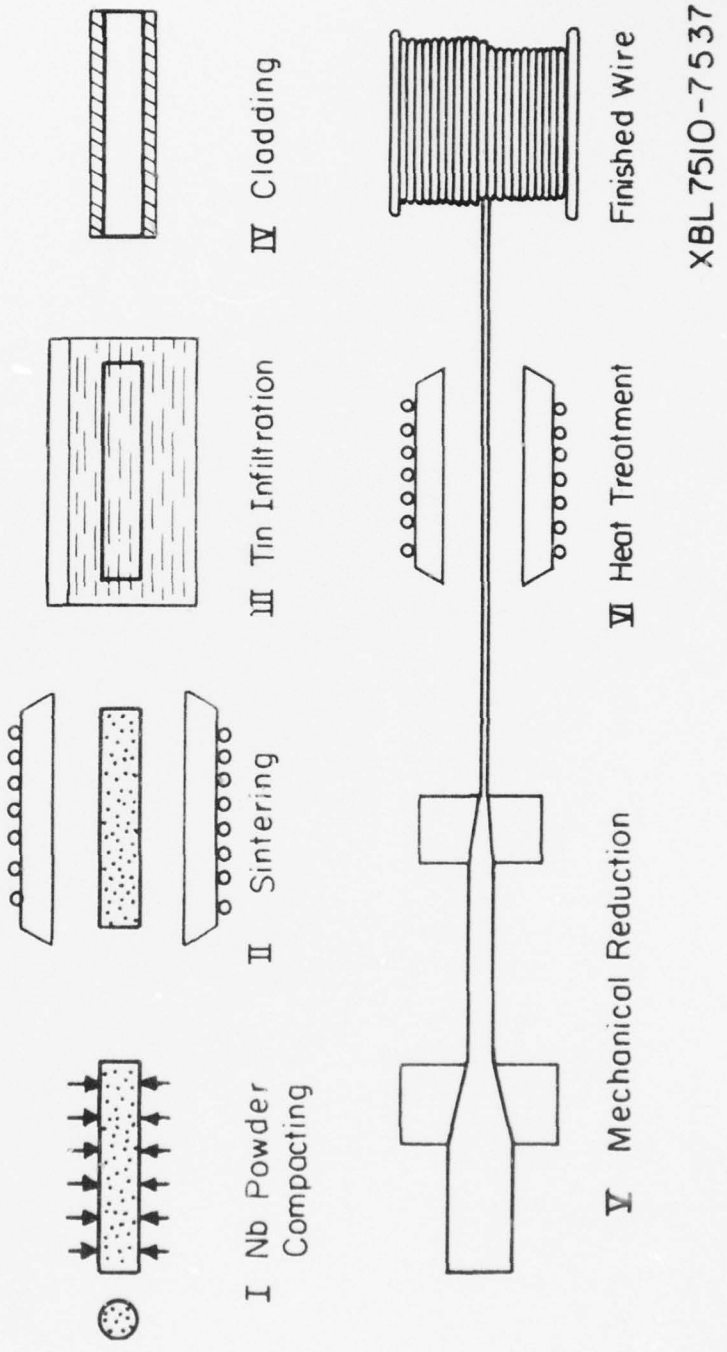

Figure 1. Schematic diagram of the filamentary wire fabrication process.

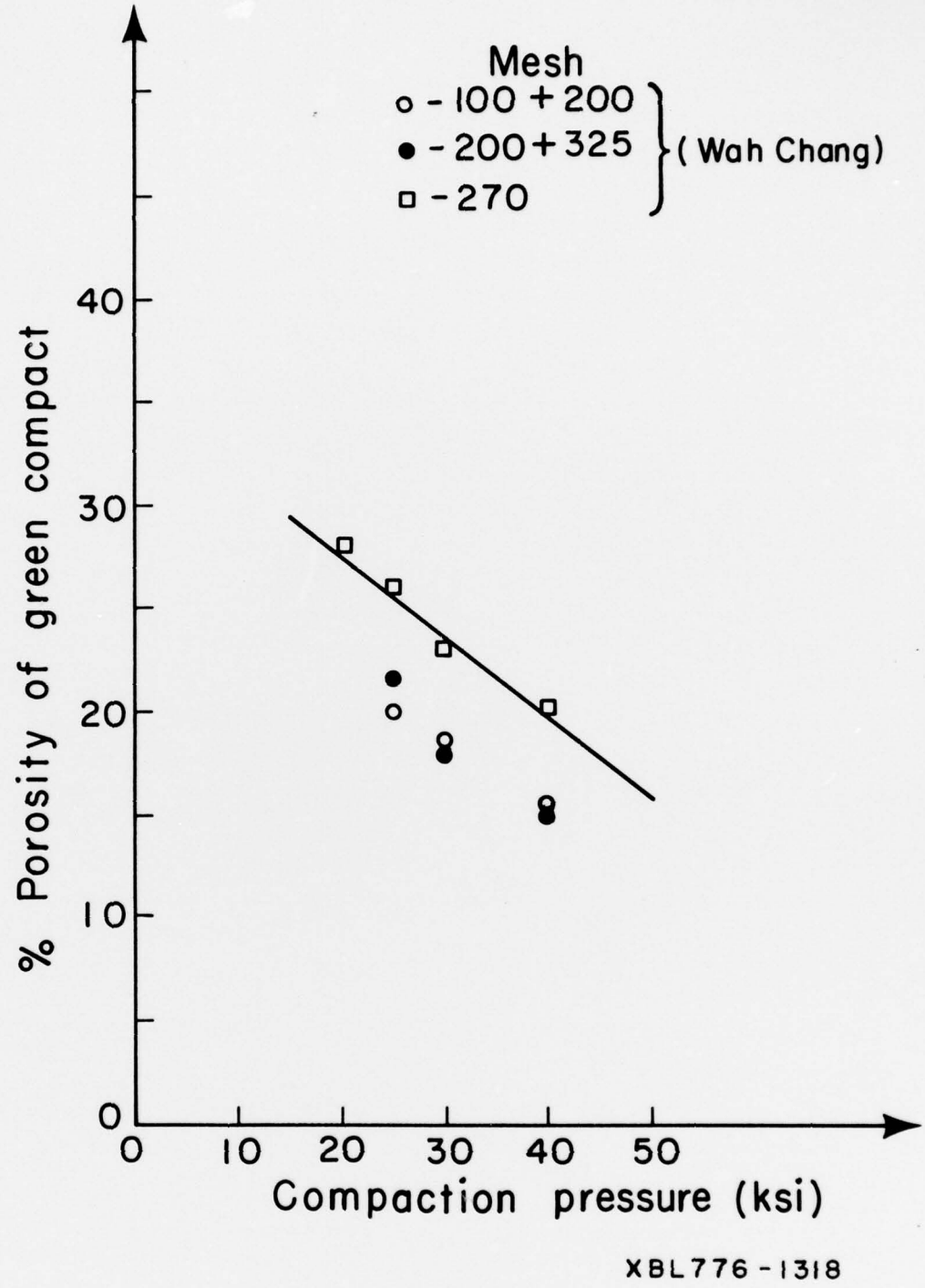

Figure 2. Green porosity vs. isostatic compaction pressure for different powders.

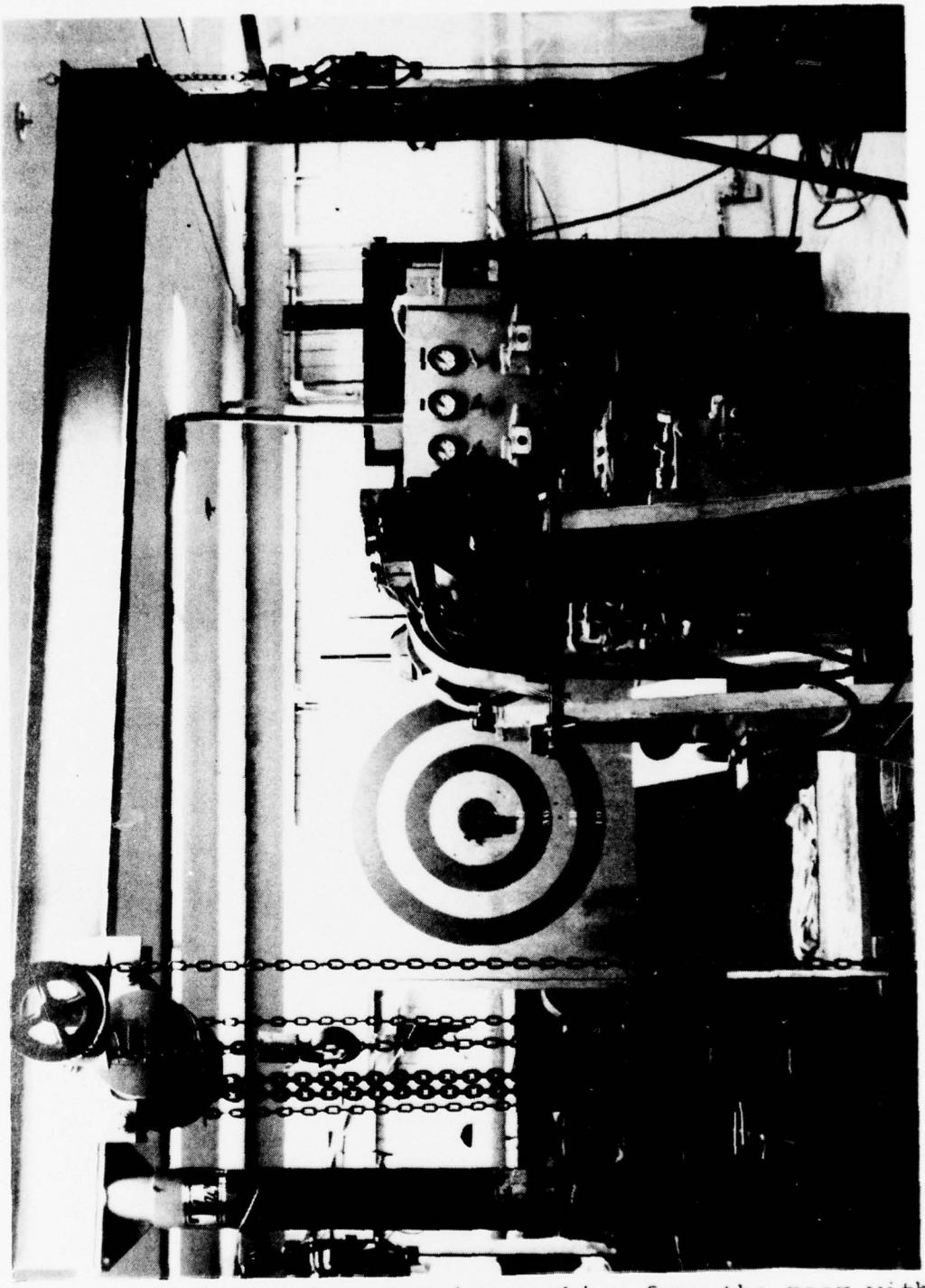

Figure 3. Hydrostatic extrusion machine from the rear with associated equipment.

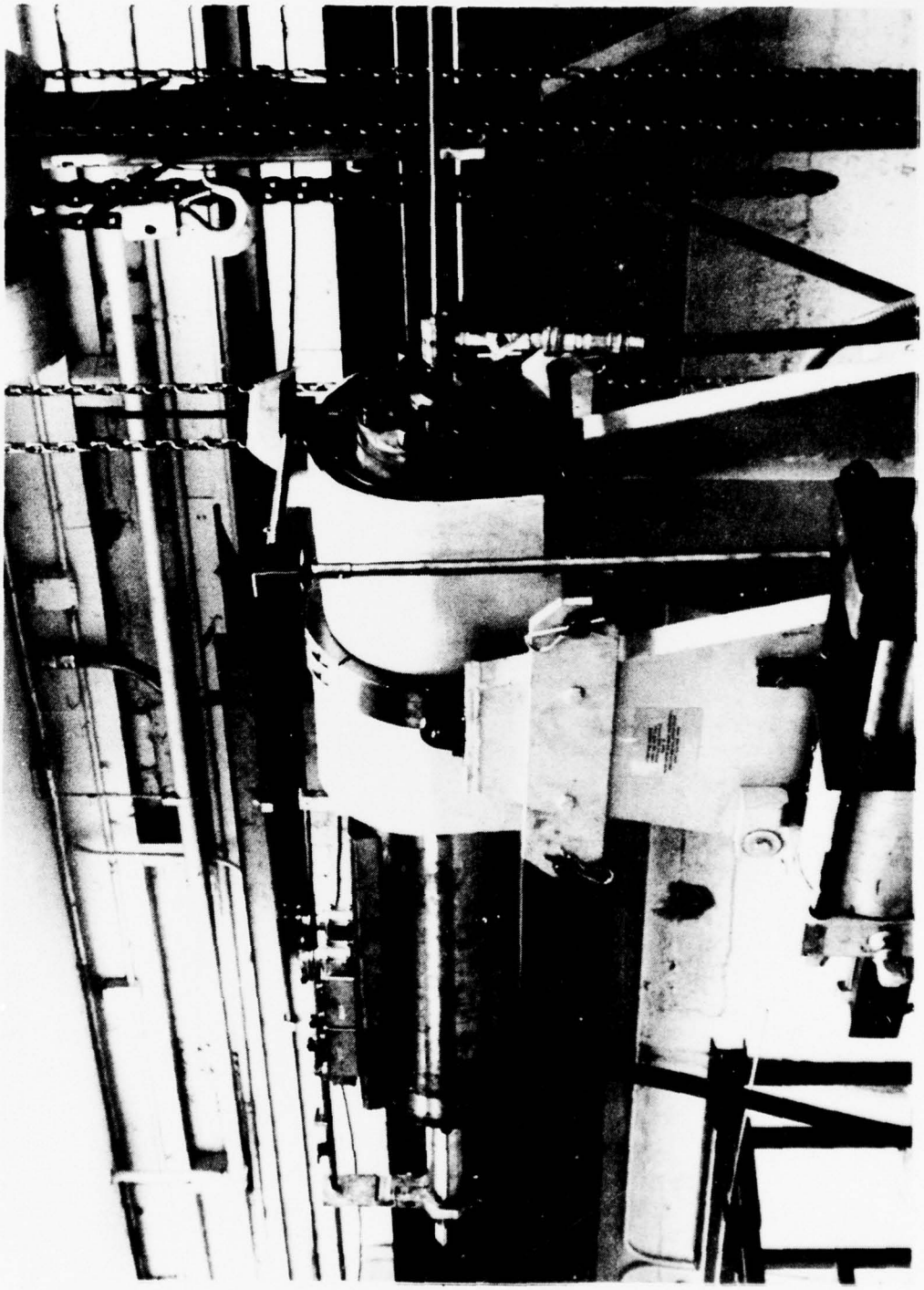

Figure 4. Side view of hydrostatic extrusion machine with cooling system attached.

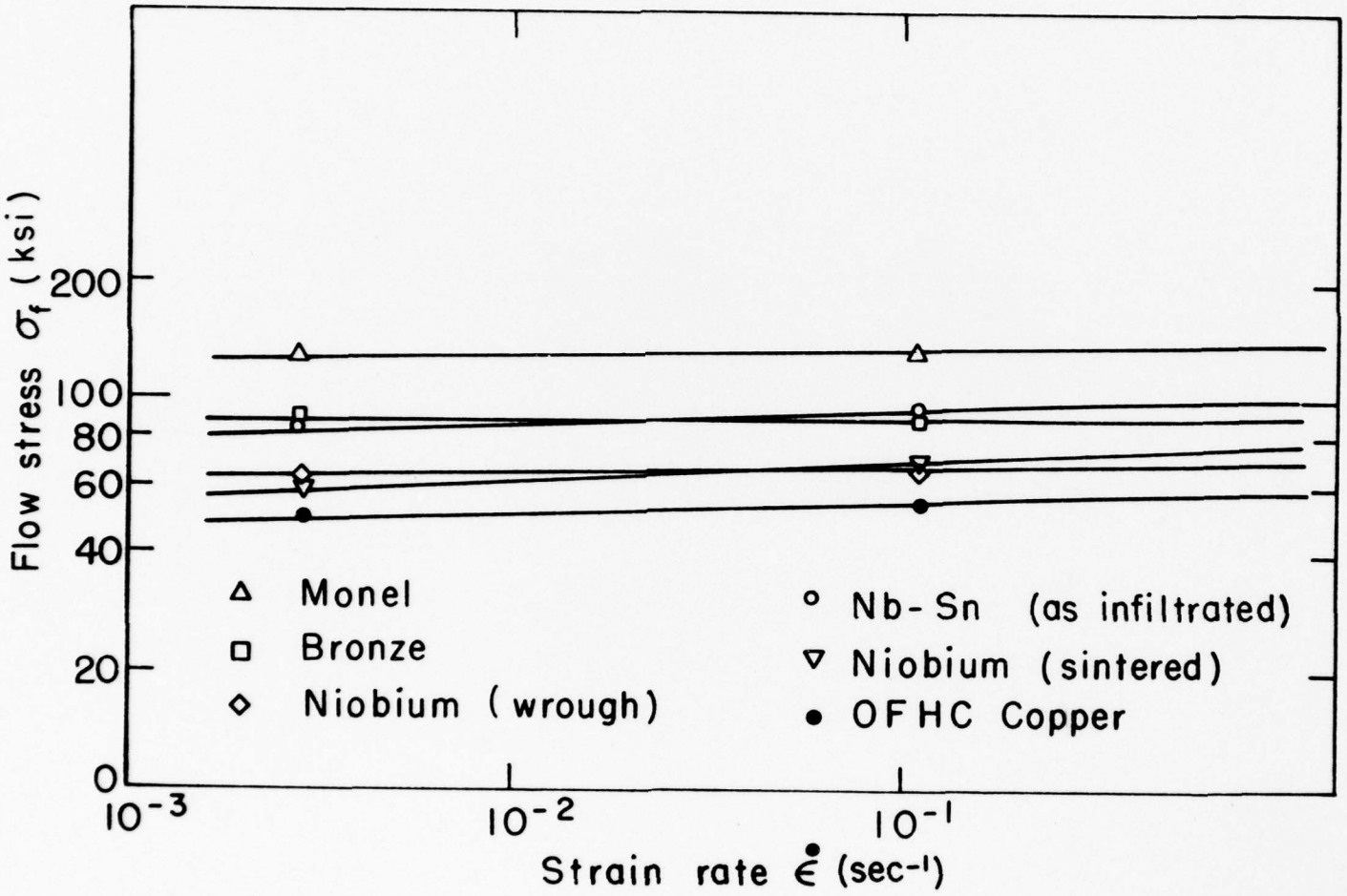

Figure 5. Log-log graph of flow stress vs. strain rate.

Figure 6. Comparison of billet designed to Avitzur's criterion; bottom, to that not designed to his criterion.

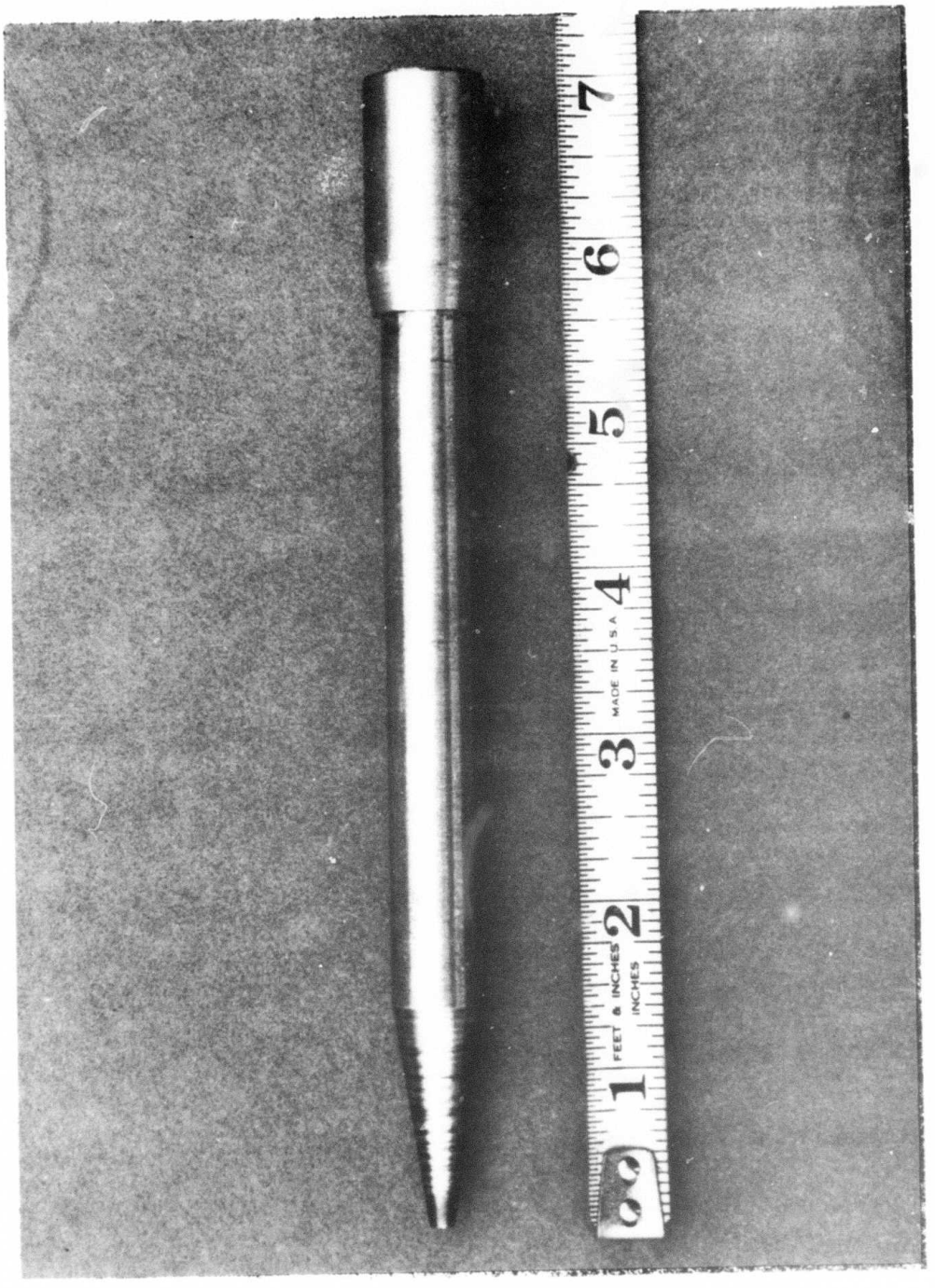

Figure 7. Billet No. 5.

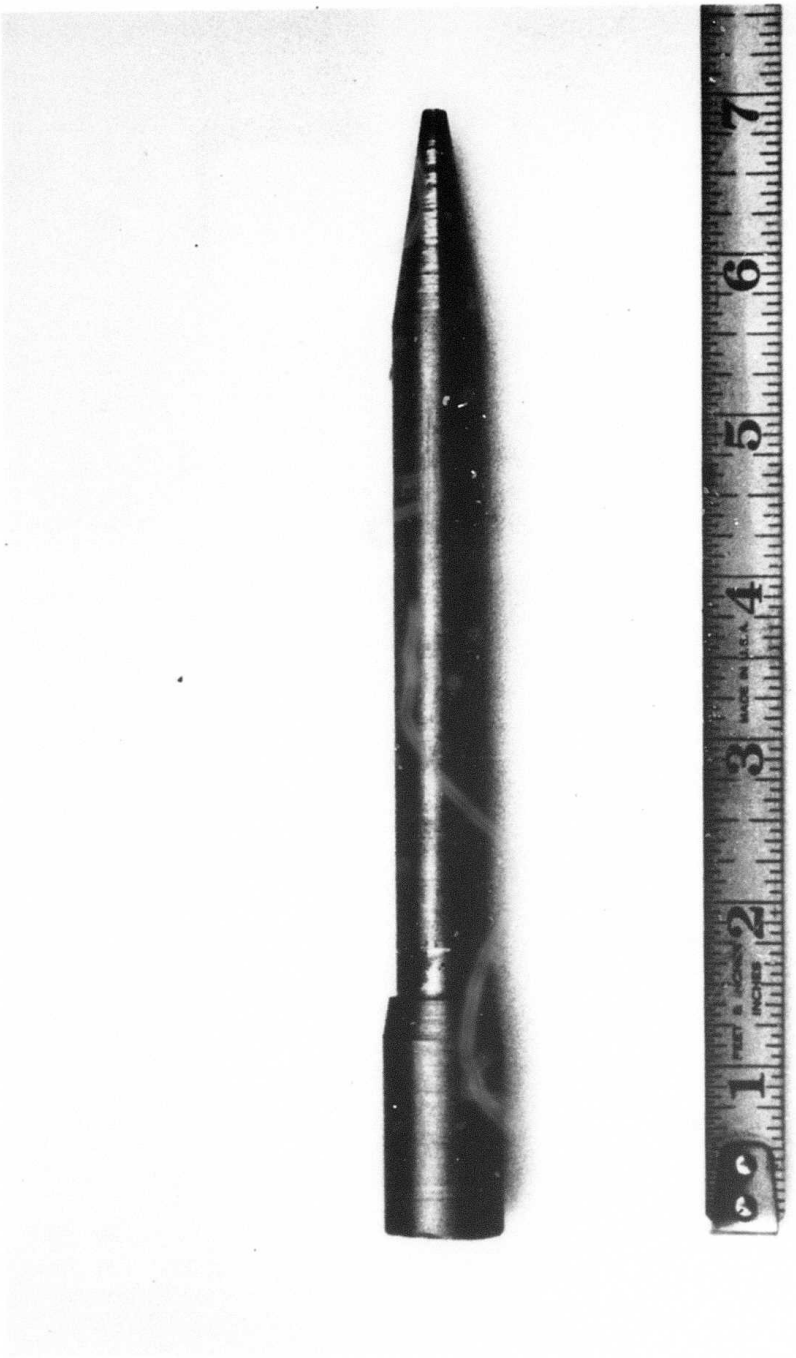

Figure 8. Billet No. 8.

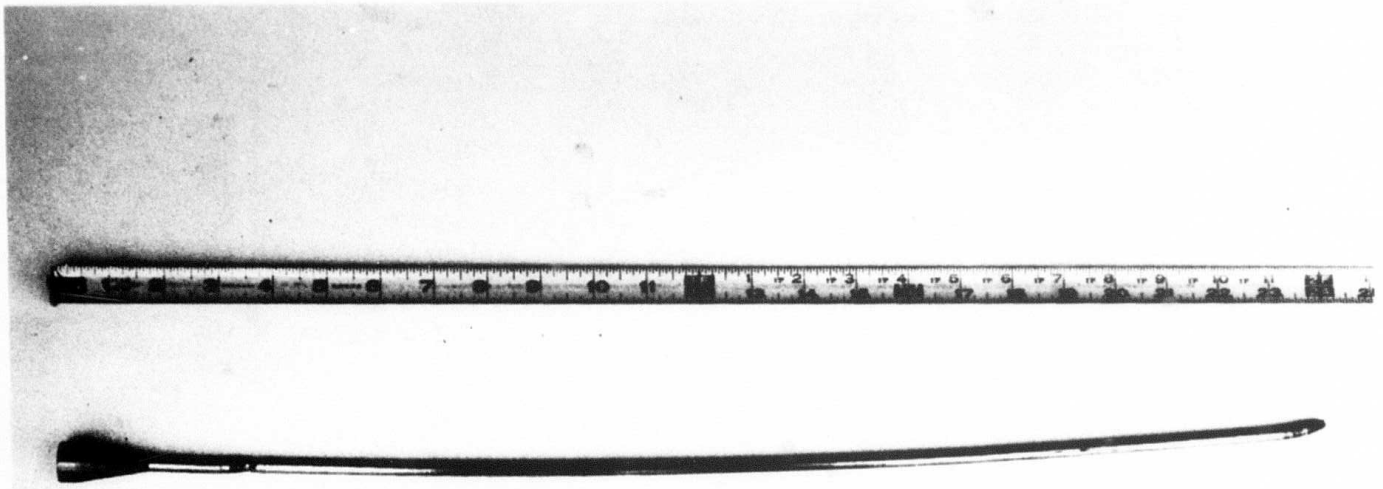

Figure 9. Extrusion of billet No. 8.

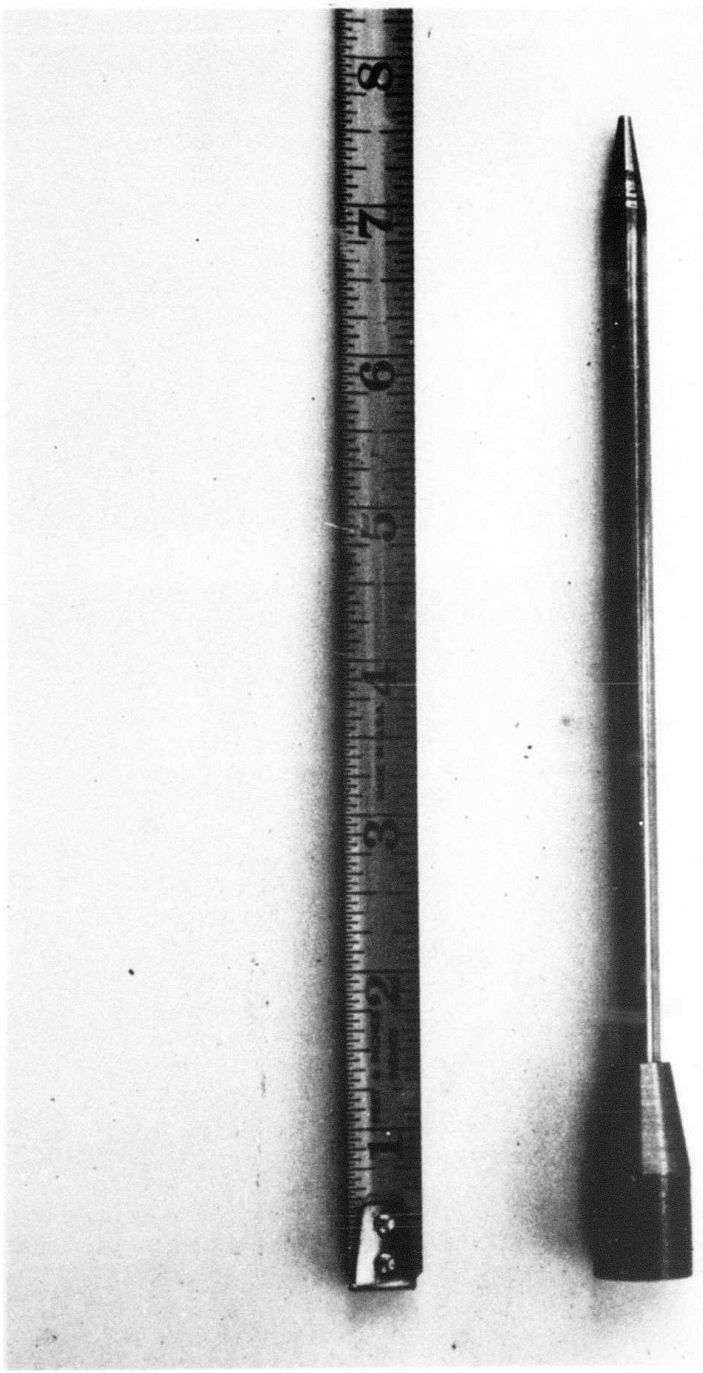

Figure 10. Billet made form extrusion of billet No. 8.

Figure 11. Extrusion of billet No. 6.

Figure 12. Extrusion of billet No. 5.

Figure 13. Extrusion of billet No. 7.

Figure 14. Second extrusion of billet No. 8.

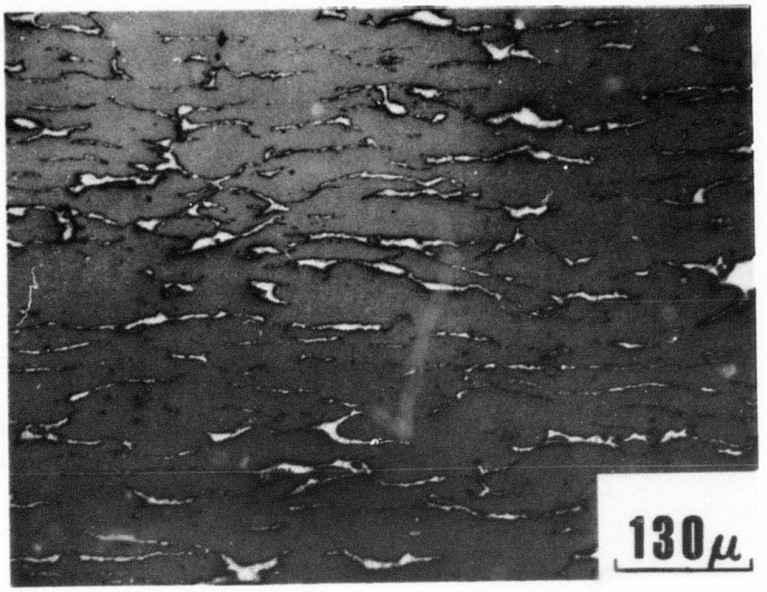

Figure 15. Longitudinal section of billet No. 5 after 69 reduction.

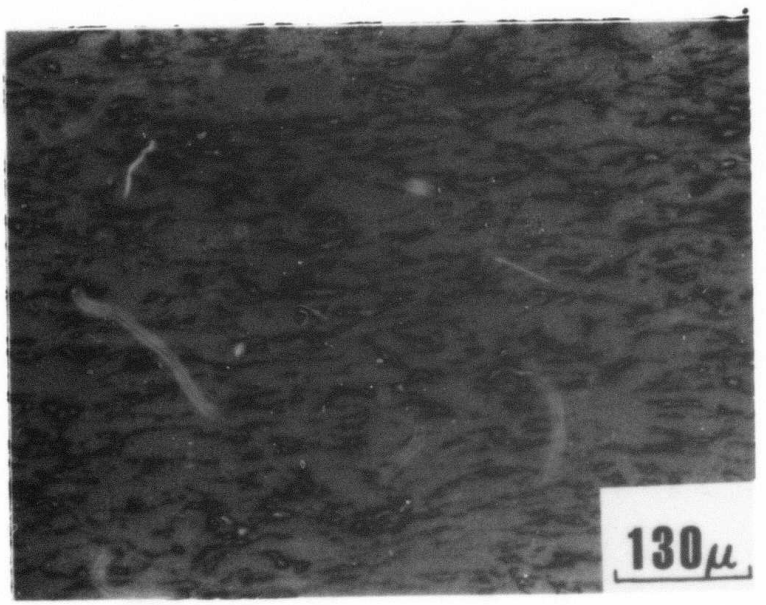

Figure 16. Longitudinal section of billet No. 8 after 77 reduction.

Figure 17. Longitudinal section of billet No. 8 after a total reduction of 95%.

Figure 18. Longitudinal section of billet No. 7 after a total reduction of 95%.

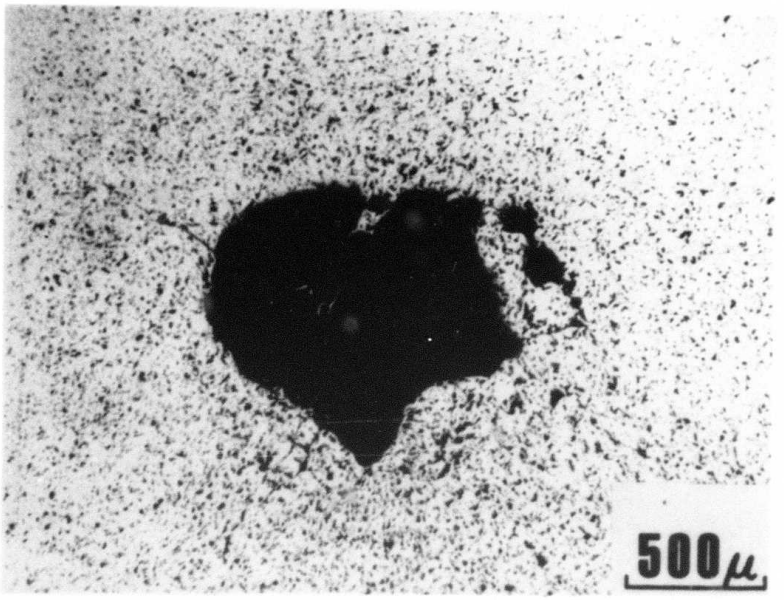

Figure 19. Cross section of an as-infiltrated rod wire drawn to a total reduction of 91%.

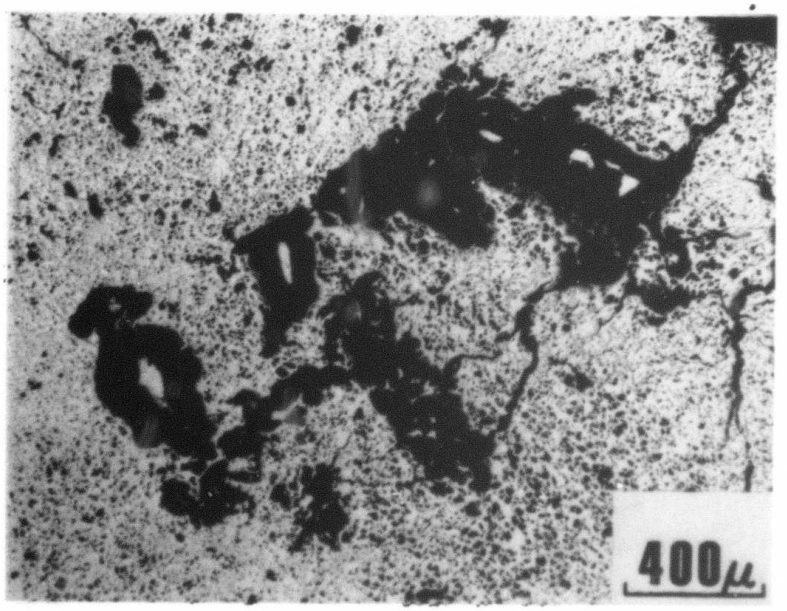

Figure 20. Cross section of billet No. 7 extruded to a total reduction of 95%.

REFERENCES

1. H. K. Onnes, Comm. Phys. Lab., University of Leyden, 119, 120, 122 (1911).
2. J. E. Kunzler, E. Buehler, F. S. L. Hsu and J. H. Wernick, Phys. Rev. Letters, 6, 89 (1961).
3. M. G. Benz, IEEE Trans. on Magnetics, Vol. Mag-2 No. 4, 760 (1966).
4. K. Tachikawa and S. Fukuda, Trans. Nat. Research Inst. Metals, 9, 39 (1967).
5. M. Suenaga and W. B. Sampson, Appl. Phys. Letters, 18, 584 (1971).
6. M. Suenaga and W. B. Sampson, Appl. Phys. Letters, 20, 443 (1972).
7. M. N. Wilson, C. R. Walters, J. D. Lewin and P. F. Smith, J. Physics D, 3, 1517 (1970).
8. M. R. Pickus and J. L-F. Wang, Paper presented at the International P/M Conf. 1976, LBL 5121, May 1976.
9. B. N. P, Babu, M. S. Thesis, LBL-437, December 1971.
10. T. N. Garrett, M. S. Thesis, LBL-448, December 1971.
11. K. Hemachalam, M. S. Thesis, LBL-1108, June 1972.
12. K. Hemachalam, D. Eng. Thesis, LBL-4181, February 1976.
13. Battelle Columbus Lab., Prog. Rep. "Experimental Evaluation of Hydrostatic Extrusion for the Fabrication of Multifilament Superconducting Wire", May 23, 1975.
14. J. M. Story, B. Avitzur and W. C. Hahn, Jr., of Eng. for Ind., 98 (3), August 1976.
15. P. W. Bridgman, J. Appl. Phys. 18, 246, 1947.
16. B. I. Beresnev, L. F. Vereschagin, Y. N. Ryabinin and L. D. Livshits, Some Problems of Large Plastic Deformation of Metals at High Pressures, Pergamon Press, 1963.
17. H. L. D. Pugh and A. H. Low, Jr., of the Inst. of Met., 93, 1964-1965.
18. B. Avitzur and W. M. Evans, Wire Jr., 2, 11, November 1969.

References (Cont.)

19. B. Avitzur, Wire Jr., 7, 11 November 1974.

20. Boaz Avitzur and B. Avitzur, Jr. of Eng. for Ind., 92, 2, May 1970.

21. W. C. Hahn, Jr., and B. Avitzur, Prog. Rep. "Forming of Compsite for Superconduting Rod", Inst. for Met. Form., Lehigh University, February 1972.

22. This work has not been published and therefore the design curves are not shown.

23. J. F. Alder and K. A. Phillips, J. Inst., Metals, 83, 80, 1954.

24. H. C. Rogers, R. C. Leech and L. F. Coffin, Jr., Bur. of Nav. Weap. Final Rep., Cont. No. 63=0671-c, July 1964.

25. E. R. Lambert and S. Kobayaski, Proc. Ninth Int'l MTDR Conf. University of Manchester, September 16-20, 1968.

(3) Hydrostatic Extrusion of 52100 Tool Steel

David Bourell

As part of our unitial efforts to test the hydrostatic extrusion machine and dies, we extruded 52100 tool steel. This was also done in conjunction with our program on the mechanical processing of high carbon steels. These materials are cold worked to produce high dislocation densities and subsequently annealed to form fine subgrains with a corresponding increase in yield strength.

Cold rolling has been the prominent method of deformation, but intermediate anneals are required after each introduction of about .4 true strain. Hydrostatic extrusion was suggested as an alternate mode of deformation which is capable of introducing large strains without intermediate annealing. The effectiveness of hydrostatic extrusion is shown in Figure 1. The material was successfully extruded to an area reduction of 60:1 or true strain of 4.12. We think further reductions would have been possible but at that time we were limited by die availability. As can be seen from the photograph, 8 passes were required to extrude to the full reduction.

Optical metallography was done and showed elongated ferrite grains with little or no change in cementite shape. Additionally, no cracks were visible in the material after the final reduction to 60:1.

As can be seen from Figure 2, the 0.2% yield stress for the 52100 tool steel continued to increase with increasing strain. We can infer from the graph that the material has not reached its saturation point and more deformation will lead to still higher yield strengths.

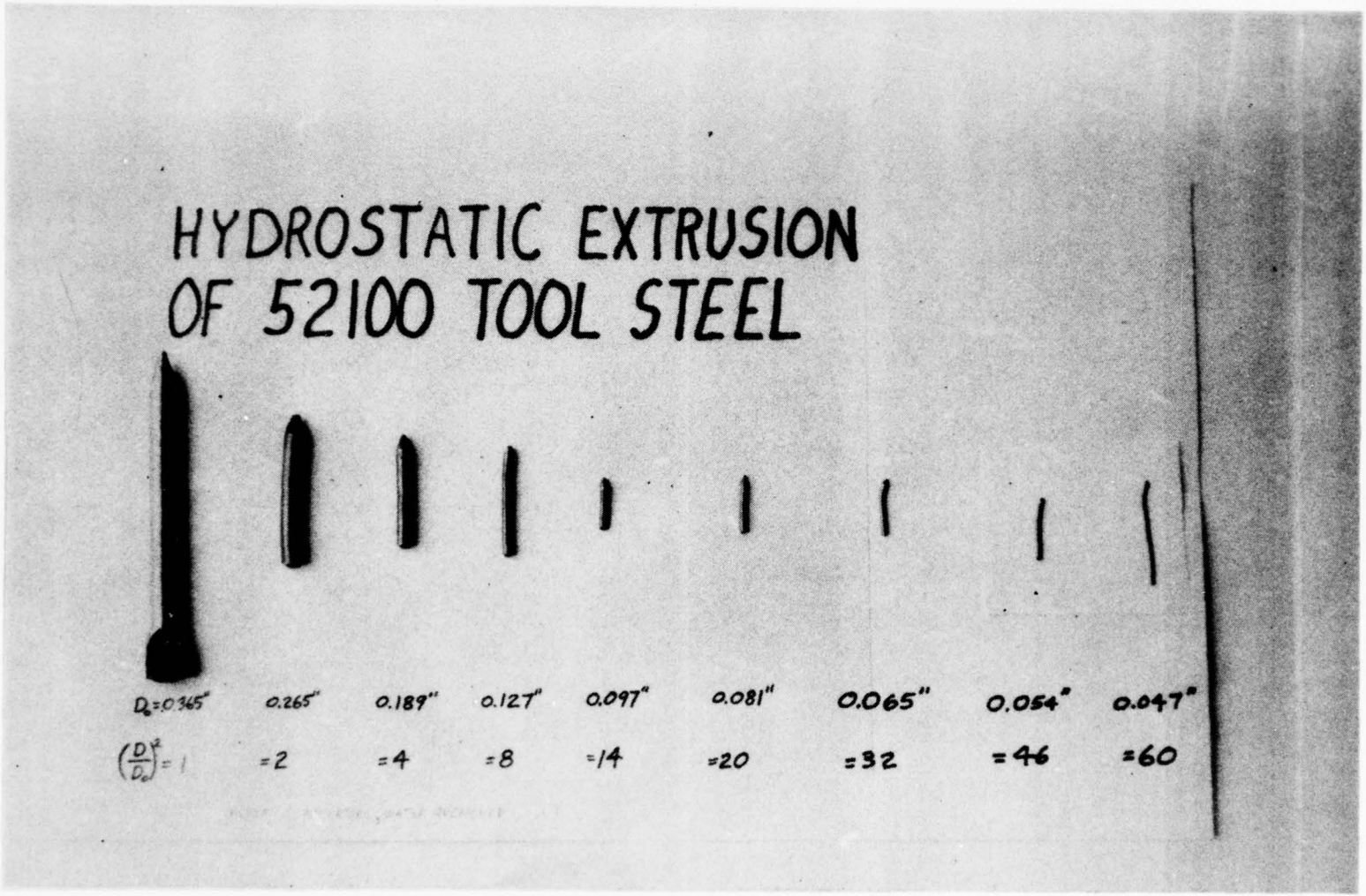

Figure 1. Room temperature multipass hydrostatic extrusion of 52100 tool steel. Total area reduction was 60:1.

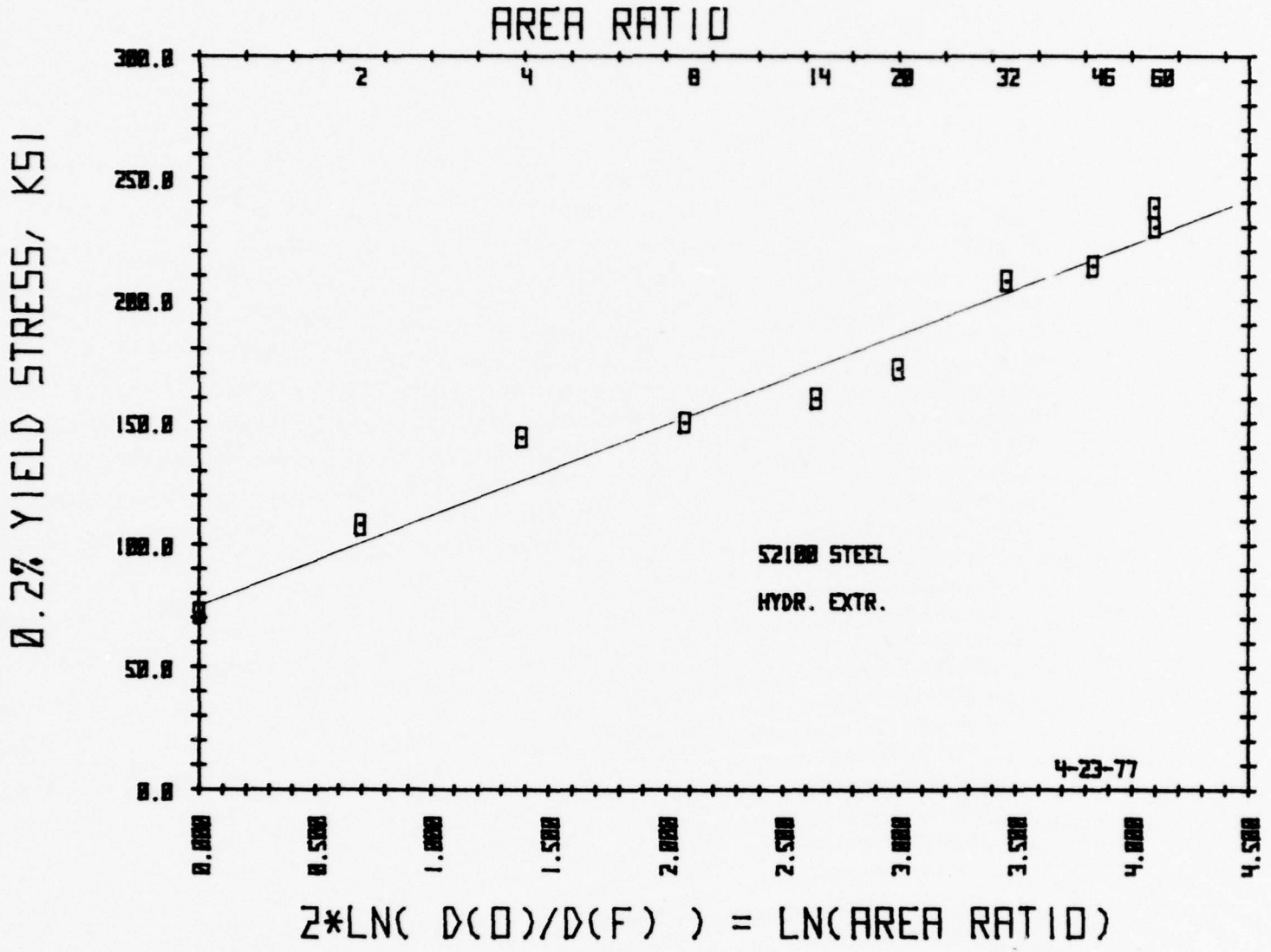

Figure 2. Plot of .2% yield stress after each successive reduction of 52100 tool steel. See Figure 1.

(4) Residual Stress Measurements in Hydrostatically Extruded Materials

Don Holcomb, W. D. Nix

We will attempt to measure experimentally the residual stresses in hydrostatically extruded rods. These results will then be compared to the residual stresses generated by the finite element program developed by our Applied Mechanics group. It is hoped that a good correlation will provide a check on the validity of the analytical work.

Residual stresses will be measured by two methods. As a first attempt we will measure only the longitudinal stresses that exist in the material. Parallel flats will be removed in small increments by milling along the longitudinal axis of the extruded rod. After each milling, the rod should undergo a small displacement in response to a force inbalance of the residual stresses. This will be measured as a strain using strain gages mounted on the rod. From the profile of longitudinal strains vs. radial position on the rod cross-section we will calculate a longitudinal residual stress field. The other technique will assume that both longitudinal and hoop residual stresses exist. The technique, known as the Sack's boring method, measures the dimensional change of both the diamter and length of the rod as the rod is bored incrementally to larger diameters. Again strains will be monitored by strain gages mounted on the specimen.

(5) A Fundamental Study of the Processing of Oxide Dispersion Strengthened Metals

Paul Gilman, W. D. Nix

Recent studies have shown that the high temperature mechanical properties of oxide dispersion strengthened superalloys depend on both the oxide dispersion and the grain shape developed during deformation processing. It is now established that the oxide dispersion determines an upper limit of creep strength that can be approached only if the grains are very large and highly elongated. However, in regard to the production of homogeneous oxide distributions and elongated grain structures in superalloys, studies have only produced certain empirical facts and the current processing methods are still largely guided by intuition. The overall goal of this research is to develop sufficient understanding of the mechanisms responsible for these desirable microstructures so that guidelines might be developed for producing these technologically significant oxide dispersion strengthened superalloys. In this regard our current research includes studies of both mechanical alloying, the repeated fracture and cold welding of alloy powders until each powder particle is of the appropriate alloy composition, and deformation processing of oxide dispersion strengthened metals.

Presently, the Al-Al_2O_3 system is being used to study the controlled variable of mechanical alloying such as attriting time, charge to ball ratio and the use of lubricants and milling atmospheres. We are especially interested in how these variables affect the final alloy powder size and morphology, the subsequent distribution of the dispersed oxides and the mechanical strength of the consolidated alloy. Hopefully by mechanical alloying the Al-Al_2O_3 system we will have produced an ODS metal with improved oxide distribution and content as well as being easier to consolidate as compared to contemporary Al-Al_2O_3 alloys.

In our study of the processing of oxide dispersion strengthened aluminum alloys

by mechanical alloying the hydrostatic extrusion press has been used and will continue to be utilized for two main reasons. First, hydrostatic extrusion of the mechanical alloyed aluminum will directionally work the material while simultaneously assuring theoretical density. This procedure closely simulates actual industrial methods of working oxide dispersion strengthened alloys. The second reason for hydrostatically extruding these alloys is to make sufficient bar stock so that subsequent tensile test specimens can be fabricated and recrystallization experiments can be performed.

C. THE ANALYSIS OF STRESS AND DEFORMATION DISTRIBUTIONS IN METAL FORMING PROCESSES

E. H. Lee, R. L. Mallett and R. M. McMeeking
Division of Applied Mechanics, Stanford University

In order to be able to predict the success of metal-forming processes, it is necessary to establish that metal-forming defects, such as the generation of internal or surface cracks, of strain localizations, or of high residual stresses, will not occur. This requires a complete stress and deformation analysis of the work-piece, including the billet before it enters the deforming region and the product after it leaves that region, since the history of the stress in an element of the work-piece is needed to predict the initiation and growth of a fracture crack, and stresses in the product constitute the residual stress distribution. Because the plastic strains generated in a metal-forming process are commonly large compared with the elastic-strain components, rigid-plastic theory is usually applied in the analysis of such processes. However the stress distribution cannot be evaluated in the rigid regions becaused the compatibility equations cannot be expressed in terms of stress. Thus elastic-plastic theory must be adopted for assessment of metal-forming processes and this calls for analysis of strains accurate to the order of 10^{-5} in the presence of strains of the order unity. In the elastic and unloaded regions, which can comprise most of the work-piece, strains must be evaluated to the order 10^{-5} in order to determine stresses to an accuracy of a few percent. An elastic-plastic finite-element program has been developed on this project to satisfy the objectives already stated. An analysis of the theory on which the program is based is given in the contract report reproduced in the following section. The finite element relations are based on a variational principal for the velocity field. Care is taken to include the convected and rotation terms in the representation of the incremental elastic-plastic

constitutive relations which express isotropic hardening based on a measured stress-strain curve. The finite element net is chosen to maintain accuracy while incorporating the effective incompressibility of the deformation when large plastic flow dominates elastic strain components.

Extrusion solutions have been carried out for chamber extrusion of both slabs in plane strain and axially symmetric rods through geometrically smooth dies having continuously turning tangent planes. Both frictionless contact between the work-piece and the die and nonzero coefficients of friction are considered. Figures 1, 2 and 3 show three cases of the distributions of longitudinal stress in elements initially at various lateral stations in the billet. The distance from the center plane or axis to the station in the billet, nondimensionalized with respect to the corresponding distance to the surface, is indicated for each curve. Each Figure is for a reduction of area of 25% and includes longitudinal stress in the billet before it enters the die, in the die and in the extrudate as indicated. It is seen that in each case the material near the center of the slab or rod experiences a tensile peak of longitudinal stress in the deforming region, $0 < x/a < 1.2$. The material near the surface of the extrudate has a peak in tensile longitudinal stress just as it leaves the die, $x/a \sim 1.6$. In the product, $x/a > 3$, there are tensile residual longitudinal stresses near the surface and compressive residual longitudinal stresses in the center of the extrudate and intermediate stresses at positions in between. When a steady state has been achieved, all stresses in the region dominated by it, $3 < x/a < 5$, are uniform in the longitudinal or extrusion direction, and, as expected from equilibrium considerations, the longitudinal direction is a principal direction for stress in this region. The aforementioned tensile peaks in longitudinal stress seem to be associated with the tendency for cracking to occur in extrusion. This failure can take the form of surface cracks formed on exit from

the die or central bursting inside the die. It has been observed experimentally that using less efficient lubrication can help to suppress central bursts. It is perhaps significant that the internal tensile peak in longitudinal stress in the deforming region of Fig. 2, $0 < x/a < 1.2$, is almost suppressed for slab extrusion where a Coulomb friction coefficient of 0.1 is used for contact between the metal and die. The frictionless rod extrusion shown in Fig. 3 involves a larger internal tensile peak of longitudinal stress, larger compressive residual longitudinal stress near the center and smaller tensile residual longitudinal stress near the surface of the product when compared with frictionless slab extrusion with the same area reduction of 25%.

A different situation occurs when the area reduction in axially symmetric extrusion is 0.69% which is about 1.5 times the yield strain in tension of the material considered. Plasticity is confined to the material near the surface of the billet and the residual longitudinal stresses are tensile in the center of the product and compressive near the surface. This reversal of residual stress states seems to offer the possibility of reducing residual stresses in a die with a slight taper after the material has passed through a die with a large area reduction. Calculations of the type presented offer the means of exploring such possibilities analytically.

The development, illustrated by the examples cited of the feasibility of carrying out complete stress and deformation analyses of metal forming processes, offers great promise in the application of basic theory to improvement in the design and selection of operating characteristics of such processes. This approach provides the opportunity to introduce fracture criteria to assess the onset of fracture in the work-piece since the history of the stress in each material element as it passes through the process can be determined. A particularly

serious extrusion defect which can be investigated in this way is central burst or chevroning, in which periodic cracks are generated across the center-line of an extrusion. This is a particularly difficult defect to detect since no evidence of its existence may appear on the surface of the product. We have shown that the currently commonly accepted theory of this defect is unsatisfactory* , and that application of the type of theory developed on this project is needed for a soundly based investigation of the phenomenon.

The calculations carried out so far have comprised a progression of increasingly difficult examples leading towards solution of the hydrostatic extrusion process. Most of the problems have been overcome, but we still have to include the influence of the unconstrained surface of the billet driven by fluid pressure in contrast to conventional extrusion in which contact with the cylinder and piston prescribes certain components of the motion of the billet surface. When this program is completed we will be able to determine analytically and in detail the effect of hydrostatic extrusion on product characteristics in contrast to conventional extrusion, for example the influence of the hydrostatic state of stress in the billet on the evolution of plastic flow and the resulting residual stresses. It is expected that such calculations will generate much greater confidence in the selection of optimum conditions for metal forming processes.

*E. H. Lee and R. M. McMeeking, "On a theory of central burst or chevroning defects in drawing and extrusion", SUDAM Rep. No. 77-1, Division of Applied Mechanics, Department of Mechanical Engineering, Stanford University, 1977. To appear in the Transactions of ASME, Journal of Engineering for Industry.

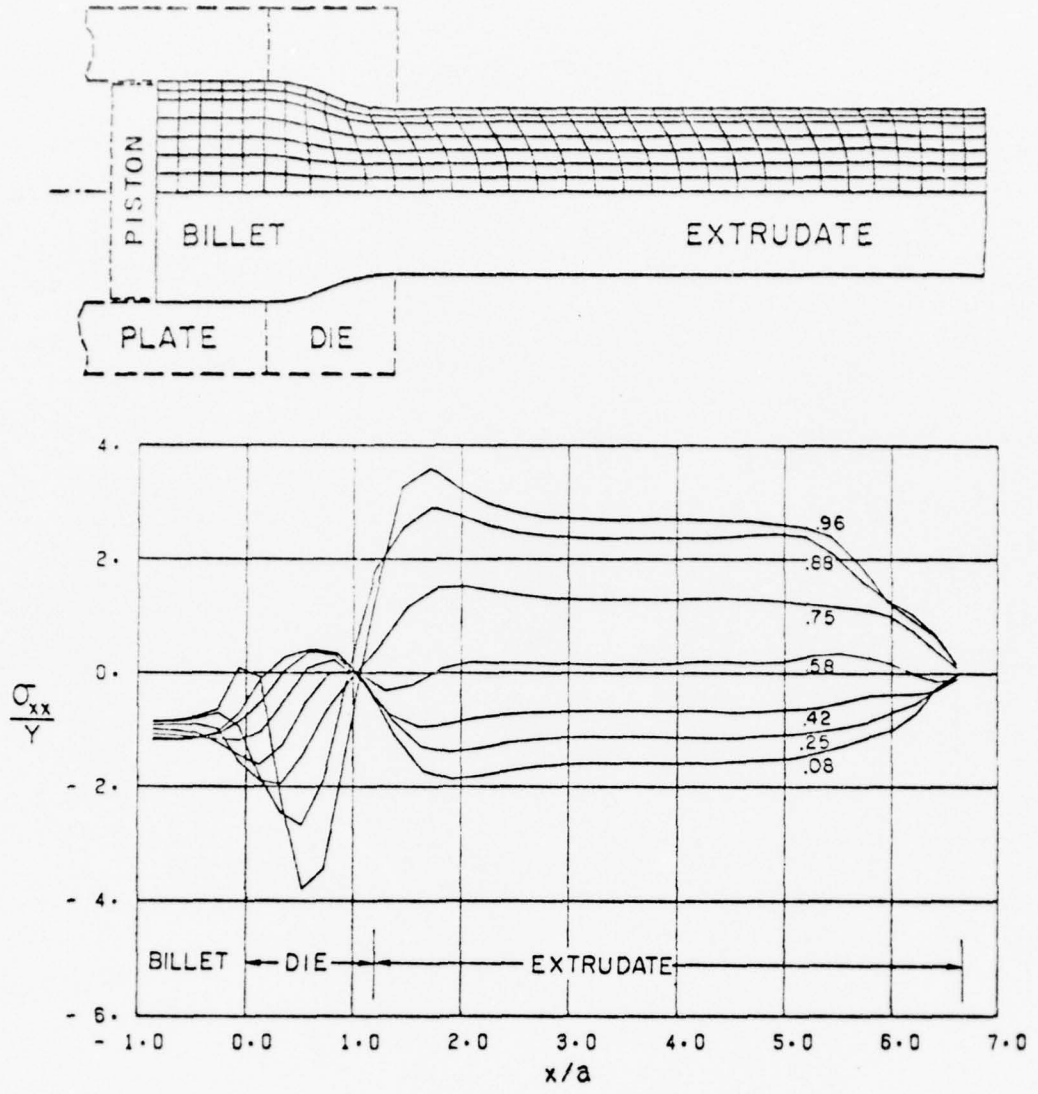

Figure 1. Longitudinal variation of normalized longitudinal stress at 7 lateral stations for frictionless plane strain extrusion with 25% thickness reduction.

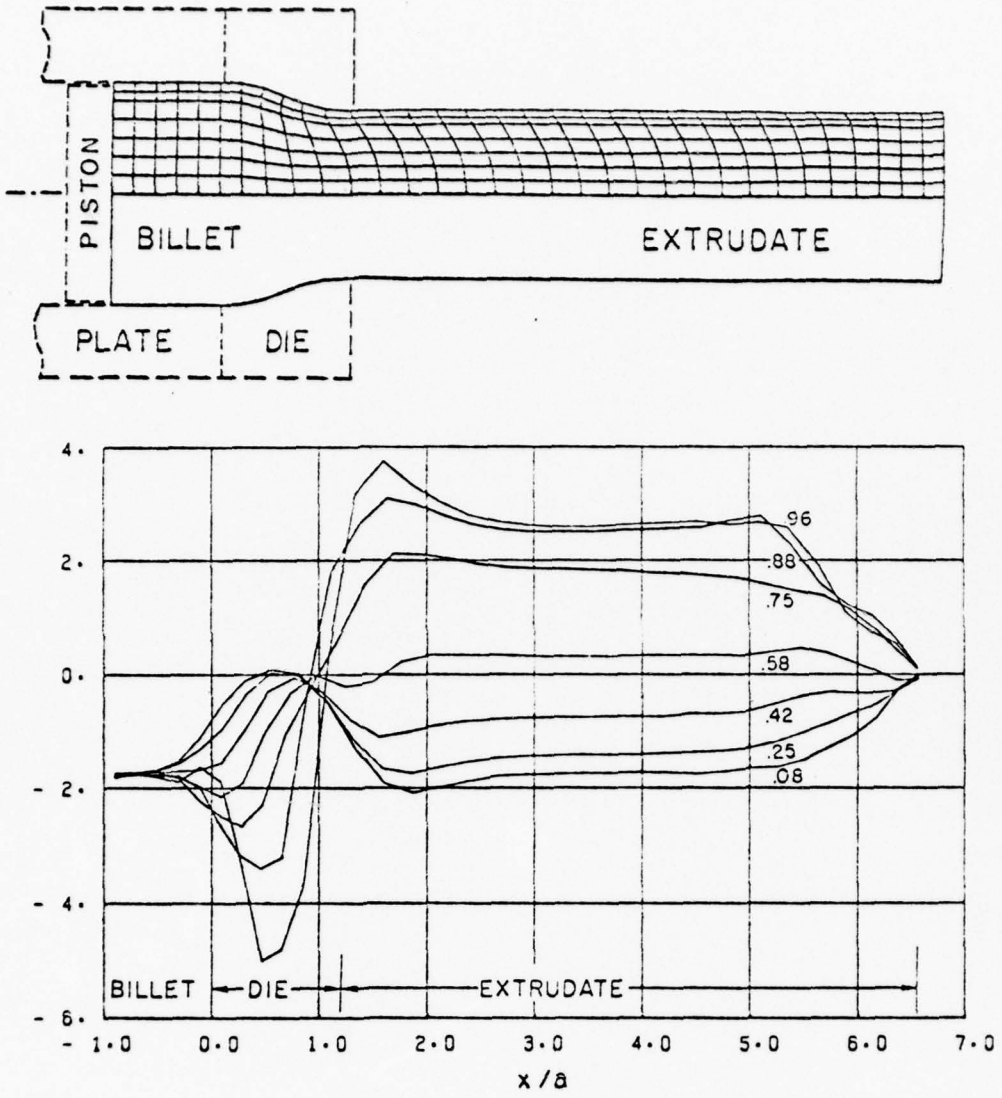

PLANE STRAIN CHAMBER EXTRUSION

$b/a = 0.75$, $\mu = 0.1$

Figure 2. Longitudinal variation of normalized longitudinal stress at 7 lateral stations for plane strain extrusion with 25% thickness reduction and $\mu = 0.1$ friction coefficient.

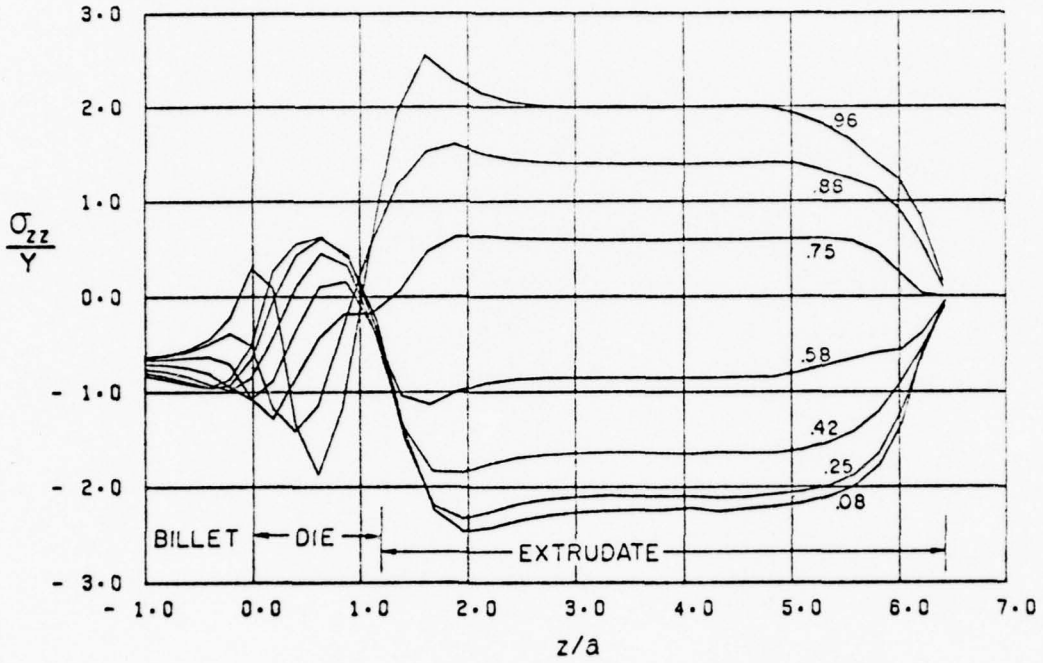

Figure 3. Axial variation of normalized axial stress at 7 radial stations for frictionless axisymmetric extrusion with 25% area reduction.

D. THE BASIS FOR AN ELASTIC-PLASTIC CODE*

E. H. Lee, Stanford University

Abstract

A complete stress-analysis of a metal-forming process is necessary in order to assess the onset of metal-forming defects such as the initiation of internal or surface cracks or the generation of residual stresses, and this demands elastic-plastic analysis. This report comprises comments on the plasticity theory formulation needed for a finite-element computer code designed for the analysis of metal forming processes. J. R. Rice has pointed out the importance of convection and rotation terms in the definition of stress-rate for inclusion in elastic-plastic constitutive relations, and that the development of uniqueness and stability analysis by R. Hill provides a convenient vehicle for including these effects. The development of these concepts is described and how they generate a convenient variational principle to form the basis of an elastic-plastic code to analyze metal forming.

---

*This report is taken from notes prepared for the Centre International des Sciences Mechanique Course: Engineering Plasticity II, arranged by Professor Lippmann of the Technische Universitat Munchen. Lecture notes of the Course will be published on behalf of CISM by Springer Verlag.

The Basis for an Elastic-Plastic Code

1. Introduction

For satisfactory analytical assessment of metal forming problems, it is necessary to evaluate the varying stress distribution throughout the work-piece since forming defects, such as the development of internal cracks, depend on stress history, and residual stresses can be important in deciding the utilization of a formed part. Elastic characteristics usually play an essential role in the determination of stress, even in combination with extensive plastic flow which may involve strains a thousand times elastic strain magnitudes. Thus analysis of metal forming problems for such assessments must be based on elastic-plastic theory. The same is true for other stress analysis problems when plastic flow occurs, unless plastic flow is occurring simultaneously throughout the entire body throughout the duration of the process, in which case plastic-rigid analysis is adequate.

Because plasticity laws are incremental in nature, they result in relations between stress-rate and strain-rate, or equivalently in numerical evaluations, between stress and strain increments. For the rate-independent laws usually adequate at temperatures low compared with the melting temperature, linear relations between stress-rate and strain-rate arise. When plastic flow is taking place, the coefficients are functions of the current stress for the common laws and below the yield

stress the elastic laws apply in incremental form. Because of the structure of these laws, elastic-plastic problems are commonly solved in terms of equations for stress-rates and strain-rates, containing stresses as coefficients. Consider the solution to have been computed up to the time t. After a time step forward, Δt, the solution for rates gives the stress at time $t + \Delta t$ in the form $\underset{\sim}{\sigma}(t) + \dot{\underset{\sim}{\sigma}}\Delta t$, and similarly for other variables. $\dot{\underset{\sim}{\sigma}}$ is the appropriate stress-rate. Then a new time step can be taken and the process repeated.

Extensive studies of the application of such laws to stability and uniqueness of solutions have been made by Hill (see, for example [1], [2], [3]* where he shows that care in the selection of stress definitions and stress-rate and strain-rate expressions is important for a satisfactory development of the theory. Rice [4] has pointed out that such questions are also important in developing a satisfactory theoretical basis for elastic-plastic stress analysis, particularly in the common circumstance that the tangent modulus in plastic flow is of the order of the stress. Convected and rotation terms then become important in the stress-rate expression, and analogously stress variables should be selected so that the influence of rate of deformation of the boundaries of the body does not complicate the variational principle commonly used to replace the equilibrium equations for evaluation of solutions. This requirement can be achieved by using the unsymmetric nominal stress

*Numbers in square brackets refer to the bibliography.

(Piola-Kirchoff I) in which the stress is defined as force per unit undeformed area. The variational principle then involves an integral over the undeformed body which is fixed.

Plastic flow is essentially a fluid type phenomenon which can be most conveniently expressed in terms of the current configuration of the material. Thus a reference configuration which remains invariant throughout the motion is not appropriate and so the configuration at time t is adopted as the reference state for evaluation of the deformation from t to $t + \Delta t$, where Δt is sufficiently small for adequacy of first order theory.

The framework described above provides a satisfactory foundation for a finite-element elastic-plastic code as discussed by McMeeking and Rice [5]. In effect, by choosing the current configuration as the reference state the Cauchy stress (or true stress in Cartesian coordinates) the unsymmetric nominal stress (Lagrange or Piola-Kirchhoff I) and the symmetric nominal stress (Kirchhoff or Piola-Kirchoff II) all have identical values at the current time which simplifies utilization of the appropriate stress for the appropriate component of the calculation. Although the stress components themselves are identical, rates of change of the different stresses are not the same.

2. Development of the Theory

Following Hill [2] and using for the most part his notation, we consider the unsymmetric nominal stress (variously referred to as Lagrange or Piola-Kirchoff I) s_{ij} defined so that the jth component of the force transmitted across a deformed element, which in the initial or

reference state had area $\overset{\circ}{dS}$ and unit normal $\overset{\circ}{\nu}_i$, is

$$\overset{\circ}{dS}\,\overset{\circ}{\nu}_i\, s_{ij} = dF_j \tag{1}$$

Hill considers (p. 214 of [2]) rate or flow type constitutive laws of the form

$$\dot{s}_{ij} = \frac{\partial E}{\partial(\partial v_j/\partial X_i)} \tag{2}$$

where X_i are rectangular Cartesian coordinates in the initial or reference configuration, E is a homogeneous function of degree two in the velocity gradients, $\partial v_j/\partial X_i$, and where $\dot{s}_{ij}$ is the partial time derivative at fixed $\underset{\sim}{X}$, i.e. a material derivative at a particle. The velocity $v_j(\underset{\sim}{X},t)$ gives the distribution at time t expressed in the initial coordinates of the corresponding material points (note that a tilde under a symbol denotes a vector or tensor in absolute notation).

Boundary value problems are considered in which for a volume $\overset{\circ}{V}$ in the reference state, at time t stress rates $\dot{s}_{ij}(\underset{\sim}{X},t)$ and velocities $v_i(\underset{\sim}{X},t)$ are sought for prescribed nominal traction rates $\dot{F}_j$ over the part of the surface $\overset{\circ}{S}_F$, velocity v_j over the remainder of the surface $\overset{\circ}{S}_v$ and body force rates $\dot{g}_j$ per unit initial volume. Then the variational principle

$$\delta\Big[\int_{\overset{\circ}{V}} E\, d\overset{\circ}{V} - \int_{\overset{\circ}{S}_F} \dot{F}_j v_j d\overset{\circ}{S} - \int_{\overset{\circ}{V}} \dot{g}_j v_j d\overset{\circ}{V}\Big] = 0 \tag{3}$$

in the class of continuous differentiable velocity fields satisfying the velocity boundary condition on $\overset{\circ}{S}_v$, characterizes the solution, for it yields the equilibrium equations

$$\frac{\partial \dot{s}_{ij}}{\partial X_i} + \dot{g}_j = 0 \tag{4}$$

and the boundary traction rate condition

$$\mathring{\nu}_i \dot{s}_{ij} = \dot{F}_j \tag{5}$$

for nominal stress, s_{ij}, and the reference geometry.

In writing the elastic-plastic constitutive relation, we wish to associate the velocity gradient in (2) with the rate of deformation or velocity strain:

$$D_{ij} = \tfrac{1}{2} \left(\frac{\partial v_i}{\partial x_j} + \frac{\partial v_j}{\partial x_i}\right) \tag{6}$$

where x_i are Cartesian coordinates expressing the position of particles in the deformed body

$$x_i = x_i(X,t) \tag{7}$$

Thus to permit simultaneous use of (3) and the plasticity laws expressed in the usual form of rate of deformation of the current configuration, Hill takes the current configuration to be the reference state, and hence

$$X_i = x_i(X,t) \tag{8}$$

for a particular t. The theory is expressed in this form for evaluation of $\dot{s}_{ij}$ and v_j and hence the solution and configuration at $t + \Delta t$, which provides a new reference state for evaluation of the next time step Δt.

Note that at the instant t, when the current and reference configurations are identical, the nominal stress components s_{ij} are equal to the Cauchy or true stress components σ_{ij}, so that at this instant s_{ij} is symmetric.

The device of selecting the configuration at time t to be the reference state for evaluation of the solution at time $t + \Delta t$ thus permits simultaneous use of the convenient variational principle (3) in terms of nominal stress s_{ij} and a fixed geometry and the familiar plasticity laws expressed in terms of the Cauchy, or true stress, σ_{ij}.

By working with curvilinear convected coordinates, ξ^{α}, having an arbitrary configuration in the reference or initial state, Hill([2], p. 219 ff.) shows that the rate potential (2) follows from associated rate potentials for other stresses and stress rate expressions, some of which are more convenient for representing elastic-plastic laws.

Consider curvilinear coordinates ξ^{α} in the initial or reference state with base vectors $\overset{\circ}{\underset{\sim}{g}}_{\alpha}$. After deformation as shown in Fig. 1 these become $\xi^{\alpha'}$, having the same values for the same material particles as ξ^{α}. Then $\xi^{\alpha'}$ are the convected coordinates and the corresponding base vectors are $\underset{\sim}{g}_{\alpha'}$, which are $\overset{\circ}{\underset{\sim}{g}}_{\alpha}$ deformed by the motion. Then the Cauchy stress tensor $\underset{\sim}{\sigma}$ has contravariant components $\sigma^{\alpha'\beta'}$ in convected coordinates such that the force $\underset{\sim}{dF}$ transmitted across an element of the deformed body of area dS and unit normal vector $\nu_{\alpha'}$ is given by:

$$\underset{\sim}{dF} = \sigma^{\alpha'\beta'} (\nu_{\alpha'} dS) \underset{\sim}{g}_{\beta'} \tag{9}$$

Since the primed coordinates are made evident by the notation ν and $\underset{\sim}{g}$ for normal and base vectors in the deformed state, the primes will usually be dropped hereafter, for $\xi^{\alpha} = \xi^{\alpha'}$ denote the same material point.

For the Lagrange or Piola-Kirchhoff I stress, s_{ij}, the force computed in the reference frame is that actually acting across the deformed element (see Fung [6] p. 437 for the usual definition in Cartesian coordinates). For the present consideration of convected coordinates, the expression for $\underset{\sim}{dF}$ thus takes the form

$$\underset{\sim}{dF} = s^{\alpha\beta}(\overset{\circ}{\nu}_{\alpha}\, \overset{\circ}{dS})\underset{\sim}{\overset{\circ}{g}}_{\beta} \tag{10}$$

For the Kirchhoff or Piola-Kirchhoff II stress, τ_{ij}, Fung points out that the force vector computed in the reference frame must be transformed by the motion to give the actual force across the deformed element, so that for convected coordinates

$$\overset{\circ}{\underset{\sim}{dF}} = \tau^{\alpha\beta}(\overset{\circ}{\nu}_{\alpha}\overset{\circ}{dS})\underset{\sim}{\overset{\circ}{g}}_{\beta}$$

becomes

$$\underset{\sim}{dF} = \tau^{\alpha\beta}\, \overset{\circ}{\nu}_{\alpha}\overset{\circ}{dS})\underset{\sim}{\overset{\circ}{g}}_{\beta} \tag{11}$$

Nanson's relation for area element:

$$\rho\nu_{\alpha}dS = \overset{\circ}{\rho}\overset{\circ}{\nu}_{\alpha}\overset{\circ}{dS} \tag{12}$$

then gives, using (9) and (11)

$$\tau^{\alpha\beta} = \frac{\overset{\circ}{\rho}}{\rho}\sigma^{\alpha\beta} = J\,\sigma^{\alpha\beta} \tag{13}$$

where J is the Jacobian of the transformation from the reference to the deformed state, i.e.

$$\underset{\sim}{g}_\alpha \cdot \underset{\sim}{g}_\beta \times \underset{\sim}{g}_\gamma = J(\overset{\circ}{\underset{\sim}{g}}_\alpha \cdot \overset{\circ}{\underset{\sim}{g}}_\beta \times \overset{\circ}{\underset{\sim}{g}}_\gamma) \tag{14}$$

Fig. 2 shows the particular situation when the ξ^α coordinates in the reference frame are Cartesian, X^α. The Cartesian coordinates representing points in the deformed body according to the point transformation, equ. (7), are x^i. The usual definition of the Kirchhoff or Piola-Kirchhoff II stress (see Fung [6] p. 439) is given in terms of this point transformation. From equ. (7), define the deformation gradient

$$\underset{\sim}{F} = \frac{\partial x^i}{\partial X^\alpha} \tag{15}$$

Then the Piola-Kirchhoff II stress $\underset{\sim}{\tau}$ is given in terms of the Cauchy stress in Cartesian coordinates $\underset{\sim}{x}$, $\overset{c}{\sigma}$ by

$$\underset{\sim}{\tau} = J \underset{\sim}{F}^{-1} \overset{c}{\underset{\sim}{\sigma}} \underset{\sim}{F}^{-1^T} \quad ([7] \text{ p. } 125) \tag{16}$$

where $J = \det(\underset{\sim}{F})$. This is in accord with (13) where $\sigma^{\alpha\beta}$ are the contravariant components of the Cauchy stress with respect to the convected coordinates $X^{\alpha'}$ for if $\overset{c}{\sigma}{}^{ij}$ are the Cartesian coordinates of $\underset{\sim}{\sigma}$ with respect to $\underset{\sim}{x}$, then the tensor change of variables law gives

$$\sigma^{\alpha'\beta'} = \frac{\partial X^{\alpha'}}{\partial x^i} \frac{\partial X^{\beta'}}{\partial x^j} \sigma^{cij} \tag{17}$$

in terms of the coordinate transformation from $\underset{\sim}{x} \to \underset{\sim}{X}'$ in the deformed geometry. Because of the property of convected coordinates that $X^\alpha = X^{\alpha'}$

for the same particle, (7) also expresses the coordinate transformation, and (13) and (17) are seen to be equivalent to (16). This connection has been pointed out by Nemat-Nasser [8]. Note that $s^{\alpha\beta}$ and $\tau^{\alpha\beta}$ are tensor densities and not absolute tensors, so that equations such as (2) are not pure tensor relations.

For rate independent constitutive relations the rate-potential function E in (2) is a homogeneous function of degree two. For the choice that the reference state is the current state, (2) follows from the existence of an associated rate potential function $F(\epsilon_{\alpha\beta})$, of the strain-rate components

$$\epsilon_{\alpha\beta} = \tfrac{1}{2}\,(v_{\alpha,\beta} + v_{\beta,\alpha}) \tag{18}$$

where $\underset{\sim}{v}$ is the velocity vector in the deforming body and the comma denotes covariant differentiation. This function generates $\overset{\cdot}{\tau}{}^{\alpha\beta}$ through

$$\overset{\cdot}{\tau}{}^{\alpha\beta} = \frac{\partial F}{\partial \epsilon_{\alpha\beta}} \tag{19}$$

where the superposed dot indicates time derivative of the convected components or convected derivative. This is equivalent to the partial time derivative at fixed X, or a material type derivative. The structure of (19) indicates that since $\underset{\sim}{\tau}$ is a tensor density, F is a scalar density and not an absolute scalar invariant.

A derivation of a relation needed in the following analyses to establish (2) is given in the Apperdix. It is the relationship between $\overset{\cdot}{s}{}^{\alpha\beta}$ and $\overset{\cdot}{\tau}{}^{\alpha\beta}$, which, for the particular choice of reference state mentioned, takes the form

$$\dot{s}^{\alpha\beta} = \dot{\tau}^{\alpha\beta} + \tau^{\alpha\gamma} v^{\beta}{}_{,\gamma} \tag{20}$$

Now from (19) and (20)

$$\dot{s}^{\alpha\beta} = \partial F/\partial(\epsilon_{\alpha\beta}) + \tau^{\alpha\gamma} v^{\beta}{}_{,\gamma}$$

multiplying both sides by $v_{\beta,\alpha}$ gives

$$\dot{s}^{\alpha\beta} v_{\beta,\alpha} = [\partial F/\partial(\epsilon_{\alpha\beta})]\epsilon_{\alpha\beta} + \tau^{\alpha\gamma} v^{\beta}{}_{,\gamma} v_{\beta,\alpha} \tag{21}$$

using (18) and the fact that $\tau^{\alpha\beta}$ is symmetric. Now $F(\epsilon_{\alpha\beta})$ is a homogeneous function of degree two since for plasticity (19) is rate independent, hence Euler's theorem for homogeneous functions permits us to write (21) in the form

$$\dot{s}^{\alpha\beta} v_{\beta,\alpha} = 2F(\epsilon_{\alpha\beta}) + \tau^{\alpha\gamma} v^{\beta}{}_{,\gamma} v_{\beta,\alpha} \tag{22}$$

Again using Euler's theorem, this is consistent with (2) in terms of convected coordinates if

$$\dot{s}^{\alpha\beta} = \partial E/\partial (v_{\beta,\alpha}) \tag{2a}$$

and

$$2E(v_{\beta,\alpha}) = 2F(\epsilon_{\alpha\beta}) + \tau^{\alpha\gamma} v^{\beta}{}_{,\gamma} v_{\beta,\alpha} \tag{23}$$

Equation (21) is a contracted scalar relation based on the tensor expression (20) and hence does not validate the tensor relation (2a) or (2). It merely prescribes the form of the rate-potential function E if such a function exists. Substitution of (23) into (2a) does yield (20) and hence establishes E as a homogeneous, second

degree, rate-potential function of $v_{\beta,\alpha}$ for the nominal stress rate $\dot{s}^{\alpha\beta}$.

A similar argument for the Cauchy stress $\sigma^{\alpha\beta}$ yields a trial potential function, which however fails to yield the correct expression for $\dot{\sigma}^{\alpha\beta}$ from the rate-potential equation. Hence a rate potential function does not exist in this case.

The laws of plasticity are normally obtained by measuring "true stress" and increments of strain defined in terms of Cartesian coordinates in the current configuration without rotations occurring. Since the theory must apply in the presence of rotations, their influence must not affect the stress rate term in the constitutive relation, hence a spin-invariant stress rate is needed, such as the Jaumann rate. We will work in terms of the configuration at time t, which is the reference configuration, and utilize Cartesian coordinates $\underset{\sim}{x}$.

In formulating the finite element theory for numerical analysis of elastic-plastic problems, we wish to use the variational relation (3) in terms of $\dot{s}_{ij}$ and a constitutive relation associated with (19) in terms of τ_{ij} since it can be conveniently associated with measurements of plasticity laws. We have seen that a law in the form (19) implies the validity of (2) and hence the variational principle. As pointed out in [5] this structure in terms of τ_{ij} leads to symmetric stiffness matrices in the finite element formulation which simplifies the numerical procedures.

Now the relationship between the nominal stress $\underset{\sim}{s}$ and the Cartesian true stress $\overset{c}{\underset{\sim}{\sigma}}$ is

$$\underset{\sim}{F}\,\underset{\sim}{s} = J\,\overset{c}{\underset{\sim}{\sigma}} \tag{24}$$

see, for example [7], p. 125, where the nominal stress is defined as the transpose of $\underset{\sim}{s}$ (or it can be deduced from (9), (10) and (17)). Taking the material derivative of (24), and noting that F and J are unity for coincident reference and current configurations, one obtains

$$\dot{s}_{ij} + s_{kj}\frac{\partial v_i}{\partial x_k} = \overset{c}{\sigma}_{ij}\frac{\partial v_k}{\partial x_k} + \overset{\cdot}{\overset{c}{\sigma}}_{ij} \tag{25}$$

The difference between the Jaumann derivative of $\overset{c}{\underset{\sim}{\sigma}}$ and its material derivative is the contribution of the rate of rotation of the axes which rotate with the body according to the anti-symmetric tensor angular velocity expression

$$\left.\frac{\partial v_i}{\partial x_j}\right|_A \tag{26}$$

where A denotes the anti-symmetric part. Using $\mathfrak{D}/\mathfrak{D}t$ to denote the Jaumann derivative, this determines (see Prager [9] p. 155)

$$\frac{\mathfrak{D}\overset{c}{\sigma}_{ij}}{\mathfrak{D}t} - \overset{\cdot}{\overset{c}{\sigma}}_{ij} = -\sigma_{ik}\left.\frac{\partial v_j}{\partial x_k}\right|_A - \sigma_{kj}\left.\frac{\partial v_i}{\partial x_k}\right|_A \tag{27}$$

Combination of (25) , (27) and (6) gives

$$\dot{s}_{ij} = \left(\frac{\mathfrak{D}\overset{c}{\sigma}_{ij}}{\mathfrak{D}t} + \overset{c}{\sigma}_{ij}\frac{\partial v_k}{\partial x_k}\right) - \left(\sigma_{ik}D_{jk} + \sigma_{kj}D_{ik}\right) + \sigma_{ik}\frac{\partial v_j}{\partial x_k} \tag{28}$$

Equation (13) defines $\tau^{\alpha\beta}$, the Kirchhoff stress, in terms of convected coordinates. Being a tensor density, definition for other coordinates is obtained by use of (17) suitably modified to incorporate the density term J . We have seen that experiments from which the laws

of plasticity were deduced involved "true stress" associated with Cartesian coordinates which, for plastic analyses, indicates the appropriateness of a Jaumann time-derivative associated with rotation of rectangular axes. Thus we need to utilize $\overset{c}{\tau}_{ij} = J \overset{c}{\sigma}_{ij}$ to incorporate the Jaumann derivative, and the first term in parenthesis in (28) can be written $\mathfrak{D}\overset{c}{\tau}_{ij}/\mathfrak{D}t$, since the derivative of the scalar density J is unaffected by rotation of axes, and at time t the instantaneous value of $J = 1$. Hill has stated ([2] p. 222) that the rate potential (19) implies a rate potential for the Jaumann derivative of $\overset{c}{\tau}_{ij}$, which provides computational advantages associated with the use of the Jaumann derivative of this stress variable.

Thus (28) takes the form:

$$\dot{s}_{ij} = \frac{\mathfrak{D}\overset{c}{\tau}_{ij}}{\mathfrak{D}t} - (\sigma_{ik}D_{jk} + \sigma_{kj}D_{ik}) + \sigma_{ik}\frac{\partial v_j}{\partial x_k} \tag{29}$$

Now combining (20) and (29)

$$\frac{\mathfrak{D}\overset{c}{\tau}_{ij}}{\mathfrak{D}t} = \dot{\tau}_{ij} + \sigma_{ik}D_{jk} + \sigma_{kj}D_{ik} \tag{30}$$

In view of (19) written for initial Cartesian coordinates, with $F(D_{ij})$ homogeneous of second order in the strain rates, multiplication of (30) by D_{ij} and using Euler's theorem gives

$$\frac{\mathfrak{D}\overset{c}{\tau}_{ij}}{\mathfrak{D}t} D_{ij} = 2F + \sigma_{ij}D_{jk}D_{ij} + \sigma_{kj}D_{ik}D_{ij} = 2F + 2\sigma_{ik}D_{ij}D_{jk} \tag{31}$$

which analogously to (21) for $\dot{s}^{\alpha\beta}$ provides a trial rate-potential function

$$G = F + \sigma_{ik}D_{ij}D_{jk} \tag{32}$$

assuming Euler's theorem. In a manner similar to that presented for $\overset{\cdot}{s}^{\alpha\beta}$, a third rate-potential function is thus established:

$$\frac{\mathcal{D}\overset{c}{\tau}_{ij}}{\mathcal{D}t} = \frac{\partial G}{\partial D_{ij}} \tag{33}$$

The classical elastic-plastic isotropically work hardening law (Prandtl-Reuss), commonly giving strain-rate as a linear function of stress-rate, can be inverted to give stress-rate and takes the form ([5] p. 606)

$$\frac{\mathcal{D}\overset{c}{\sigma}_{ij}}{\mathcal{D}t} = \frac{E}{1+\nu}\left[\delta_{ik}\delta_{jl} + \frac{\nu}{1-2\nu}\,\delta_{ij}\,\delta_{kl} - \frac{3\overset{c}{\sigma}'_{ij}\,\overset{c}{\sigma}'_{kl}\,\left(\frac{E}{1+\nu}\right)}{2\bar{\sigma}^2\left(\frac{2}{3}h + \frac{E}{1+\nu}\right)}\right] D_{kl} \tag{34}$$

where E and ν are Young's modulus and Poisson's ratio, σ' denotes stress deviator, $\bar{\sigma}$ is the current tensile yield stress and h the current gradient of the true-stress logarithmic plastic strain curve in a tension test. The Jaumann derivative is used for stress-rate as mentioned above in order to eliminate rotation effects, and the last term in the brackets is dropped when the increment of deformation is elastic. We have shown that there is a rate-potential function G for $\overset{c}{\tau}_{ij}$, but not one for $\overset{c}{\sigma}_{ij}$. This means [5] that a non-symmetric finite-element stiffness matrix would be deduced using (34). Replacing $\overset{c}{\sigma}_{ij}$ by $\overset{c}{\tau}_{ij}$ in the stress-rate term would yield a symmetric stiffness matrix which would simplify the numerical analysis. Moreover such a change is appropriate in terms of its representation of the physical laws. The J term in

$$\overset{c}{\tau}_{ij} = J\,\overset{c}{\sigma}_{ij} \tag{35}$$

arises in more accurate representation of the laws of elasticity than Hooke's law used in classical elasticity. It is associated with geometrical non-linearity which expresses the non-linear influence of finite strain. In effect it expresses the fact that energy density per unit initial volume yields a simpler energy conservation statement, for per unit current volume implies change of energy density simply because the amount of material containing it changes. For example, the term (ρ/ρ_o) appearing in equation (26) of [10] is equivalent to replacing $\underset{\sim}{\sigma}$ by $J\underset{\sim}{\sigma}$, and it was pointed out in that paper (p. 935) that such a term provides a good approximation to non-linear elasticity of metals with input of only the two classical elastic constants. A similar modification of the classical laws of plasticity was suggested in [11] where it was found compelling to express the yield stress in terms of $J\underset{\sim}{\sigma}$ (equs. (33) and (34) of [11]). Again this was based on the requirements of geometrical non-linearity, which of course are independent of specific material characteristics.

Introduction of (2) into the variational principle (3) expresses it in the form

$$\int_{\overset{\circ}{V}} \dot{s}_{ij}\, \delta\left(\frac{\partial v_i}{\partial x_i}\right) \overset{\circ}{dV} - \delta\left(\int_{\overset{\circ}{S_F}} \dot{F}_j v_j \overset{\circ}{dS} + \int_{\overset{\circ}{V}} \dot{g}_j v_j \overset{\circ}{dV}\right) = 0 \qquad (36)$$

which, since the reference state is the current state ($\underset{\sim}{X} = \underset{\sim}{x}$) can be written

$$\int_V \dot{s}_{ij}\, \delta\left(\frac{\partial v_i}{\partial x_i}\right) dV - \delta\left(\int_{S_F} \dot{F}_j v_j dS + \int_V \dot{g}_j v_j dV\right) = 0 \qquad (37)$$

Substitution of (29) and applying algebraic manipulation based on

symmetries then yields the variational principle in the form (see equ. (5) of [5])

$$\int_V \left[\frac{\mathcal{D}^c\tau_{ij}}{\mathcal{D}t}\,\delta(D_{ij}) - \tfrac{1}{2}\sigma_{ij}\,\delta(2D_{ik}D_{kj} - v_{k,i}\,v_{k,j})\right]dV$$

$$-\delta\left(\int_{S_F} \dot{F}_j v_j\,dS + \int_V \dot{g}_j v_j\,dV\right) = 0 \tag{38}$$

where the subscript $,i$ denotes the operation $\partial/\partial x_i$. Now utilizing (33), the principle takes the form (see equ. (15) of [5]).

$$\delta\left[\int_V G(D)\,dV - \tfrac{1}{2}\int_V \sigma_{ij}(2D_{ik}D_{kj} - v_{k,i}\,v_{k,j})dV\right.$$

$$\left. - \int_{S_F} \dot{F}_j v_j\,dS - \int_V \dot{g}_j v_j\,dV\right] = 0 \tag{39}$$

By (33), and using Euler's theorem

$$\frac{\mathcal{D}^c\tau_{ij}}{\mathcal{D}t} = \frac{\partial G}{\partial D_{ij}} = \frac{\partial^2 G}{\partial D_{ij}\partial D_{kl}}\,D_{kl} = \mathcal{L}_{ijkl}\,D_{kl} \tag{40}$$

since $\partial G/\partial D_{ij}$ is homogeneous of first degree in $\underset{\sim}{D}$, hence $\mathcal{L}_{ijkl}$ is symmetric in $ij \leftrightarrow kl$ as well as $i \leftrightarrow j$ and $k \leftrightarrow l$. Since G is homogeneous of second degree

$$G(\underset{\sim}{D}) = \tfrac{1}{2}\frac{\mathcal{D}^c\tau_{ij}}{\mathcal{D}t}\,D_{ij} \tag{41}$$

The symmetry implicit in the variational principles (38) and (39) with (40) and (41) imply symmetric stiffness matrices which carry through to the finite-element formulation [5].

3. Discussion

As discussed by Rice [4] and McMeeking and Rice [5], the development reviewed in these notes brings out the importance of convection

effects and appropriate stress-rate definitions in formulating elastic-plastic theory. Thus the precise analysis of continuum theory must be applied to obtain reliable results. Common small strain assumptions are not valid even for incremental theory based on small strain increments. This situation is implicit in comparison of the first and second terms in the first volume integral in the variational principle (38). In plastic flow the coefficient of $\delta \underset{\sim}{D}$ in the first term is $\sim h\underset{\sim}{D}$, where h is the gradient of the tensile stress-plastic strain curve, whereas the second term is $\sim \underset{\sim}{\sigma D}\delta \underset{\sim}{D}$. The second term and the difference between the Jaumann derivative and other simpler time derivatives can only be neglected if $h >> \underset{\sim}{\sigma}$. The relative error in neglecting such terms is effectively independent of the magnitude of the strain increment adopted, so that small steps do not permit simplification in this regard. For many metals $h \sim \sigma$.

It is interesting to note that the complications which arise in elastic-plastic analysis result from the elastic component of strain, and not the plastic. For stress and strain deviators, elastic-ideally plastic deformation with a Mises yield condition, $J_2 = \sigma'_{ij}\,\sigma'_{ij}/2 = k^2$, satisfies

$$D'_{ij} = \dot{\sigma}'_{ij}/2G + \dot{\lambda}\sigma'_{ij} \qquad (42)$$

where λ is a parameter. Multiplication of (42) by σ'_{ij} gives

$$\dot{\lambda} = \sigma'_{ij}D'_{ij}/2J_2 \qquad (43)$$

For isotropic work hardening with a Mises yield condition, (42) takes the form

$$D'_{ij} = \dot{\sigma}'_{ij}/2G + f(J_2)\dot{J}_2\sigma'_{ij} \qquad (44)$$

The first terms on the right hand sides of (42) and (44) are the elastic strain rate components. Thus rigid-ideally plastic theory ((42) with the $\dot{\sigma}$ term deleted) gives a relation between stress and velocity gradient with no complications due to a stress rate term, which greatly simplifies the analysis, apart from the difficulty of determining the rigid regions. Similarly for work hardening rigid-plastic analysis ((44) with the $\dot{\sigma}$ term deleted), only the rate of change of a stress invariant occurs, which is simpler to include than a tensor rate. For elastic-plastic theory it is the elastic term which introduces stress-rate and the consequent complications.

Many technologically important metal-forming problems are steady state processes in which $\partial\sigma_{ij}/\partial t|_{\underset{\sim}{x}} = 0$. In planning to use an analysis of the type considered here to evaluate such situations, it is fortunate that the stress-rate terms appearing in the variational principle, $\dot{s}_1$, or $\mathcal{D}\overset{c}{\tau}_{ij}/\mathcal{D}t$, do not approach zero in the steady case, hence singular computational conditions need not be anticipated. This is not the case in some simpler and inadequate approaches to this problem in which sufficient care was not devoted to the appropriate choice of stress-rate definition.

On the basis of the theory described, a finite-element program has been written to evaluate stress and deformation histories in an extrusion problem. The case of a billet being pushed through a die until a steady-state configuration was reached has been completed.

The stress field exhibits features which are consistent with the known development of extrusion defects, such as the appearance of surface cracks.

4. Acknowledgement

In studying the material preparatory to writing this review, I benefited from helpful conversations with Professors J. W. Hutchinson, R. J. Kaul, R. L. Mallett, J. Mayers and S. Nemat-Nasser of Harvard, State of New York, Stanford, Stanford and Northwestern Universities respectively, and with Dr. R. M. McMeeking of Brown University

This work was sponsored in part by the Materials Science Division, U. S. Office of Naval Research on a contract with Stanford University, and was carried out in part while the author held a John Simon Guggenheim Memorial Fellowship.

5. References

1. R. Hill, A general theory of uniqueness and stability of elastic-plastic solids, *Jl. Mech. Phys. Solids*, 6, 236-249, 1958.
2. R. Hill, Some basic principles in the mechanics of solids without a natural time, *Jl. Mech. Phys. Solids*, 7, 209-225, 1959.
3. R. Hill, Eigenmodal deformations in elastic-plastic continua. *Jl. Mech. Phys. Solids*, 15, 371-386, 1967.
4. J. R. Rice, A note on the "small strain" formulation for elastic-plastic problems. Technical Report N00014-67-A-0191-0003/8, Division of Engineering, Brown University, 1970.

5. R. M. McMeeking and J. R. Rice, Finite-element formulations for problems of large elastic-plastic deformation, *Int. Jl. Solids Structures*, 11, 601-616, 1975.

6. Y. C. Fung, *Foundations of solids mechanics*, Prentice Hall, 1965.

7. C. Truesdell and W. Noll, *The non-linear field theories of mechanics*, Handbuch der Physik, Band III/3, Springer-Verlag, 1965.

8. S. Nemat-Nasser, Continuum bases for consistent numerical formulations of finite strains in elastic and inelastic structures. Finite element analysis of transient nonlinear structural behavior, Eds. T. Belytschko, J. R. Osias and P.V. Marcal, ASME, 1975.

9. W. Prager, *Introduction to mechanics of continua*, Ginn and Co., 1961.

10. E. H. Lee and T. Wierzbicki, Analysis of the propagation of plane elastic-plastic waves of finite strain, *Jl. Appl. Mech.*, 34, 931-936, 1967.

11. E. H. Lee, Elastic-plastic deformation at finite strains. *Jl. Appl. Mech.*, 36, 1-6, 1969.

6. Appendix

For simplicity, relations are developed for Cartesian axes in the reference state which is instantaneously coincident with the current state. The general theory for convected coordinates carries through in a similar manner but can be technically much more involved.

Equations (16) and (24) yield the relation,

$$\underset{\sim}{\tau}\,\underset{\sim}{F}^{T} = \underset{\sim}{s} \tag{A1}$$

Material differentiation of this relation gives

$$\dot{\underset{\sim}{\tau}}\,\underset{\sim}{F}^{T} + \underset{\sim}{\tau}\,\dot{\underset{\sim}{F}}^{T} = \dot{\underset{\sim}{s}}$$

and for the special reference configuration

$$\underset{\sim}{F} = \underset{\sim}{1}\,, \quad \dot{\underset{\sim}{F}} = \frac{\partial v_i}{\partial X_j} = \frac{\partial v_i}{\partial x_j}\,, \quad \text{hence} \quad \dot{s}_{ij} = \dot{\tau}_{ij} + \tau_{ik}\frac{\partial v_j}{\partial x_k} \tag{A2}$$

Figure 1. Convected coordinates, $\xi^{\alpha} = \xi^{\alpha'}$.

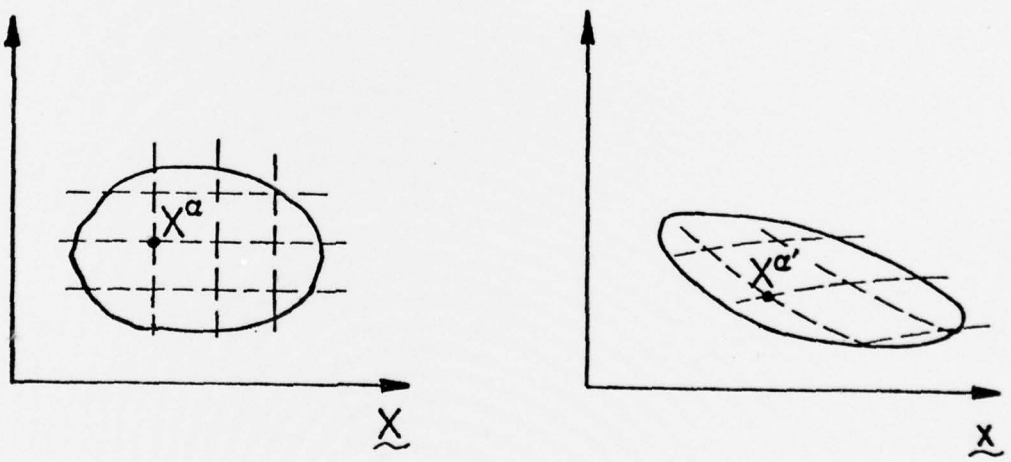

Figure 2. Cartesian reference coordinates, X^{α} .